THESIS FOR THE DEGREE OF DOCTOR OF PHILOSOPHY

Partial discharges studied by dielectric response method

Xiangdong Xu

High Voltage Engineering
Department of Material and Manufacturing Technology

CHALMERS UNIVERSITY OF TECHNOLOGY

Göteborg, Sweden 2015

Partial discharges studied by dielectric response method

XIANGDONG XU

ISBN: 978-91-7597-187-2

Doktorsavhandlingar vid Chalmers tekniska högskola
Ny seire nr. 3868
ISSN 0346-718X

High Voltage Engineering
Department of Material and Manufacturing Technology
Chalmers University of Technology
SE-41296 Göteborg
Sweden
Telephone + 46 (0)31-772 1000

Chalmers Bibliotek, Reproservice
Göteborg, Sweden 2015

道可道，非常道

A road sign shows the usual way, the best one is ever changing

Partial discharges studied by dielectric response method

XIANGDONG XU
High Voltage Engineering
Department of Material and Manufacturing Technology
Chalmers University of Technology

Abstract

The increasing demand of integrating various renewable energy recourses in power system requires extensive use of power electronic solutions, which allows energy conversion between different frequencies and stabilizes the system. Consequently, other than the traditional 50/60 Hz sinusoidal voltage stresses act on the high voltage insulation systems. Therefore a need for elaborating fast and accurate characterization methods arises for facilitating studies of the different types of voltage waveforms on the behaviour of insulation materials and systems.

Two commonly applied non-destructive insulation characterization techniques, dielectric response and partial discharge (PD) measurements, are addressed in the project. Several methods based on the so called Arbitrary Waveform Impedance Spectroscopy (AWIS) technique have been developed to enable fast and accurate characterization of dielectric material frequency response. This approach was further adopted to study the behaviour of PDs in various types of test objects, including needle-plate electrode arrangement, twisted pair enamel wires and dielectrically insulated cavities, by simultaneously applying the dielectric response measurements and the stochastic PD detection. Various experiments, involving occasionally changing voltage level, circulating air around a specimen, and modifying conductivity of cavity walls, were performed and allowed identifying additional PD current components in the total current response, which are in the following named as excess currents.

It is shown among others, by comparing the excess currents with simultaneously detected PD pulses, that contributions from weak discharges lying below the conventional PD detection threshold as well as slow contributions to the current caused by charge movements within the partial discharge area can be identified and evaluated. An important component of the excess current is a non-PD excess current that repeatedly appears in all studied types of objects and causes a decay or even disappearance of PD activity with time. At longer exposures of the dielectrically isolated cavities, it also yields oscillating interchanges between PD activity and the excess current.

Keywords: AWIS, dielectric characterization, partial discharge, frequency domain spectroscopy, partial discharge excess current, non-PD excess current.

Acknowledgments

This work has been carried out within ELEKTRA projects no. 36085 and 36262, jointly financed by the Swedish Energy Agency, Elforsk and ABB. Financial supports from Stipendiefonden till minne av Erik Feuk, Wilhelm och Martina Lundgrens vetenskapsfond and Chalmerska forskningsfonden for participating in scientific conferences and study visits have also been thankfully received.

I am very grateful to my examiner Prof. Stanislaw Gubanski for consistent support, carefully revising all my manuscripts, putting tricky questions, keeping me alert, providing excellent platform for promoting the work and providing solid theoretical support in the dielectric world. My supervisor, Prof. Tord Bengtsson has shared his great expertise, teaching me the philosophy of research and life. He has always been ready for discussing any issues, sharing valuable ideas and providing exciting inspirations. Through his continued guidance and encouragements, lab becomes enjoyable and writing becomes confidence. My other supervisor Prof. Jörgen Blennow has continuously served as an inspiration for both my master and PhD studies. In addition, we have shared many other interesting discussions throughout the years at Chalmers.

The reference group members are acknowledged for providing a great source of ideas and support.

Ron Brammer from Bombardier; Fredrik Sahlén and Sari Laihonen from ABB CRC; Tina Törnström from ABB karlskrona, are sincerely acknowledged for supplying testing materials.

Colleagues from High Voltage Engineering group has helped to create a pleasant atmosphere and with various matters. Fellows from KTH, Lund and Uppsala are also thanked for sharing valuable ideas and discussions during conferences and courses.

My parents are sincerely thanked for all the supports and encouragements, you are the ones who led me the person I am today. (在此，我也由衷的感谢我的父母：徐成钦，向清如，对我付出的一切支持和鼓励，是你们的努力成就今天的我). At last, but not least, my wife, Yu Liu, is specially thanked for all her love, understanding, and support to make this work possible.

Xiangdong Xu

Göteborg, Sweden

May, 2015

Table of Contents

1 Introduction

Today, the demand of sustainable electric power solutions is at the top of strategic development agendas over the world. To integrate renewable energy sources as well as to balance energy production and consumption, power electronic solutions in combination with solid dielectric insulations are integrated into the systems. In such systems, the insulation is subjected to increasingly higher dielectric stress and in many cases to stresses at higher frequencies than the traditional power frequencies. Thus, there is a growing interest in testing methods for fast and accurate dielectric characterization under different voltage levels as well as at high frequencies for material selection and development.

Measurement techniques are essential in all stages of high voltage equipment life time, from first conception to retirement decision. Dielectric response (DR) and partial discharge (PD) measurements are two major effective and non-destructive insulation testing techniques in high voltage applications. The history of dielectric response measurements can be dated back to late 1800 [1], whereas the measurements of partial discharges were initiated in the 1940s [2].

In this work, the focus is on exploration of a nearly virgin field, i.e. measurements of currents associated with PD activity in model insulation systems. Throughout the work, the technique, Arbitrary Waveform Impedance Spectroscopy (AWIS) [3, 4] is utilized in parallel with a stochastic PD detection [5, 6] in order to determine slow and fast charge movements associated with the PD activity.

1.1 Background and motivations

The AWIS technique has been developed to a versatile tool for insulation dielectric diagnostics and its primary advantage, as compared to conventional DR methods is that a well-defined sinusoidal waveform with precisely known frequency is no longer required for performing high-precision measurements. It is capable of determining a broad dielectric spectrum from one measurement, provided the test voltage is rich enough in harmonics. The high accuracy is achieved by adopting a large flexibility in selecting measuring circuit parameters to create the best possible conditions for a specific task.

Presence of partial discharges is an important indicator of weak points or degradation in insulation systems. Measurements based on amplified and band-pass filtered electrical detection of significant fast PD pulses are mostly applied for high voltage diagnostics and material studies [7]. The limitation of such an approach is that it does not allow detecting slow charge movements and the discharge pulses need to be well separated and well above noise level, as PDs are essentially dielectric breakdowns that only partially bridge the insulation distance between two conductors. When PDs occur, high frequency transient current pulses appear with rise times of nanoseconds and duration up to microseconds. These distinct fast features facilitate detecting

millivolt PD signals on kilovolts background. Thus, anything below the threshold is disregarded. In addition, in various insulation systems, PDs may not only cause fast current transients but also slower current contributions due to charges generated by preceding PDs.

In studies of insulation system ageing, time to breakdown is often the measured quantity and various trials have been made to adopt other observable parameters of the ageing process [8, 9] to reduce the necessary testing efforts. PD occurrence appears as a natural choice for such an observable, though proven not easily interpretable. For example, studies [10-14] have exemplified that both PD number and their amplitude may decrease to very low values shortly after an ageing test is initiated and only after a substantial part of the lifetime consumed, the parameters return to levels similar or higher to the initial ones. One explanation is that this effect is closely related to space charge dynamics as well as to generation of decomposition by-products. A pertinent question in relation to these studies is if there are small undetected discharges or possibly currents of other types present when the PD intensity has changed. To answer this question, another type of approach to PD measurement is proposed in this thesis.

1.2 Aims and contributions

The aim of the work reported here is to develop a new technique, which enables measurements of both fast and slow charge movements during PD activity and facilitates a comparison of the total charge resulting from a few sizeable PD events to that from many small ones. Such a measurement should be a desired complement to the conventional PD detection methods that provides additional insights into the mechanism of PD activity. The use of dielectric response measurement, represented here by AWIS, provides a possibility to overcome the limitations of the traditional detection methods and to quantify the charge involved in the PD activity. By measuring dielectric response currents through a test object without and with PD activity, the additional current components generated from the discharges is quantified. To some extent, the developed method is an advancement of the tan δ 'tip-up' test. The difference is however that the discharge current is resolved in phase and can thus be compared to conventional PD phase distributions. This method provides a possibility to measure the true additional current related to the PD apparent charges, but without a necessity for calibration.

Discussions in the thesis provide more details of how the PD excess currents are measured and what complementary information can be gained. In addition, a new way of presenting the dielectric response results as the excess current is introduced in the thesis and it is compared with the simultaneously obtained results from the conventional stochastic PD detection [5, 6]. Interesting similarities and differences between the PD excess current and the simultaneously detected pulse PD current are observed for a variety of test objects.

1.3 Content overview

The author's complete PhD project work consists of two integral parts. The first part of the project was dedicated to the enhancements in dielectric response characterization of insulation materials and was presented in the licentiate thesis [15]. A resume of this work is provided in section 2.3 and it is thus not fully included in this

thesis. This thesis only reports on the second part of the project work, i.e. on the partial discharges excess current measurements. However, the common denominator in both studies is that very similar techniques and circuits are utilized, albeit with different objectives and interpretation.

Chapter 2 serves as literature review of PD test techniques and background of the project. In chapter 3, the definition of the PD excess current, different possible approaches to resolve the current as well as detailed measurement setups are discussed. The used test objects and voltage waveforms are presented in chapter 4. Chapter 5 is dedicated to verify existence of an PD excess current. Followed by different PD patterns observed in prolonged PD exposure of the test objects in chapter 6, including decay and oscillation of PD activity. Finally, analyses of non-PD excess current identified in these measurements are provided in chapter 7. The last chapter, chapter 8, presents conclusions and suggestions for the future work.

1.4 List of publications

Licentiate thesis:

I. Xiangdong Xu, Tord Bengtsson, Jörgen Blennow and Stanislaw Gubanski, "*Harmonic Limited Test Waveforms for Fast AWIS Dielectric Studies*", 22nd Nordic Insulation Symposium (NORDIS 11), June 13-15, Tampere, Finland, p. 199-202

II. Xiangdong Xu, Tord Bengtsson, Jörgen Blennow and Stanislaw Gubanski, "*Arbitrary Waveform Impedance Spectroscopy used for Accurate Contact-free Dielectric Characterization*", 2012 International Conference on High Voltage Engineering and Application (ICHVE 2012), (Article no. 6357019) p. 170-173

III. Xiangdong Xu, Tord Bengtsson, Jörgen Blennow and Stanislaw Gubanski, "*Enhanced Accuracy in Dielectric Response Material Characterization by Air Reference Method*", IEEE Transactions on Dielectrics and Electrical Insulation, Vol. 20, No. 3, pp. 913-921, 2013.

IV. Xiangdong Xu, "*Enhancements in Dielectric Response Characterization of Insulation Materials*", Licentiate thesis, Materials and Manufacturing Technology, High voltage engineering, Chalmers University of Technology, Gothenburg, Sweden, 2013.

V. Xiangdong Xu, Tord Bengtsson, Jörgen Blennow and Stanislaw Gubanski, "*Correction of Geometric Influence in Permittivity Determination*", NORD-IS 13, Trondheim, Norway, pp. 71-74, 2013.

PhD thesis:

VI. Xiangdong Xu, Tord Bengtsson, Jörgen Blennow and Stanislaw Gubanski, "*On Excess Current During and After Partial Discharge Activity*", IEEE Conference on Electrical Insulation and Dielectric Phenomena - (CEIDP 2014), Des Moines, IA, USA, pp. 27-30, 2014.

VII. Xiangdong Xu, Tord Bengtsson, Thomas Hammarström, Jörgen Blennow and Stanislaw Gubanski, *"Loss Current Studies of Partial Discharge Activity*", IEEE Transactions on Dielectrics and Electrical Insulation, Vol. 22, No. 1, pp. 472-481, 2015.

VIII. Xiangdong Xu, Tord Bengtsson, Thomas Hammarström, Jörgen Blennow and Stanislaw Gubanski, "*Study of Partial Discharge Activity by Excess Current*", to appear in IEEE Transactions on Dielectrics and Electrical Insulation, 2015.

IX. Xiangdong Xu, Tord Bengtsson, Jörgen Blennow and Stanislaw Gubanski, "*Spontaneous Partial Discharge Oscillations Studied by Excess Current*", IEEE Conference on Electrical Insulation and Dielectric Phenomena - (CEIDP 2015), Ann Arbor, Michigan, USA, 2015.

2 Literature review and background

This chapter starts with a review of conventional PD test techniques, followed with the history of the techniques used in this work, including AWIS and stochastic PD detection [5]. In addition, a summary of the first part of the project, enhancements in dielectric response characterization of insulation materials, is also presented with some highlighted results.

2.1 Conventional PD test techniques

The importance of PD studies was realized back in the 1940s [2]. Initial works on detection, measuring as well as location of PD phenomena were performed and a large numbers of effective measurement techniques were introduced. Later, with adequate acquired PD data, various interpretation schemes were introduced, involving different time scales. The following literature review is therefore divided into two parts with the first part focused on PD measurement techniques and the second part devoted to PD data analysis.

The partial discharge phenomenon can be subdivided into a number of classes dependent on the dominating physical mechanism of the discharge. Despite the duration and magnitude of individual discharges may vary over many orders of magnitude, most of them are thought to contribute to material ageing [16]. Of these, some discharge types are classified in [16] as difficult or impossible to detect by conventional PD detection techniques, namely glow, Townsend and swarming partial micro discharges. Also the surface conductivity influences are hardly detectable. Thus, conventional PD detection techniques are not guaranteed to indicate an ongoing ageing process.

2.1.1 PD measurement techniques

Partial discharges are characterized by fast rise time and short duration, in the nanosecond range, which create a series of fast current pulses in an external circuit and exhibit a non-linear voltage behaviour. These pulses can also be observed as high frequency fluctuations of the terminal voltage. Therefore, various frequency bands are used in PD measurement systems by coupling either the fast current pulses or the rapid voltage fluctuations [17]. Electrical PD measurement techniques rely on such characteristics and can therefore be divided into three levels, depending on how the PD signal is resolved and the detection bandwidth in the frequency domain.

The first level requires resolving nanosecond time scales and the used detection bandwidth is ultra-wide band, over 1 GHz , which allows the true PD current pulse shape to be resolved [18]. This type of tests often requires dedicate instrumentation characterized by excessive sampling rate. However, a limitation of such measurements is that only a few PD pulses can be studied.

PD signals resolved in micro second range can be considered as the second level of PD measurement techniques, where the original PD pulse shape is not resolved, only the time of concurrence and its amplitude are quantified. The bandwidths of these types of instrumentation range from tens of kilohertz up to several hundred kilohertz and the pulse shape obtained is determined by the detection circuit. This type of measurement technique is often used to count amplified PD pulse signals. A coupling device, usually known as quadripole, converts the input current pulses into an output voltage signal and the frequency response of the coupling device is selected to attenuate the excitation voltage. The response of these instruments to a PD pulse is a high frequency transient with its peak to peak value proportional to the apparent charge [17, 19]. The limitations of such a measurement approach are that it is not possible to detect slow charge movements and the discharge pulses need to be well separated and significantly above the noise level. Nevertheless, the band-pass filtered electrical detection of significant PD events remains today the most commonly used method in industrial applications, often being an important part of factory acceptance tests.

The third level of PD measurement techniques is based on detecting PD activity without resolving the individual pulses with narrow bandwidth often below tens of kilohertz, the time scales involved is thus seconds. A typical example of such a method is the radio interference voltage (RIV) PD measurement [19]. Tan δ 'tip-up' testing [20, 21], and changes in measured capacitance during PD activity [22, 23] also belongs to this category. This type of measurements often relies on the non-linear voltage dependence of PD activity and provides only qualitative information. The PD excess current measurement discussed in this thesis is a further development of this line of work.

Studies based on dielectric response technique were earlier reported in [24, 25]. In [26, 27], currents arising from PD activity were also explored. These studies were however limited to low-frequency AC applications. Nevertheless, interesting features (similarities and differences) between PD apparent charges measured by the dielectric spectroscopy method and the pulse PD method were observed in different test objects. In [28], a weak decaying resistive current was found to have some correlation with PD activity bursts.

As a primary challenge in PD detection is the noise level, it has always been desirable to detect as weak PDs as possible. The theory of signal analysis states that white noise amplitude is inversely proportional to bandwidth and therefore narrow band measurements have the potential of being the most sensitive. To obtain nanosecond resolution, the noise must be seriously considered. A large number of publications [29, 30] is devoted to signal processing of PD signals in order to reduce the noise.

Apart from electrical measurements, PDs can also be detected by means of optical [31, 32] and acoustical [33] methods. These are primarily utilized to localize PDs, but require that the construction of test objects allows detection of such signals [34].

2.1.2 PD data analysis

After recording enough data from a PD measurement, interpretation becomes important. PD analysis has been established as a reliable diagnostic tool within power industry. Similar to the PD measurement techniques, the PD data analysis can also be

divided into three different resolved time levels, i.e. nanoseconds level, milliseconds level and second level, depending on the analysed PD properties.

The nanosecond resolved PD properties often reflect the physical process of individual PD events and may reveal some direct connections between the defects [35, 36] and the shape of the PD signals [37, 38]. The PD current shape is also an important part in the pulse sequence analysis [39, 40].

The second and the most commonly resolved level is in the millisecond range, where the obtained PD information is often phase resolved with relation to the excitation voltage [41, 42]. The averaged PD parameters, occurrence time and amplitude, are integrated over small bins or windows dividing the voltage phase angle range. Many studies [33, 43-48] have been devoted to interpret PD patterns at this time scale level and various types of defects may be identified by means of these techniques.

The third level of resolved PD activity is often used in time to breakdown studies [10-14], where the changes in PD activity are observed during longer time scale. This analysis level has historically attracted the least interest. The time development of PD excess current presented in the thesis belongs to this level of PD data analysis.

2.2 Background of the used approach

Two measurement techniques, AWIS and stochastic PD detection, have been utilized in this work for partial discharge studies. Both techniques were developed within our research group in the context of four PhD project works, of which three were earlier presented in [6, 49, 50]. A common feature of the techniques is that they are based on relatively simple but carefully designed electrical circuits and flexible but versatile acquisition and analysis software. Thus, a large freedom and responsibility is entrusted to the operator to design the best possible conditions for various challenging measurement tasks, as resumed below.

2.2.1 Arbitrary waveform impedance spectroscopy

With help of modern instrumentation technology and computational ability, AWIS [3, 4] has been developed as a dielectric response technique for insulation diagnostics [49, 51, 52].

In the development of the AWIS concept, a measurement toolbox was gradually built in order to meet the high demands on precision in the dielectric response characterization, typically in the order of 10^{-4}. Efforts were made to limit the stray capacitances and line inductances. At the same time, the inherent properties of the circuit components were considered. However, stray capacitance as well as line inductance cannot be completely eliminated. In order to cope with the reality, modelling of the measurement circuit over a broad frequency spectrum (from 100 Hz to 100 kHz) was carefully performed for both low and high voltage setups. For the high voltage setup (voltage levels higher than the voltage specification in the DAQ card), a voltage divider was applied with consideration of its frequency responses.

The realized AWIS setup was first employed to perform fast dielectric frequency response characterization using semi-square voltage waveforms. By adjusting the fundamental frequency of the applied voltage as well as the sampling rate of DAQ, the

aliasing effect could be suppressed and a broad dielectric spectrum was determined from one measurement utilizing voltage harmonics.

The dependence of capacitance and loss on voltage, temperature and time were studied and significant effects were found. This resulted in a general formulation of how to calculate dielectric heating under voltages with a high harmonic content [53].

Further, first studies of dielectric material degradation mechanisms using AWIS technique were performed. The PD behaviour of different objects was studied by monitoring the discharge current in both frequency and time domain. This study gave an indication of a weak conductive current, as seen in Figure 2.1, which was one motivation of for undertaking the PD excess current investigations performed within this work. As a particular example, the change of dielectric properties during electrical tree growth in LDPE samples was studied by monitoring capacitances on the level below 1 pF [23, 54].

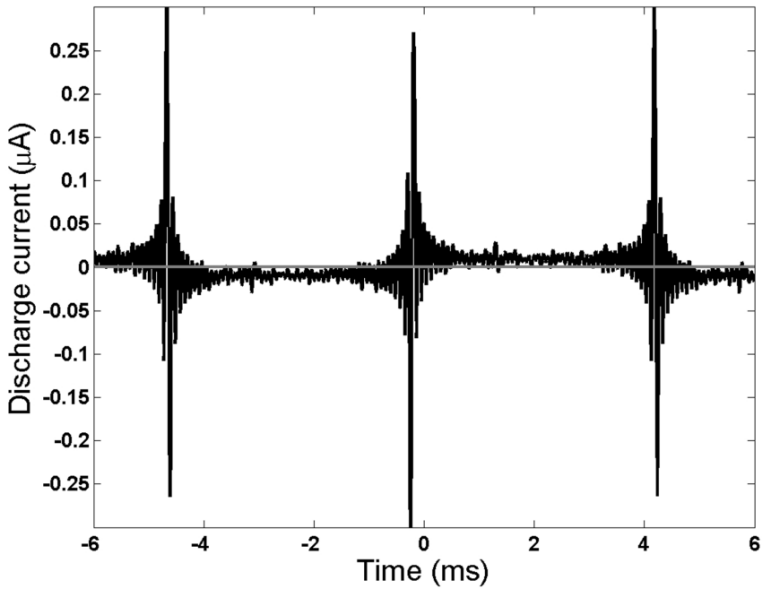

Figure 2.1. The observed resistive-like current which is related to partial discharge activity [55].

2.2.2 Stochastic PD detection

Today, with increased use of power electronic solutions, it is important to understand the impact of rapidly changing voltages originating from pulse width modulated (PWM) voltages on insulating systems. A new research direction towards understanding of ageing and breakdown mechanisms of electrical insulation under power electronic wave shapes has started in 2003 and a PD measuring system, the first version of stochastic PD detection [50], was developed. It enabled studies of the influence of the voltage steepness on the PD behaviour [56, 57]. Further, a scan of PD extinction voltage dependence on rise time for various types of PD sources was performed and the results were found to vary for different types of insulation systems [58]. In addition, it was found that PD appearance in paper-oil insulation could be prohibited by increasing the frequency, as PDs often require a few milliseconds to be formed in such systems [59].

The measurement system has thereafter been developed further [6]. One important enhancement was a more elaborate design of the electric circuit, the PD decoupler [60], which became more versatile to allow a more efficient suppression of the voltage remnant without lowering the PD signal amplification. The PD decoupler circuit is adjustable to different voltage shapes by only changing a few of its components and thus allows the use of a low resolution digitizer, such as an oscilloscope.

Investigations on dielectrically insulated cavities revealed that the voltage rise time has a significant influence on the PD characteristics and its mechanism [61]. The obtained result suggests that the rise time indeed affects the degradation with possible implications on the design and production of electrical apparatuses.

With the development of the PD measurement system, stochastic PD detection [5] was realized, which is the one employed in this thesis for simultaneous PD pulse detection. The implemented system is able to detect PDs under PWM voltage, which requires accepting both timing jitter and a non-integer relation between carrier and modulating frequency. Tests under PWM voltage shape confirmed the observations found for semi-square wave voltages. Further investigations on PWM voltage shape of different smoothness provides a possibility to determine a sufficient smoothing level when designing insulations systems exposed to fast transients [62, 63]. An example of PD detection under smoothed PWM voltage is shown in Figure 2.2.

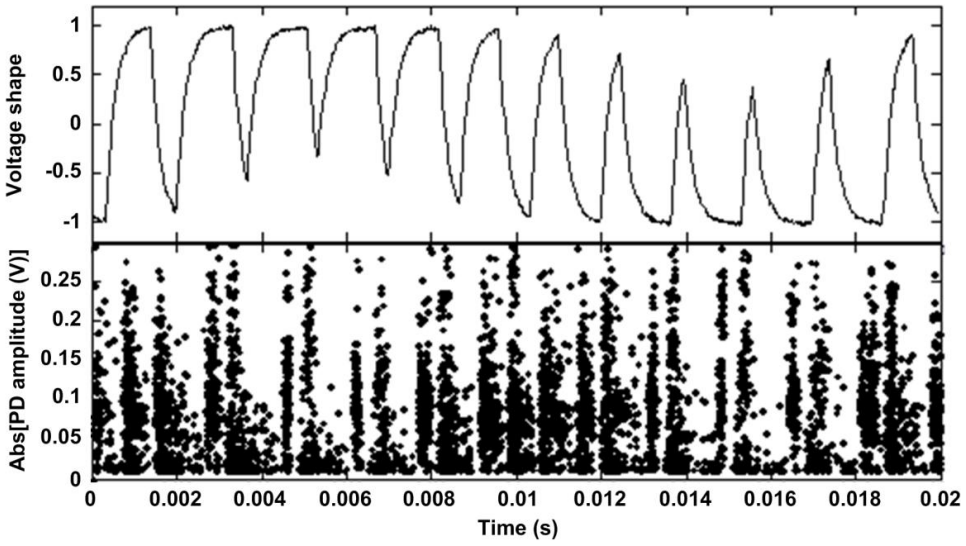

Figure 2.2. PD events detected by stochastic PD detection system under smoothed PWM voltage [6].

2.3 Enhancements in dielectric response characterization

In this project, the continued development of the AWIS technique concentrated initially on enhancements in dielectric response characterization of solid insulation materials, which provides a foundation for later development of PD excess current measurement. These research activities were concentrated on two main aspects. One was related to the measurement time and the other was focused on the measurement accuracy. Both aspects are complementary and the main outcomes of this work are summarized below.

2.3.1 Fast dielectric characterization

Harmonic limited waveforms [64] and contact-free electrode arrangements [65] are implemented to enable fast dielectric response measurements.

Signals with high harmonic content can be used by the AWIS technique to determine a wide dielectric frequency response spectrum from one measurement. However, a too high harmonic content will limit the measurement accuracy due to aliasing. To avoid signal aliasing, the harmonics limited waveform must be generated by considering the fundamental frequency, the number of samples in the waveform and the sampling rate in the measurement. This was facilitated by the equations that reveal the apparent frequencies of aliased signals. With a frequency spectrum determined from one measurement, the optimized test waveforms enabled all the frequency responses to be determined under identical test conditions and to eliminate possible systematic errors. A selected result of such measurements is highlighted in Figure 2.3, where loss factors from fast dielectric characterization using voltage harmonics are compared with swept results by traditional measurement. Both measurements were performed under continuously changing temperature in the specimen.

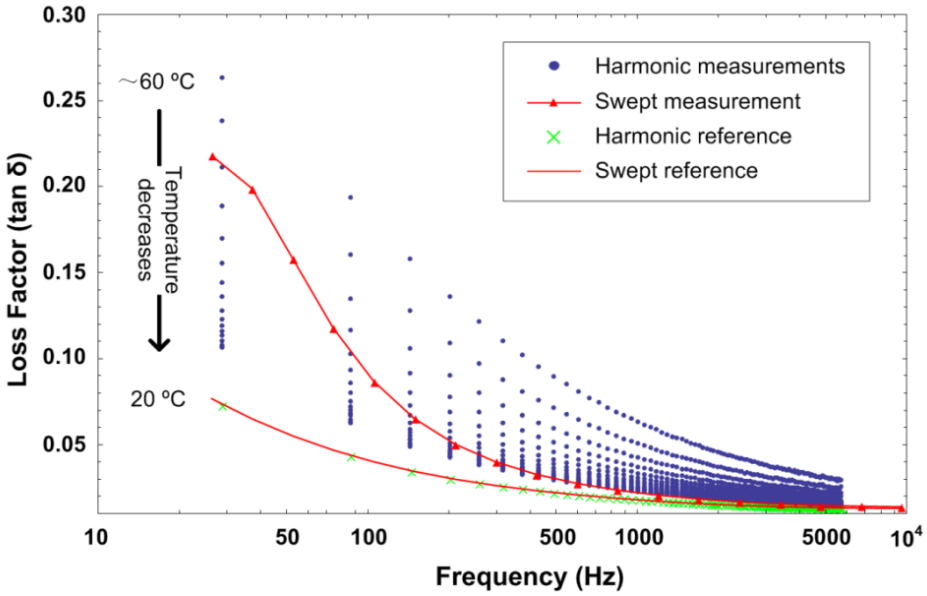

Figure 2.3. Dielectric response characterization of a pressboard sample measured under continuously changing temperature. More details can be found in [15].

Elaborated specimen preparation procedures in solid dielectric characterizations are often time-consuming and complicated. Further, in contact specimen-electrode arrangement, the applied pressure from electrodes may deform the specimen and influence the accuracy of the determined permittivity. Contact-free electrode arrangement was therefore investigated to avoid elaborate specimen preparations and to increase the measurement accuracy.

The combination of harmonic limited waveforms and contact-free electrode arrangements enable the use of AWIS for fast dielectric characterization and study of dielectric materials under rapidly changing environmental conditions.

2.3.2 Accuracy improvement

To improve the accuracy of measurement, the work was first focused on optimization of the AWIS setup. A measurement noise at ppm level was achieved by implementing a shielded box, a voltage supply with batteries and a proper grounding. With additional help of a voltage divider, a voltage follower as well as separation channels, crosstalk interferences were largely reduced down to the noise level.

Further, the accuracy of the dielectric response parameters, loss factor and permittivity, were improved in this work by implementing an air reference method and considering the geometric influence in the electrode setup.

The air reference method [66] was demonstrated to improve instrument accuracy by performing a calibration with a known medium, air, under the same conditions as the dielectric is tested. Thus, the detailed voltage and current sensing properties are eliminated from the final results. This requires that the instrument have the same sensitivity in the reference and the specimen measurements. The experimental results indicate a substantial improvement in accuracy as compared to direct measurements. In particular, this method may improve loss factor sensitivity into ranges required for characterization of modern insulation materials. In addition, any poor surface contact between specimen and electrode will result in a significant increase of losses at high frequencies due to a series connected surface resistance. On the other hand, as the measured loss at low frequency is often dominated by the material's DC conductivity, it masks all other simultaneously acting polarization processes. An example is shown in Figure 2.4, in which differences between contact and contact-free measurements at the low frequencies are shown.

To apply a contact-free measurement, the air reference method is required as the dielectric properties of the specimen are found from the difference of two capacitance measurements. There is inevitably some reduction of sensitivity as an air gap contribution need to be eliminated from the result whereas this method may significantly reduce specimen preparation time and improve reproducibility. The air reference method eliminates one important source of error, the sensor calibration error. In cases where this error dominates, an improved accuracy may be obtained despite the reduction of accuracy due to the air gap. One such example is shown in Figure 2.5, where the accuracy of a commercial instrument has been increased about 3 times by utilizing the air reference method.

Material permittivity is often determined based on capacitance measurements of a two-electrode fixture, therefore electrode edges, shielding box, and other parts of the surroundings influence the accuracy in cases a non-negligible voltage is generated at the measuring electrode over a current shunt. Two methods to either compensate or shield the interferences from electrode test set-up were proposed to improve the accuracy of dielectric permittivity determination.

The geometric correction derived from finite element model calculations [67] provides one possible way to increase the accuracy of permittivity measurement by an order of magnitude, provided that the voltage on the measurement electrode is accounted for. By analysing finite element based compensation, a shielding guard electrode system has been conceived. In contrast to ordinary guard rings, the system allows eliminating the need for the geometric corrections. It is however required that the shielding guard

has the same potential as the measuring electrode and that it covers the backside of the measuring electrode.

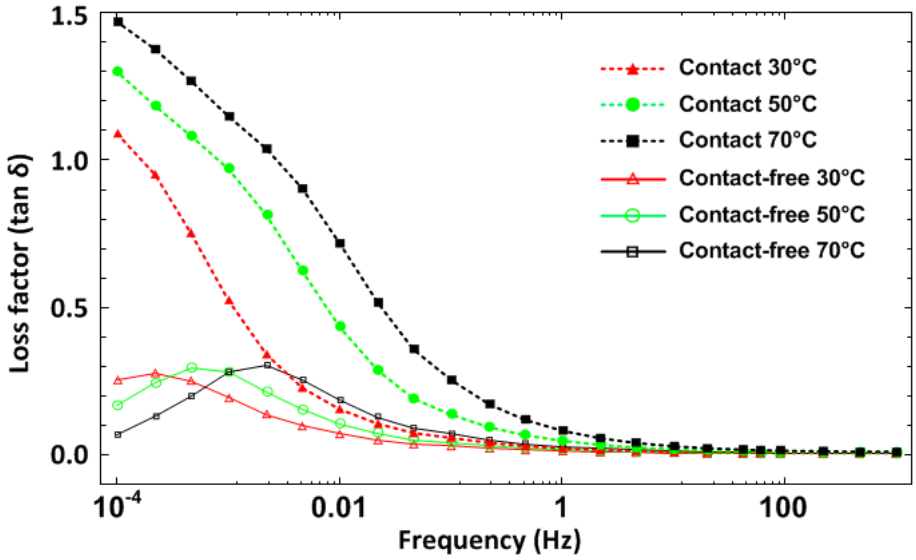

Figure 2.4. Loss factor of a HTV silicon rubber measured at three different temperatures with contact-free electrode arrangement and air reference method at low frequency range. As a reference, results obtained by contact electrode arrangement with direct measurement are also shown. Error bars are not visible for the used scaling, thus omitted in the figure.

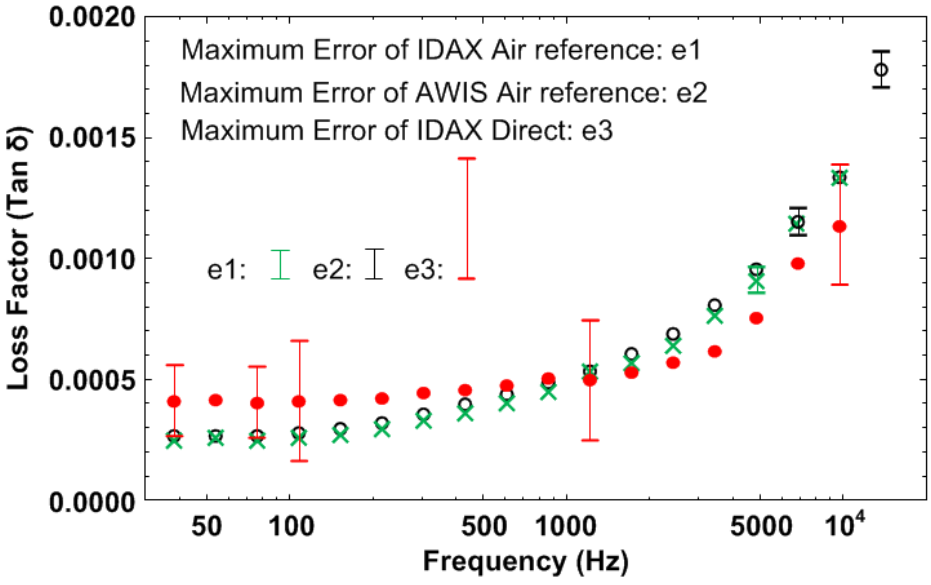

Figure 2.5. Loss factor of a polycarbonate specimen measured by AWIS with the air reference method and measured by IDAX with both the air reference method and the direct contact method. To improve the readability, only a few data points are marked with error bars as they are within the same uncertainty ranges for each frequency [68].

3 Partial discharges measured as excess current

The majority of conventional measurement techniques applied to detect partial discharges rely on the vast difference in frequency content of the fast discharge and the background voltage signal. As PDs are very fast and weak events, the detection requires resolving millivolt signals in a kilovolt background. This type of methods mainly allows detecting discharge pulses stronger than a noise threshold, while pulses below the threshold are ignored, even if they are very many. Further, as mentioned in section 2.1, some discharge types are not possible to be detected by conventional PD detection techniques but may contribute to material aging [16].

It is thus of interest to complement the conventional PD measurements by measurements detecting slower charge movements and also properly compare the total charge released by a few large discharges to that of numerous small ones. Such a possibility appears when simultaneously applying the dielectric response technique, AWIS, as described in the previous chapters. Up to the voltage level where PD starts, the PD inception voltage (PDIV), only a capacitive component is registered in the current response of a test object. When passing this level, a drastic change of the response current is observed, containing additional current components. This is separated from the total measured current by subtracting the estimated capacitive component to extract an entity called the excess current. It is shown in the following that detailed studies of the excess current provide valuable complementary information on the PD behavior in various types of test objects.

To verify and complement the excess current results, a conventional pulse PD detection system, stochastic PD detection [5] was applied simultaneously with the excess current measurement. The way in which the two systems are connected is illustrated in Figure 3.1.

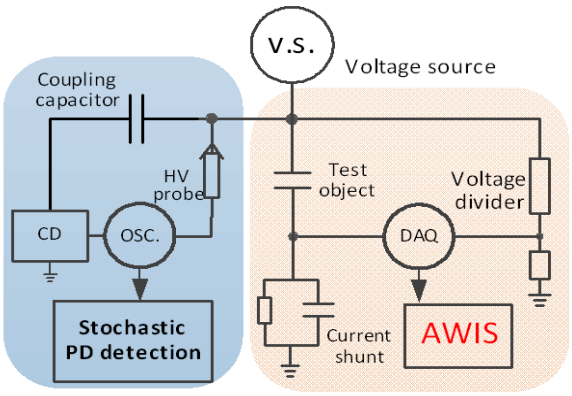

Figure 3.1. Measurement setup combining excess current measurement (AWIS) and pulse PD detection (stochastic PD detection).

3.1 PD excess current - overview

The PD excess current is defined as a difference of the actual measured current during PD activity and the estimated dielectric current. It is determined from two measurements of voltages V_0 and V_1 (Figure 3.2) under similar voltage waveforms but of amplitudes below and above the PD inception voltage (PDIV). The excess current due to PD activity is then calculated as follows:

$$I_{exc} = I_{tot} - I_{cap} = \frac{V_1}{Z_{sh}} - \frac{kV_0}{Z_{to}} \tag{3.1}$$

where $Z_{to} = \frac{kV_0^{ref} \cdot Z_{sh}}{V_1^{ref}}$ is the impedance of the test object without PD activity and k is the ratio of the voltage divider. The current obtained with voltage below PDIV (measured voltages V_0^{ref} and V_1^{ref}) is used as a reference to estimate the capacitive response of the test object. Here, it is assumed that the capacitive current is linearly dependent on the voltage amplitude around PDIV.

The quantities in equation (3.1) may be waveforms, real scalar values or vectors of harmonic amplitudes. The principle of calculation remains the same but the choice has significant influence for the quality of the results.

Measurement of PD excess currents can be realized by a conventional time domain approach, provided the time resolution and the sensitivity of the system are sufficient. Due to the stochastic nature of PDs, the measurements often require some time to obtain statistically significant results. With the short duration of the PD pulses, this seems to demand excessive computational ability and sampling rate. The current sensing method can, however, be used to reduce the requirements on the sampling rate as discussed below, whereas the AWIS technique provide proper time averaging by frequency analysis. Combined together, these allow sensitively measuring partial discharge currents. More detail discussions of the time and frequency domain analysis approaches are presented in section 3.3.

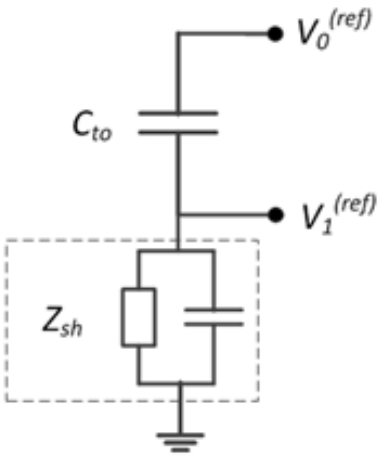

Figure 3.2. Basic circuit of PD excess current measurement.

A very important element in this measuring circuit is the design of the current shunt, built of a resistor in parallel with a capacitor. With such a shunt, the capacitor stores the fast PD pulse charge which then slowly discharges via the resistor. Fast charge movements can thus be quantified by integration, which facilitates a sufficient time constant for the data acquisition (DAQ) to record the event. For selection of the shunt parameters, both sampling rate, impedance of test object as well as applied voltage harmonic content should be considered to obtain an optimal resolution. The current shunt is discussed in more detail in section 3.2.1.

With the chosen current shunt, the fast PD pulse charge is immediately reflected in the shunt response voltage V_1. The sharp front appears as wide frequency response in the measured current. Due to the stochastic nature of PD activity, this high frequency

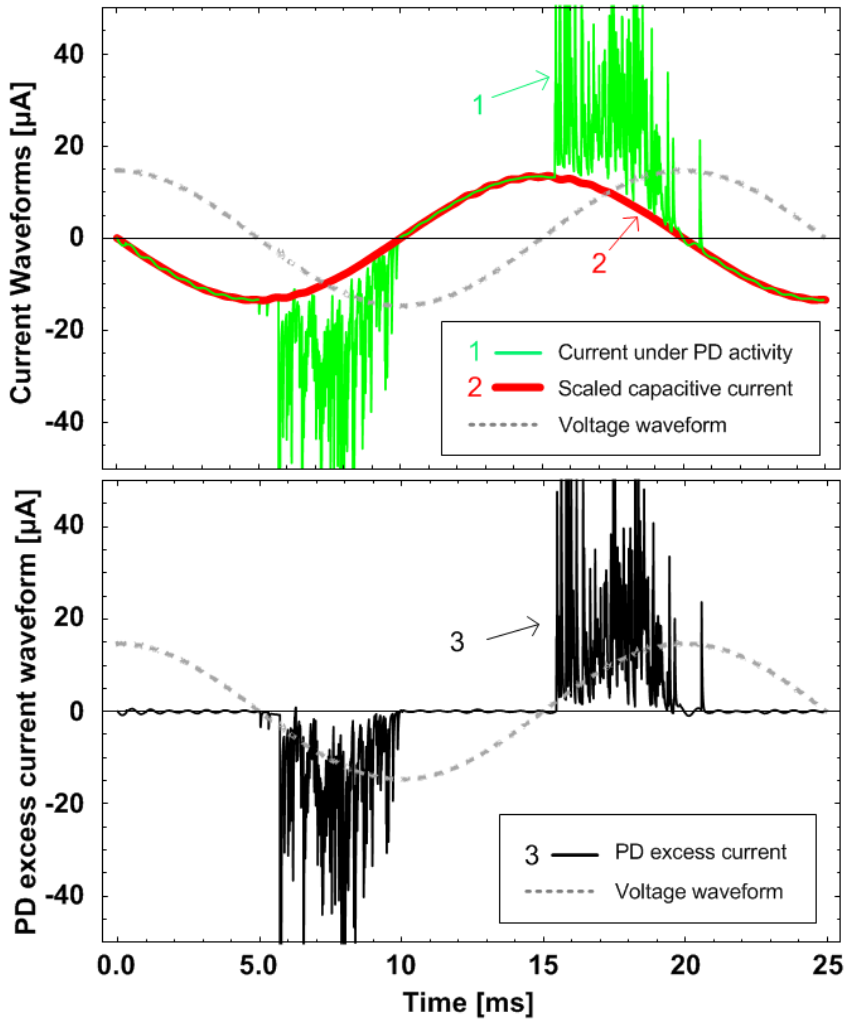

Figure 3.3. Two current signals directly sampled at 2.6 and 1.5 kV; the total current under PD activity and the estimated capacitive current obtained at a voltage below PDIV and scaled with the voltage ratio. The shape of the applied voltage waveform is also shown for a reference. PDIV is about 1.6 kV. Due to large peaks in the measured PD current signal, only parts of the currents are shown to provide a good resolution.

contribution will be observed as undesired additional noise. To reduce the noise generated, a series connected front resistor can be used to slow down the fast fronts. The front resistor choice should consider the sampling rate and the capacitance of the test object. This is discussed further in section 3.2.2.

To further illustrate the PD excess current measurement, the two current waveforms acquired during the measurements below and above PDIV are plotted in Figure 3.3 (recorded from a twisted pair test object). The waveform obtained below PDIV is scaled with the voltage amplitude ratio to estimate the capacitive part of the one that is measured under PD. The excess current is then obtained by subtracting the capacitive current from the total current. The waveforms presented in Figure 3.3 are directly obtained time domain signals, which require a very stable voltage source. Further, an average PD activity can usually not be deduced from a measurement during only one period, as in some cases there can only be one PD event in a few periods. An alternative solution is to average and reconstruct the waveforms via the frequency domain transformation, Figure 3.4 illustrates the frequency domain processed current waveforms based on the same acquisition as the signals shown in Figure 3.3 however the waveforms shown represent an average over 200 periods. The differences between the two figures indicate that individual PDs strongly influence the time domain signal even for a twisted pair object with many PDs per cycle.

If a study of PD activity over a long period of time is desired, the information on excess current behavior can further be condensed by integrating the reconstructed current waveforms over half a cycle. This provides a possibility to evaluate the development of total PD activity over time. To facilitate such studies, the measurement and calculation process requires a minimum time of 2 s between measurements in the used system.

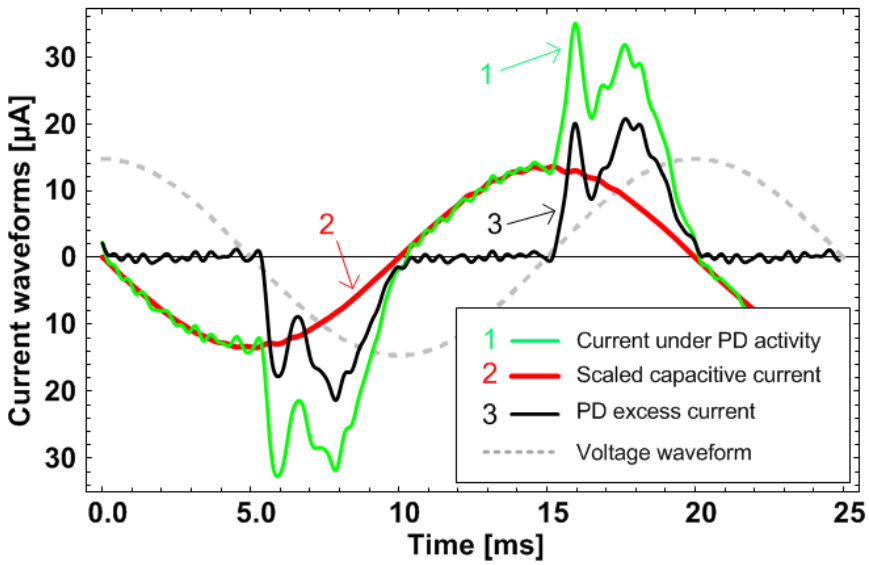

Figure 3.4. Two current signals reconstructed via a frequency domain transform; total current under PD activity and estimated capacitive current. The difference between the two waveforms is the excess current.

3.2 Measurement circuit optimization

In this section, optimization of both the current sensing shunt and the front resistor are discussed in details.

3.2.1 Current shunt

Except for converting a current signal into a measureable voltage signal, the role of the current shunt in this application is to enable the fast current pulses from PDs to be properly integrated by sampling at a relatively slow rate. The conservation of charges caused by PD activities is achieved via a current shunt built of a capacitor in parallel with a resistor. The integral of the shunt voltage will namely always reflect the total charge, no matter how fast it is deposited. The advantage of this solution is that the fast discharge current pulses are stored in the capacitor and discharge via the resistor within a sufficient time constant for the data acquisition to capture the event. Parameters of the shunt components also need to be matched with the impedance of test object, ratio of the voltage divider as well as harmonic content of the voltage waveform for achieving suitable amplitudes of signals in respect to the noise level. Fulfilment of these criteria yields an improved resolution of the DAQ. However, with the high precision of AWIS technique, a very accurate determination of the shunt parameters is not critical anymore; precision within a few digits is fully acceptable as the shunt only influence the current magnitude, not the proportion of excess current, see equation (3.1).

To measure the charge of fast discharge pulses with a limited sampling rate, a current shunt with rather long time constant is desired. A longer time constant will, however, result in lower amplitudes and thus a lower signal to noise ratio. Figure 3.5 presents how the estimated error in a single PD pulse integration depends on the shunt's time

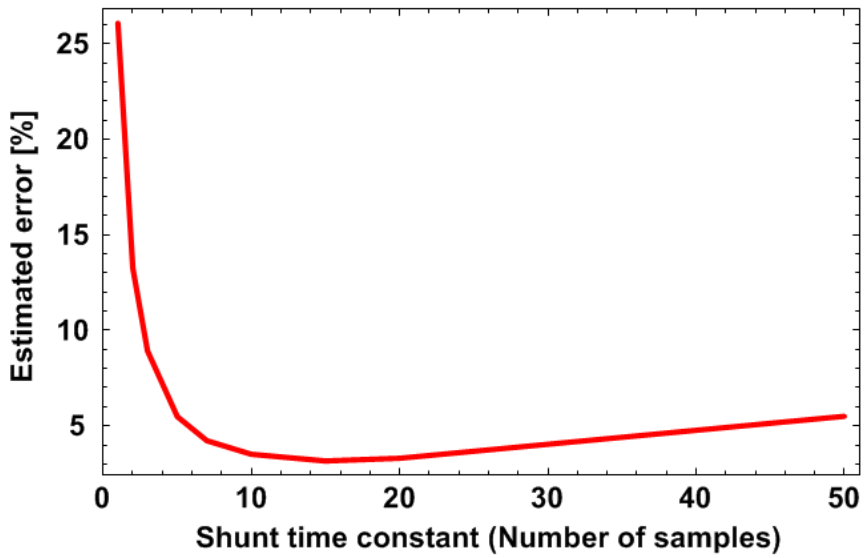

Figure 3.5. Dependence of estimated maximal error in a single PD pulse current integration on the shunt time constant represented by number of samples, a constant noise level of 0.01 is assumed for a single PD pulse.

constant; the latter being represented by the number of samples. It can be observed that the lowest error (~3 %) is obtained if 10 to 20 samples are acquired per single PD pulse. As in a typical measurement performed in this work over 200 voltage periods are analysed in one sequence, only a negligible error is introduced into the final result as the integration error is randomly distributed.

For one of the here used DAQ card, 400 kS/s is the maximum sampling rate per channel and the time constant of the current shunt should then be about 40 μs or 16 samples. This is the criterion for selecting the shunt capacitance once the resistance is defined. In addition, the time constant defines the time resolution of the PD excess current, a shorter time constant provides more details of the PD distribution over time.

The amplitude of the measured signals is another factor in the shunt optimization as it strongly affects the accuracy of data acquisition. For the applied voltage signal, the voltage divider defines the measurement range. The same sensing range as for the responding current signal is in general desired for a good resolution and less crosstalk. As the setup aims to measure PD activity, with current pulses appearing around the peak of the capacitive current, a higher sensing range is therefore required. The amplitude of a discharge pulse depends on PD apparent charge and shunt capacitor and can thus easily be estimated if the expected PD magnitude is known. However, a sensing range of about a few times the capacitive current is considered adequate in most cases and it can further be optimized from additional tests.

For frequencies lower than 25 kHz (cut-off frequency of a shunt with a 40 μs time constant), the shunt impedance is mainly determined by the shunt resistance R_{sh}. To exemplify the shunt selection process, two test voltage waveforms and one test object are employed. One of the voltage is a 50 Hz sinusoidal wave and the other one is a 105.7 Hz semi-square wave. The used test object is a twisted pair with capacitance C_t of 10 pF. The shunt resistance R_{sh} is thus determined from:

$$R_{sh} \approx Z_{sh} = \frac{1}{2\pi f C_t(\alpha k - 1)} \approx \frac{1}{2\pi f C_t \alpha k} \tag{3.2}$$

where α is a safety margin, estimated from the peak ratio of the total and capacitive currents; k is the ratio of the voltage divider.

A pre-testing is however desired, as generally the PD amplitude is not known. For waveforms with one dominating frequency, such as 50 Hz sinusoidal, it is relatively easy to select the shunt resistor. Usually α in the range of $2 \sim 5$ is a good initial value as the waveform resolution is not strongly affected by such a small range extension. As illustrated in Figure 3.6, PDs occur close to the capacitive current peak and are about twice as large as the peak capacitive current, therefore, $\alpha = 3$ is chosen. By using equation (3.2), the shunt resistance becomes 53 kΩ. A 50 kΩ resistor is thus selected. The shunt capacitor is defined by the time constant and a 120 pF capacitor is suitable.

To select a shunt for testing under voltage waveforms without any clearly dominating frequency in its harmonic spectrum, finding the shunt parameters becomes more complicated. For testing under semi-square wave waveforms, the frequency obtained from the inverse of the rise time can be used to define the shunt resistance. For the case illustrated in Figure 3.7, with about 0.25 ms rise time, the dominating frequency is thus 4 kHz. Further, as PDs often occur after the capacitive current has peaked, the

sensing range can be defined by the capacitive current ($\alpha = 1$). The shunt resistor value calculated based on equation (3.2) is 1989 Ω. Similarly to the previous case, a 2 kΩ resistor and a 3.3 nF capacitor are chosen. The peak amplitudes should thereafter be checked for the optimal sensing range and the procedure repeated until a satisfactory result is achieved.

To better illustrate the responses of the selected current shunts for testing under different voltage waveforms as well as under PD events, the respective frequency responses of the shunts are plotted in Figure 3.8 and their impulse responses in Figure

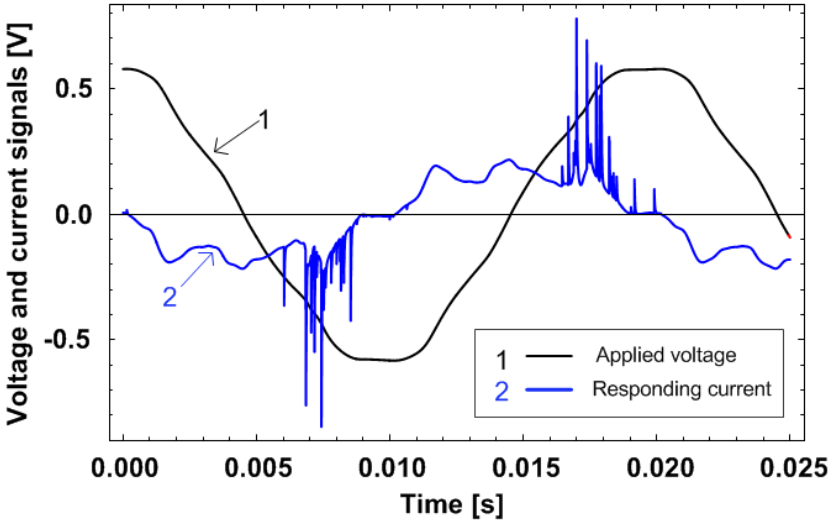

Figure 3.6. Sampled voltage and current signals of a twisted pair object under 50 Hz sinusoidal waveform with a 50 kΩ // 120 pF current shunt.

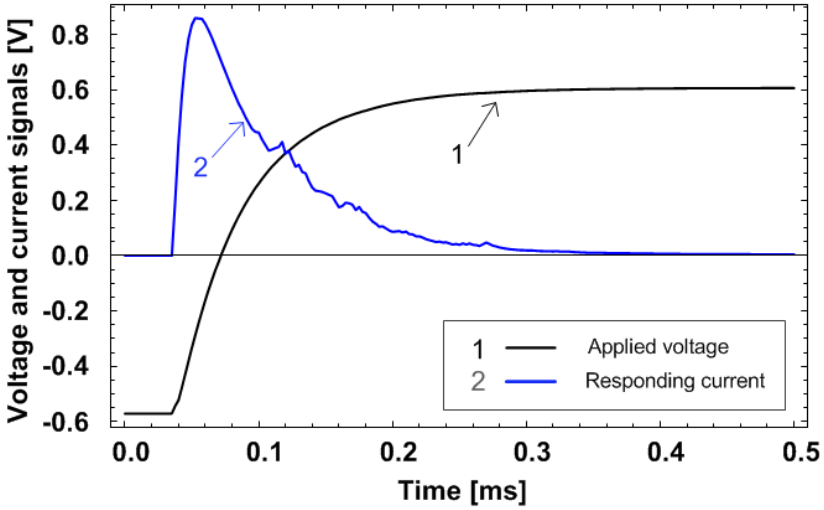

Figure 3.7. Sampled voltage and current signals of a twisted pair object under 105.7 Hz semi-square wave voltage with a 2 kΩ // 3.3 nF current shunt.

3.9. The frequency responses has the same cut-off frequency of 25 kHz, allowing for a proper noise attenuation, but different impedances for good amplitude matching of voltage signal in the DAQ. The impulse responses of the shunts, shown in Figure 3.9, are used to exemplify the responses to a PD event. In the figure, the shunts step responses show a 40 µs decay, which allows 16 data points to be measured with a sampling rate of 400 kS/s.

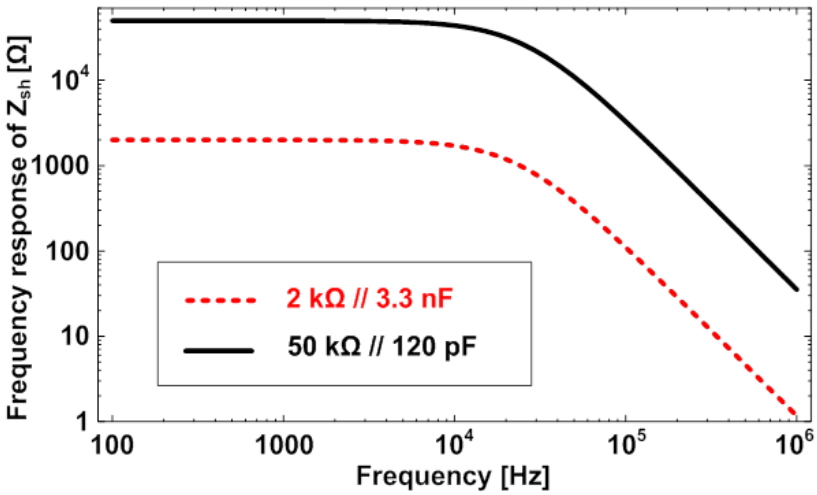

Figure 3.8. Frequency response of the tested current shunts. The cut-off frequencies of the shunts are at about 25 kHz to match the sampling rate of 400 kS/s.

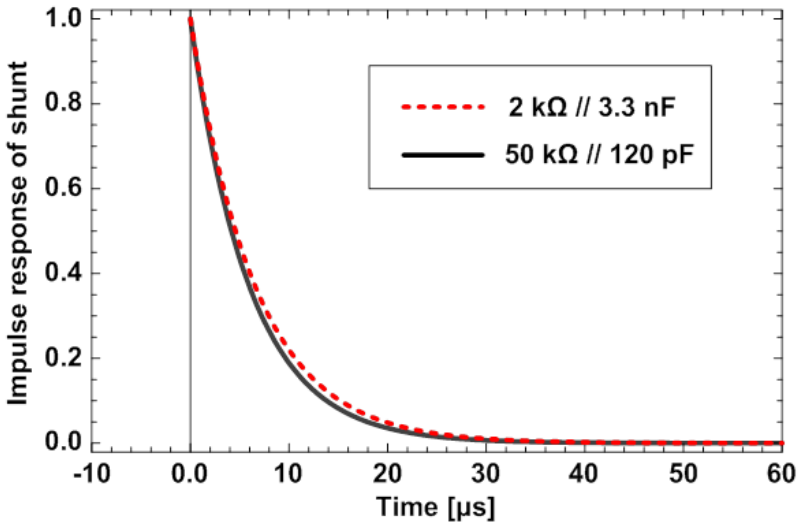

Figure 3.9. Impulse responses of the tested current shunts. The desired time constant for both shunts is about 40 µs and thus 16 samples describe the shape at the used sampling rate (400 kS/s). The peak amplitudes of both shunts are normalized in this figure.

3.2.2 Front resistor

The noise level is of central importance in PD excess current measurements as the current contribution from PD activity often shares only a small portion of the total current measured. To significantly resolve the PD excess current, the noise level needs to be kept as low as possible. A high noise level would otherwise severely reduce the signal resolution or even make the measurements impossible.

A change in noise level has been noticed when performing the PD excess current measurements with the AWIS technique. As shown in Figure 3.10, the noise level in the excess current measured at the voltage below PDIV, without PD, is nearly 3 ~ 5 time lower than the noise level observed during PD activity. To understand the appearance of the increased noise level, simultaneously detected PD events by the pulse PD detection method, accumulated from 23 cycles, are also plotted for a reference. It becomes evident that the increase of noise level does not only appear at the times where PD events are detected but in the entire reconstructed trace.

A trace of the current directly sampled around a voltage polarity shift is plotted in Figure 3.11. It shows that a PD event is registered as a pulse of a very short rise time with relatively longer tail time. The long tail time is a desired effect of the current shunt used. The charge transfer from the test object to the shunt capacitor still remains too fast and therefore difficult to be captured with a limited sampling rate. The fast signal fronts together with the stochastic nature of PD events introduce the observed higher signal noise when converted via frequency domain.

The noise level of the current under PD activity can be reduced by slowing down the fast front of the observed PD pulses. This can be achieved by introducing a front resistor (R_f) between the test object and the current shunt as shown in Figure 3.12.

The value of the front resistor is determined by desired front time of PD pulses, the

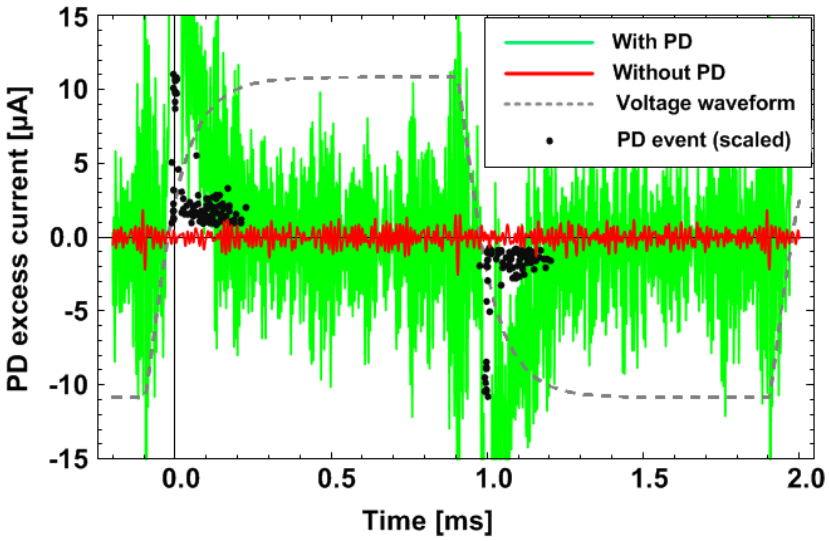

Figure 3.10. Two reconstructed excess current waveforms from a twisted pair test object. One with PD activity, measured at 2.3 kV, the other one without PD, measured at 1.55 kV. PDIV is about 1.6 kV. The PD events detected by pulse PD detection are accumulated from

time needed for charge transfer between the two capacitors. As the capacitance of the used shunt is often several times larger than that of the test objects, the front time is mainly determined by the test object capacitance and the front resistor. The front resistor is an additional component in the circuit. It reduces the voltage amplitude applied to the test object and delays the recorded PD current pulse. Therefore, a low value of the front resistor is advantageous and can be roughly estimated as:

$$R_f \approx \frac{\tau_f}{C_{to}} \tag{3.3}$$

where τ_f represents the desired front time of PD pulses. To ensure a proper sampling of the rising front, at least two data point should be sampled. This determines the shortest acceptable front time and the smallest value of the front resistor. With a rise time of two sampling time intervals, the cut-off frequency is around the Nyquist

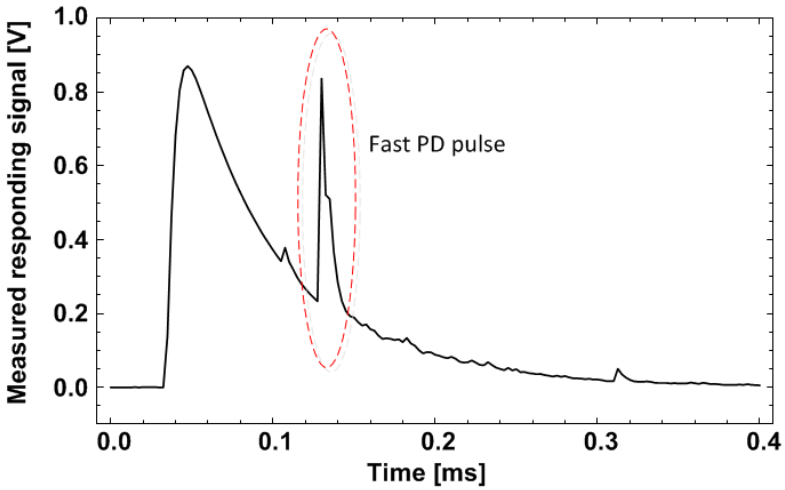

Figure 3.11. Trace of a sampled current signal around the polarity shift, measured at 2.3 kV, being a part of the signal used to calculate the excess current shown in Figure 3.10.

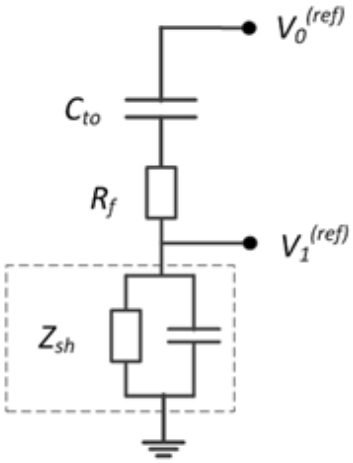

Figure 3.12. Basic circuit of PD excess current measurement with the front resistor R_f.

frequency [69], above which aliasing will occur that may interfere with the lower frequencies used for excess current calculations.

For sampling rate of 400 kS/s the desired front time, used to select a front resistor, is about 5 μs. In addition, the test objects are often characterized by low capacitance, less than 100 pF. For a test object of 100 pF, the front resistor used in this study is selected to be 50 kΩ. Ideal PD responses, with and without the front resistor, are illustrated in Figure 3.13.

To additionally demonstrate the effect of front resistor, the frequency spectra of currents measured with and without R_f, are plotted in Figure 3.14. As seen from the figure, both high order harmonics and the noise level are substantially reduced by implementing R_f. The PD excess current waveforms that are recreated from the spectra are plotted in Figure 3.15, which clearly indicates that R_f has reduced the noise by over 10 times and is of importance for enabling sensitive studies of the PD excess current. Even though the figure shows a delay and a reduction in the current peak in the case of measurement with R_f, the charge integrated over a half period remain the same for both measurements (7.20 nC). The absolute peak value of the excess current is not of interest in these measurements as long as the peak is resolved within the DAQ resolution. As the delay of the peak is due to the front time constant, this will influence the time resolution of the obtained excess current waveforms. With the applied voltage of 500 Hz, the delay time is about 0.5% of a half period for the used sampling rate (400 kS/s). If a better time resolution is needed, it is necessary to increase the sampling rate of DAQ.

The front resistor also influences the voltage level on the test objects. For a test object impedance of a few MΩ, the front resistor shares about 10 V of the total voltage of 2 kV. Considering the resolution required for the conventional PD measurements and the stability of the voltage source, a few percent uncertainties are considered as good

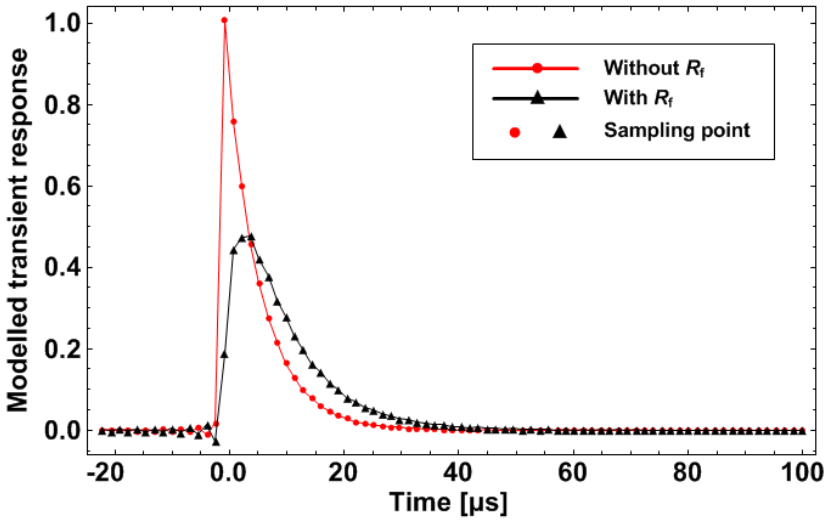

Figure 3.13. Modelled impulse responses of circuits with and without front resistor R_f. By introducing the front resistor R_f, the sharp signal front is delayed by about 5 μs, which allows for sampling 2 data points. The tail time remains the same, 40 μs, for both the cases.

accuracy. This influence can therefore be disregarded.

The front resistor was however not implemented in all the measurement circuits used, particularly in the beginning of the study. Initially the achieved resolution of the excess current measured by frequency domain reconstruction was considered well enough for comparing it with the distribution of detected PD events. In the later studies, for observing additional behaviour of excess current, much higher resolution was needed and the front resistor became necessary. Detailed information on the circuit parameters are defined for each specific test object and listed in section 4.1.

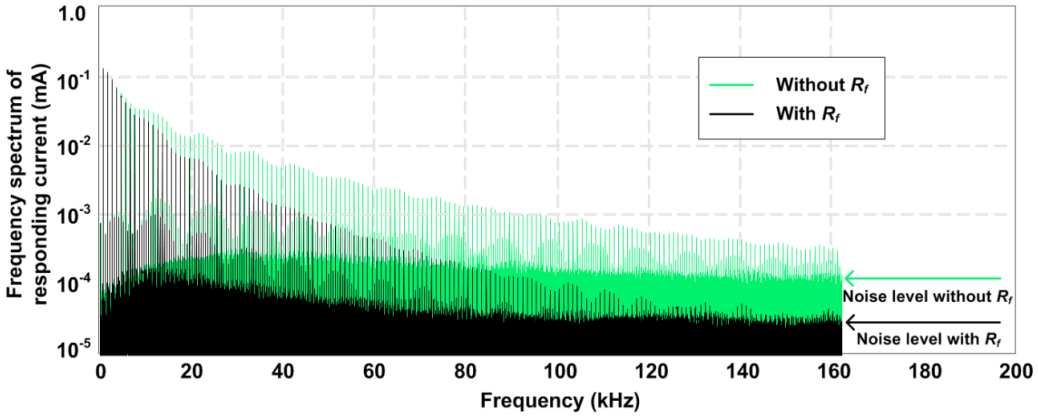

Figure 3.14. Frequency spectrum of two responding currents under PD activity with and without a 50 kΩ front resistor from a twisted-pair test object. The used current shunt is 1 kΩ // 3.3 nF, and the applied voltage is a 500 Hz semi-square wave voltage of 2.3 kV $V_{p\text{-}p}$. PDIV is about 1.6 kV.

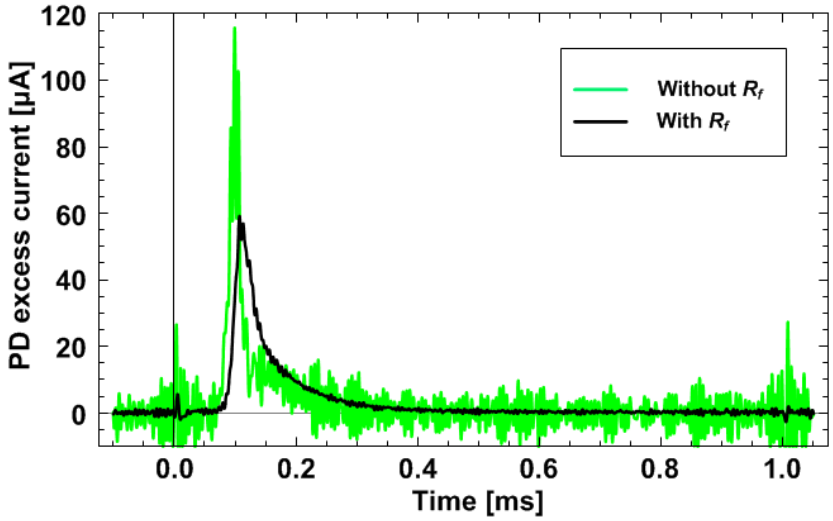

Figure 3.15. Two recreated PD excess current waveforms, with and without R_f from the frequency spectra shown in Figure 3.14.

3.3 Time and frequency domain analyses

The PD excess current can be resolved either in the time or in the frequency domain. Both have their advantages and disadvantages depending on applied voltage deficiencies. For an ideally stable test voltage waveform, both approaches should perform equally well. Common to both approaches is that a time-domain wave shape reflecting the average current during one period should be constructed. To obtain the one-period average, many periods need to be recorded and analysed. It is clear when analysing Figures 3.3, 3.6, 3.7 and 3.11 above that the single period analysis is much affected by individual PD events.

In this section, the principle of the time domain solution is introduced first and is followed with a discussion of how the excess current is reconstructed via the frequency domain. The latter method is adapted in this study. Finally, two examples of waveform deficiencies that influence the choice of time or frequency domain analysis are discussed.

3.3.1 Time domain approach

The technical challenge of time domain processing is to find and extract single periods from a long recording. If the test frequency and the sample rate are exactly known and the period corresponds to an integer number of samples, this becomes a trivial task. However, the frequency generation and the sampling are generally controlled by different clocks; the difference in clock rates may thus introduce severe errors in the extraction of the last periods of a long record. This problem becomes even worse if the test voltage comes directly the power mains. If the frequency is only known within about 1 %; the zero crossings may be 10 % off already after 10 periods. A more precise method to extract the single periods is thus desired.

One possible approach is to first identify the approximate position of each period, extract them with some margin and align them in time to one sample accuracy. As the current signal may be strongly varying with voltage and PD activity, the identification and alignment should preferably be performed using the applied voltage signal. The corresponding responding current signals can then be averaged for each sample in a period to form the desired total current. This is similar to the approach presented in [6] to properly assign PD events to the voltage steps of a PWM waveform, which has steps of varying length.

Thus a time domain analysis seems fully feasible but has not been tested as it requires relatively extensive software development and testing. The alignment procedure conceivably requires a substantial computational effort and, depending on the chosen algorithm, it may become more computationally intensive than a frequency domain reconstruction. Certain advantages are however clear; a time domain approach will not suffer from the noise increase discussed in the previous section.

3.3.2 Frequency domain approach

An alternative approach allowing for determining the PD excess current is to first perform a measurement in the time domain for many periods of a repetitive voltage signal, then use FFT to convert the signal into the frequency domain and extract its complex harmonic amplitudes v_i for each of the harmonic frequencies f_i. The reconstructed voltage waveform $V_R(t)$ can thereafter be obtained from the extracted harmonics as follows:

$$V_R(t) = Re\left[\sum_{harmonics} v_i \, e^{j\,2\pi f_i\,t}\right] \tag{3.4}$$

The main advantage of this approach is that averaging over many signal periods is achieved and the capacitive current can be calculated using impedance spectroscopy technique. Thus the reference capacitive current is defined from the test object impedance, a complex function of frequency, as in equation 3.1. In this case a very stable voltage shape is not required as moderate changes in harmonic content are accounted for. However, the base frequency must be relatively stable as the harmonics frequencies from the actual and the reference measurements need to match.

A further advantage of this approach is that it is simple to correct for frequency dependent sensor transfer functions, just like in dielectric spectroscopy. The harmonic amplitudes v_i are then divided by the measured or derived transfer function value at the harmonic frequency f_i. This is applied to correct for the properties of the voltage divider, whereas the responding current is defined through the shunt resistor value. To perform a similar correction in the time domain, a convolution or, equivalently, two Fourier transformations would be required, and all simplicity with that approach would be lost.

Though the frequency domain analysis offers an improved stability, presentation of the results in the time domain is still required. The time resolution of the reconstruction in equation (3.4) is defined by the number of harmonics used. In principle, the more harmonics, the better resolution. On the other hand, due to the interference from aliasing, too high harmonic content may degrade the result. To reduce this interference one can use harmonic limited waveforms as the testing voltage. A simpler approach is, however, to leave a certain range of free spectrum for attenuation of the high-frequency content down to the noise level. The latter solution is a good option for on-line testing but requires a much higher sampling rate.

As discussed in section 3.2, fast discharges will be integrated and converted into signals below the cut-off frequency of the shunt. However, due to the limited attenuation of the passive filter, some information will remain, extending the harmonic range by $3 \sim 4$ times of the cut-off frequency, depending on the noise level. Figure 3.16 presents three reconstructed current signals, all based on the same measured data, but using different harmonic contents of 50, 100 and 800 harmonics. The original signal was generated by a 105.7 Hz semi-square wave voltage with PD activity and the cut-off frequency of the current shunt was about 25 kHz. The three different harmonic contents cover the frequency spectra up to around 5 kHz, 10 kHz and 82 kHz, respectively.

A clear indication of the accuracy of the reconstructed signal is the ringing effect seen in Figure 3.16, which is an unwanted oscillation of a signal, particularly in the step

response. The cause of the ringing is the Gibbs phenomenon [70], where the Fourier series of a piecewise continuously differentiable periodic function oscillates at a jump discontinuity. With 800 harmonics the ringing effect nearly disappears from the step response at zero seconds, in contrast to the other two waveforms.

Apart from the ringing effect, the time resolution of the reconstructed waveform is another factor that affects the accuracy. Figure 3.17 shows three calculated PD excess current waveforms from the three current waveforms shown in Figure 3.16, the time resolution for using 800 harmonics is about 20 μs, whereas the other two waveforms have much lower time resolutions. Therefore, to obtain the best time resolution, the

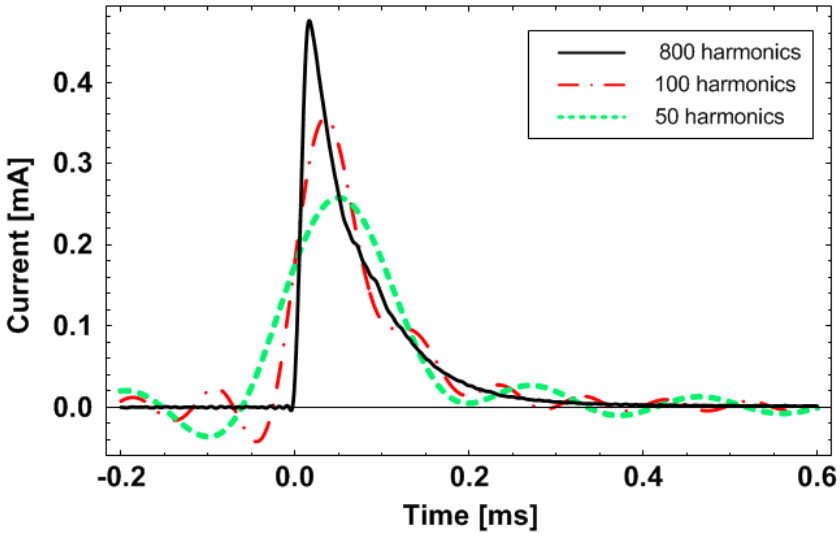

Figure 3.16. Reconstructed total current waveform generated by a semi-square wave voltage, using 50, 100 and 800 harmonics of the same signal.

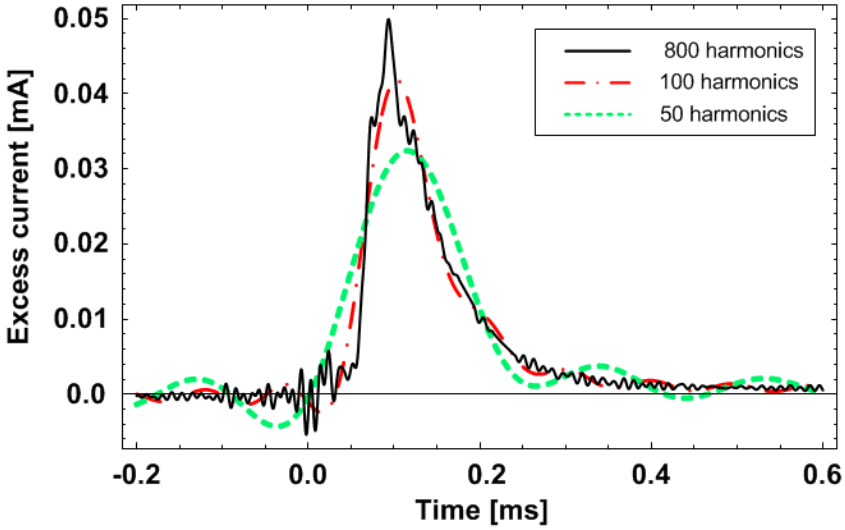

Figure 3.17. Illustration of the different time resolution of PD excess current waveforms calculated from three current waveforms shown in Figure 3.16.

used harmonics content should be 3 ∼ 4 times the shunt cut-off frequency. If the demand on time resolution is less, fewer harmonics are needed. For example, to obtain the total charge during a half period, already the first few harmonics provide a satisfactory estimate.

With a total available frequency spectrum up to 200 kHz (sampling rate of 400 kS/s), four times the shunt cut-off frequency covers half of the frequency spectrum. The other half of the frequency spectrum provides an extensive free spectrum for attenuation of the aliased high frequency components down to the noise level.

3.3.3 Choice between time and frequency domain

The time and frequency domain approaches are, in principle, equivalent but characterized by some subtle differences arising from the used calculation procedures. Thus, it is partly a matter of free choice which of the approaches that is to be preferred. It has been found, however, that certain voltage waveform instabilities imply that one is to be preferred over the other.

A case when the frequency domain approach has advantage is when the harmonic content of the test voltage is not stable, such as when it is taken from power mains. In this case the wave shapes used during the reference and the PD containing measurements may differ so much that it becomes difficult to extract the excess current with the time domain approach, as illustrated by the following example.

Figure 3.18 compares PD excess currents obtained by the time and frequency domain approaches using the power mains waveform. The time domain approach is here simulated by scaling the recorded non-PD current (with applied voltage below PDIV) with the ratio of the voltage magnitudes. As the voltage waveforms are not perfectly stable in shape, the PD excess current is not well resolved. In sharp contrast, the same PD excess current determined from the frequency domain approach provides a much better resolution as the influence of each harmonic is accounted for in the frequency dependent impedance, Z_{to} in equation (3.1). Thus, the capacitive current is precisely estimated even though the voltage waveform slightly varies. The simultaneously performed PD pulse measurement, shown in Figure 3.19, confirms that discharges only occur when indicated by the frequency domain approach. Thus, the current pulses from the time domain approach in the time ranges 0 ∼ 4 ms and 10 ∼ 15 ms seen in Figure 3.18 are not associated with PD activity, they rather are considered as a consequence of the slight variations in the voltage waveform.

As a counter example, the frequency domain approach may not be optimal if voltage waveform periods are not of the same length. Such waveforms may be generated by sources utilizing high voltage switches and are a cause of an increased noise in the measured signal if the sampling rate is high enough. This is exemplified in Figure 3.20 which shows the spectra from two recordings, made directly after each other with the sampling rate of 8 MS/s. Voltage signal 2 in the figure shows a low noise level of about 10^{-5} V as the switch happened to be stable during this recording. In contrast, voltage signal 1, showing a noise in the $10^{-4} \sim 10^{-3}$ V range, exemplifies the response as the jitter of the switch was more severe, about 2 ∼ 3 μs. Here, a time domain approach may be favourable as the cutting and aligning procedure should be able to correct for this deficiency. However, for a low sampling rate that cannot resolve the

jitter, a frequency domain approach can still be a good solution in terms of the calculation efficiency as well as being able to handle an unstable voltage shape.

In this thesis, only the frequency domain solution was implemented in the calculation of the PD excess current. In addition, the used sampling rate is low enough to not affect the measured signals by the switch jitter.

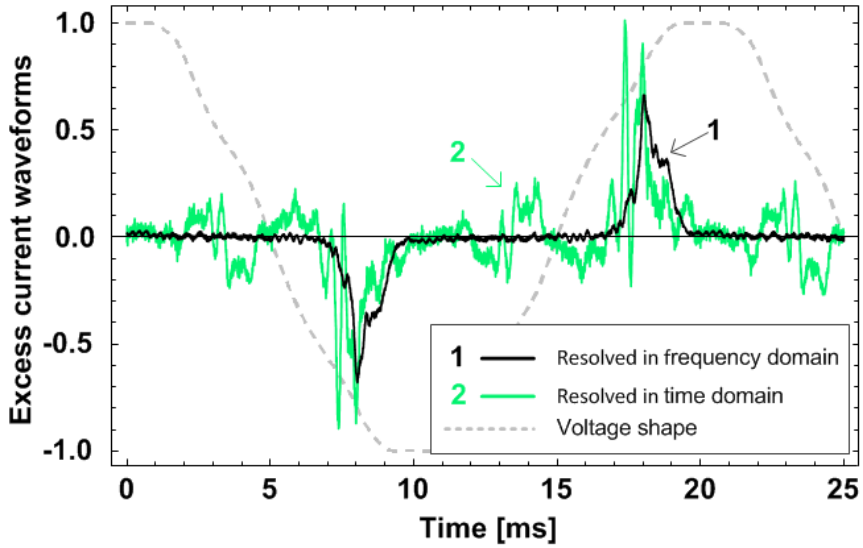

Figure 3.18. PD excess currents derived from the same measurement by the frequency and time domain approaches. The voltage source is an ordinary 50 Hz power mains supply. Both voltage and current waveforms are normalized for a better comparison.

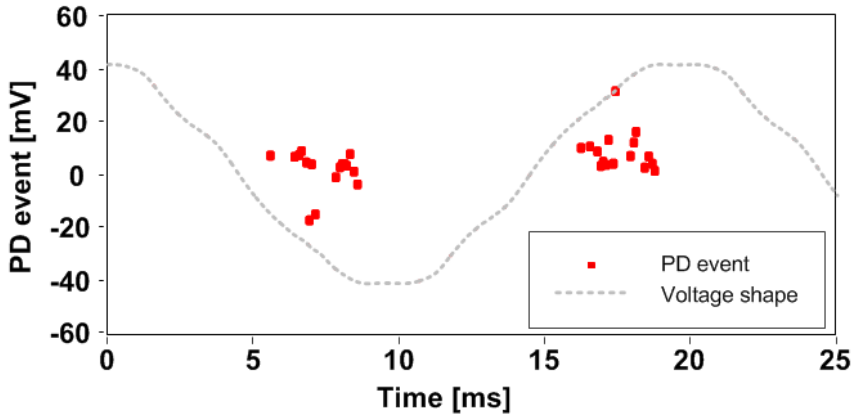

Figure 3.19. Amplitudes and phase position of PD events measured simultaneously to the signals presented in Figure 3.18 by pulse PD detection method. Note that position of PD events coincide with the current peaks in time intervals 5 ~ 19 ms and 15 ~ 20 ms.

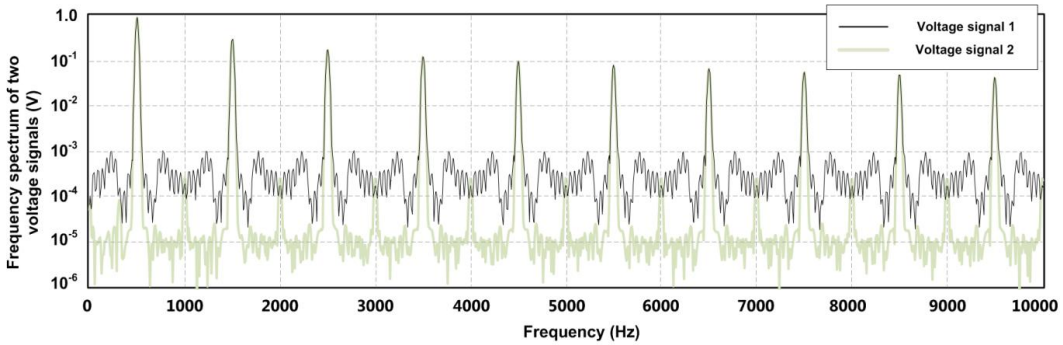

Figure 3.20. Spectra from two sequential measurements with semi-square wave source. The used sample rate is 8 MS/s, which is high enough for the switch jitter to influence the frequency analysis.

3.4 Error analysis and feasibility

The accuracy and resolution of PD excess current measurement is degraded by the uncertainties arising from the stability and accuracy of components used in the measurement circuit. This effect can be quantified by analysing the error sources as well as their propagation. Degradation of the test object during the measurements may also introduce some additional uncertainties, as the measurements will not be fully repeatable. However, as this is a characteristic of the measured object, such an uncertainty is not considered in the standard error analysis.

According to equation (3.1), three error sources can be identified. The first one relates to the shunt impedance (absolute error and drift error); the second error is brought up by the voltage sensing DAQ card, which is present in all the measured voltage signals; the third error appears due to the drift of the voltage divider Δk. As the PD excess current is obtained by subtraction of the capacitive current from the total current, uncertainties in each current are addressed separately to simplify the analysis.

For evaluating the uncertainty of the measured total current, $\Delta(I_{tot})$, the divider drift is not considered as only two error sources are involved:

$$\Delta(I_{tot}) = I_{tot}[\frac{\Delta(Z_{sh})}{Z_{sh}} + \frac{\Delta(V)}{V}] \tag{3.5}$$

Moreover, to further simplify the analysis, the drift of the Z_{sh} is neglected as well, as only one measurement is performed. Further, if the offset of Z_{sh} can be calibrated to 0, $\Delta(I_{tot})$ only contains the measurement noise.

The error in the capacitive current $\Delta(I_{cap})$ measurement can roughly be calculated as:

$$\Delta(I_{cap}) = I_{cap}[\frac{\Delta(Z_{sh})}{Z_{sh}} + \frac{\Delta(k)}{k} + \sqrt{n}\frac{\Delta(V)}{V}] \tag{3.6}$$

Further, the drift in both Z_{sh} and k need to be considered in contrast to that in the total current measurement, as the capacitive current determination uses two measurements

at different times. It creates a possibility for the drift. Note that *n* is the number of measured voltages, 2 in this case.

With these independent error estimates, the resulting error in PD excess current is calculated as:

$$\Delta(I_{exc}) = |\Delta(I_{tot})| + \left|\Delta\left(I_{cap}\right)\right| \tag{3.7}$$

As exemplified in Figures 3.21 and 3.22 for continuous measurement during about 2000 seconds, the drift and noise in the applied voltage are respectively 0.1 % and 0.02 %; the drift and noise of the voltage obtained from Z_{sh} become 0.03 % and 0.005 %. Using the highest uncertainties observed, the maximum error in the PD excess current measurement is estimated to about 0.2 %.

In the above presented considerations, the influence of the absolute value of the Z_{sh} has been neglected which causes some systematic error in determination of the PD excess current amplitude. The accuracy requirement in PD studies is, however, generally quite low, in the range of 10 % or more.

Even though the general accuracy requirements on PD pulse detection are quite low, this error analysis also provides information on the feasibility of PD excess current measurements. To be significantly detectable, the PD excess current must be larger than its estimated error. This imposes a limitation on test object capacitance; with a large capacitance it may be impossible to resolve the PD excess current with sufficient sensitivity. If one considers, as an example, a 10 pF test object at 1 kV and 50 Hz, which gives a capacitive current of 3 µA. With 0.1 % accuracy, the smallest observable PD excess current is about 3 nA, which corresponds to 60 pC/period. Compared to pulse PD detection, this detection limit is quite high and it increases with test object capacitance, applied voltage and frequency. Thus PD excess current measurements may only be feasible for test objects characterised by a low capacitance.

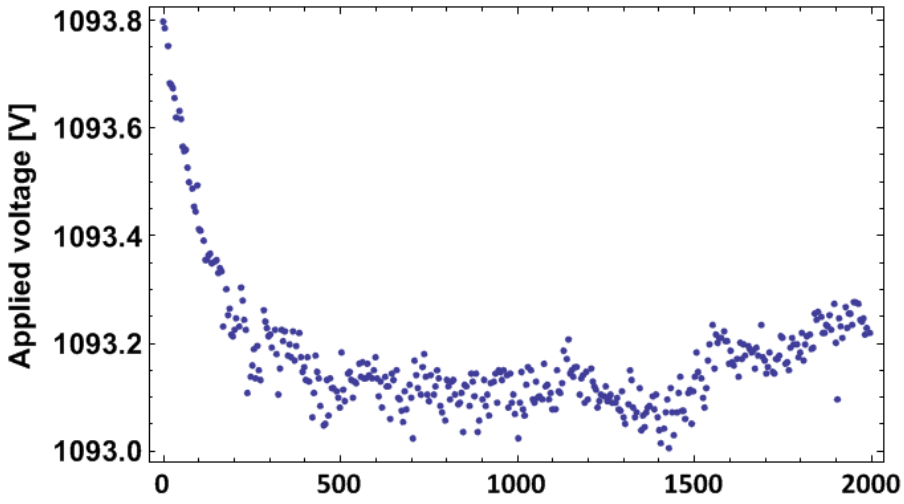

Figure 3.21. Measured applied voltage during 2000 seconds, illustrating voltage divider drift and noise.

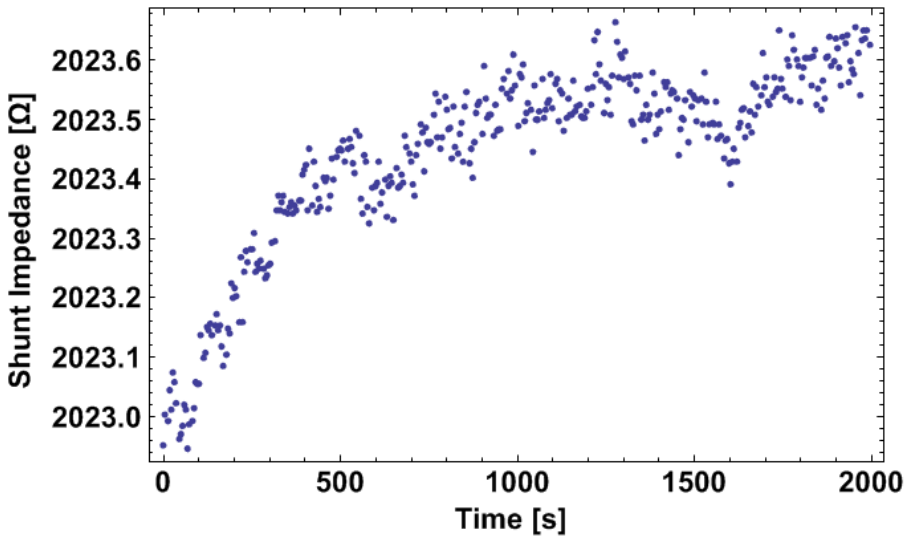

Figure 3.22. Illustration of the current shunt drift and noise during 2000 seconds.

3.5 Stochastic PD detection

As indicated earlier, for verifying the PD excess current measurement approach, a conventional pulse counting PD detection system, known as stochastic PD detection [6], is simultaneously employed in this thesis.

Detection of PD pulses with excitation at power frequency is well defined in standards [19] and available with many commercial instruments. However, the standard measurement technique is not well suited for investigations of PD activity under semi-square wave voltage waveforms, characterized by large controllable derivatives of their fronts followed by periods of constant amplitudes. Such voltages are employed in this study as they are often utilized in power electronic applications and, in the authors view, are more informative than sinusoidal waveforms. Thus, special detection techniques need to be applied and we adopt here the approach presented in [6], stochastic PD detection, which differs from the standard technique in two ways. Firstly, PDs are detected by a comparison to a floating average of the acquired signals; therefore the detection circuit does not need to fully suppress the applied voltage waveform. Secondly, it employs a resonant detection circuit to enhance PD signals with the resonance frequency above 10 MHz. This means that any signals with frequency content below 10 MHz cannot be detected by the pulse PD detection system. The PD magnitude is measured by the peak amplitude, thus several PDs occurring close in time are not summed to a larger value as the largest one will determine the observed magnitude. A more detailed description of the technique can be found in [5, 6].

One limitation of the resonant detection is that the signal amplitude cannot directly be converted into apparent charge by calibrating the system with a standard PD calibrator, as the standard calibrators are often designed for detections below 1 MHz. For some sources and with use of a high precision acquisition card, PD signals may however be detected directly in the applied voltage [5]. Thus, by knowing the capacitance of the test object and that of the coupling capacitor, the charge decrease caused by a PD event can directly be calculated from the observed voltage drop. Examples of such voltage drops are shown in Figure 3.23. The average PD calibration constant obtained from 100 similar events were used to convert the measured PD voltage drop to the apparent charge, as the PD current pulse presents a transient oscillation with the peak to peak values proportional to the apparent charge. A conversion factor of 350±50 pC/V was found for the applied measuring system. It may be of value to mention here that a conventional calibrator (designed for use below 1 MHz) indicated a factor that deviated more than ten times from this value.

For comparison to the excess current measurements, which provides the excess current waveform as well as integration of this waveform during a half cycle, the amplitude of the PDs that occur within one half period are summed to obtain an average PD current. A number of cycles need to be analyzed to obtain a reasonably detailed phase distribution of the pulse PD current. For a twisted pair test object, as there are often many PDs per half period, this number can be relatively low, for example 10 cycles. For other test objects, having typically one PD per half period, more cycles need to be analyzed. Figure 3.24 shows PD obtained from a twisted pair object over 57 positive half cycles. These PD events can further be converted into a PD current with consideration of pulse amplitude and calibration factor.

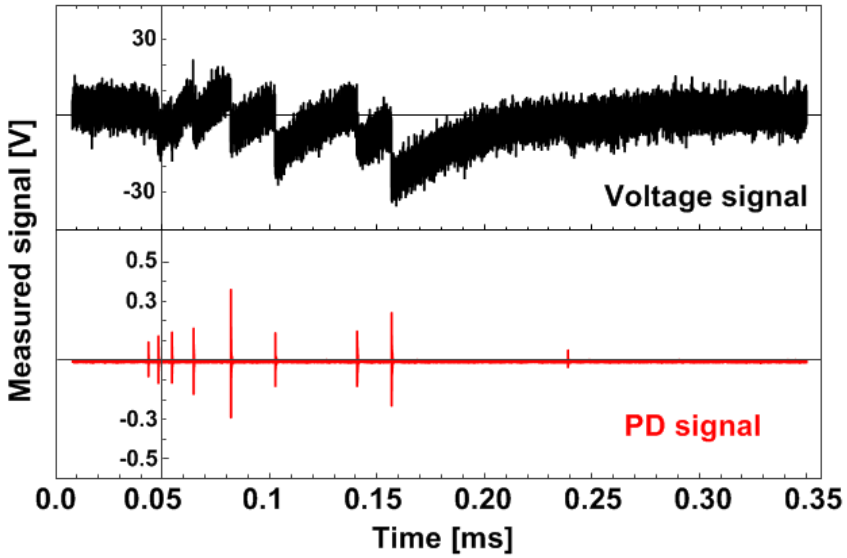

Figure 3.23. Signals used for conversion of pulse PD amplitudes into charge obtained during PD detection in a needle-plate test object at 6.5 kV. The used coupling capacitor was a 50 pF gas insulated capacitor. The voltage signal shows the difference between one voltage recording and the average of all voltage recordings where the fast dips indicate presence of PDs, as confirmed by the signal from the pulse PD detection circuit.

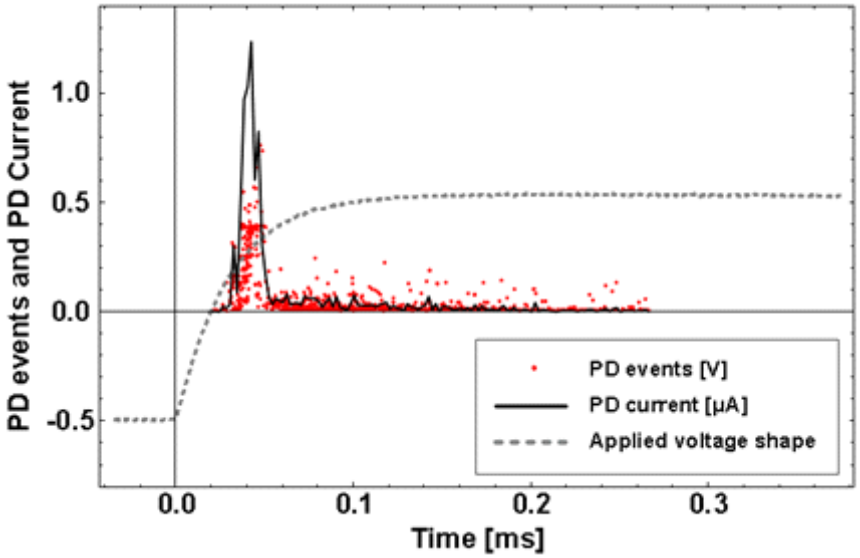

Figure 3.24. PD events measured by stochastic PD detection method on a twisted pair object subject to 500 Hz, 2.7 kV semi-square voltage waveform. The PD events are accumulated during 57 positive half cycle traces. The curve “PD current” is calculated according to equation (3.8).

The principle of the conversion PD pulses into a PD time dependent current is by averaging the charges that are displaced by PD events within small time intervals of one period. The PD current is calculated as the summed PD charge that occurred within the time step (Δt) around the time t as:

$$I_{PD}(t) = \frac{\sum q_{PD}}{N\,\Delta t} \qquad if \;\; |t_{PD} - t| \leq \frac{\Delta t}{2} \tag{3.8}$$

Where q_{PD} is the charge from each PD event, this is obtained by applying the calibration factor to the measured PD amplitude and t_{PD} is the time of each measured PD events. N is the total number of cycles that are used to accumulate PD events for averaging. The time step Δt is chosen to maximize the time resolution while perserving a relatively smooth PD current shape. Thus the time step choise is influenced by the number of PDs available for averaging.

4 Experimental setup

In this chapter, three different types of test objects and the two voltage waveforms employed in the PD excess current studies are presented. Further, the full test setup for simultaneous excess current and pulse PD measurements is described in details.

4.1 Test objects

In this section three test objects, needle-plate, twisted pair and cavity are introduced as they are used for demonstrating the feasibility of excess current measurements in later chapters. In addition, the test voltage waveforms, the used current shunts and the front resistors are also listed for each test object as a reference for later experiments.

4.1.1 Needle plate

The needle-plate test specimen, presented in Figure 4.1, is employed to demonstrate corona discharges and is made from two parallel plate electrodes with one needle mounted on the center of the top high voltage electrode. To perform excess current measurements, the bottom low voltage electrode is required for connecting to the current sensing circuit. The needle diameter is 0.7 mm with a tip radius of 50 µm. The distances between the needle tip and the low voltage electrode as well as between the two electrodes are adjustable. In the case of this study, the distance is adjusted to achieve the specimen capacitance of 10 pF.

This specimen is only used as an introductory example to illustrate how the well-known corona discharge properties under sinusoidal voltage appear when studied by the excess current. The used current shunt was a 50 kΩ resistor in parallel with a 120 pF capacitor and no front resistor was added to the circuit.

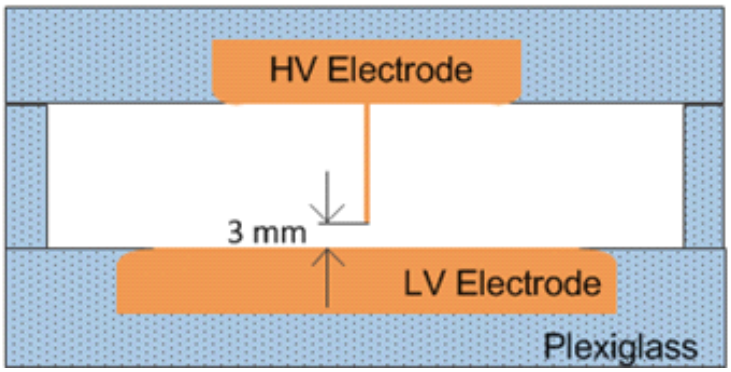

Figure 4.1. Illustration of needle-plate test setup.

4.1.2 Twisted pair

Twisted-pair specimens are made of a standard enamel motor wire winding and prepared according to IEC standard [71]. The enamel layer thickness is about 50 μm and the wire diameter is 1.2 mm, as depicted in Figure 4.2. The specimen is directly connected to the measuring system with one wire to the high voltage source and the other one to the current shunt. To ensure that PDs only appear between the two wires, the end of the wires were covered with semiconducting rubber clots.

Twisted pair specimens were tested under both sinusoidal and semi-square wave voltage waveforms with various frequencies. The table below lists the conditions and circuit parameters used during the experiments presented later.

Voltage waveform	Current shunt	Front resistor	Section
Sinusoidal 50 Hz	50 kΩ // 120 pF	0 Ω*	5.2
Sinusoidal 500 Hz	2 kΩ // 3.3 nF	50 kΩ	7.2
Semi-square 105.7 Hz	2 kΩ // 3.3 nF	0 Ω*	5.3
Semi-square 500 Hz	1 kΩ // 3.3 nF	50 kΩ	6.1.1

* *In the initial excess current measurements, there was no need for a front resistor as the resolution obtained was enough for a comparison to pulse PD results.*

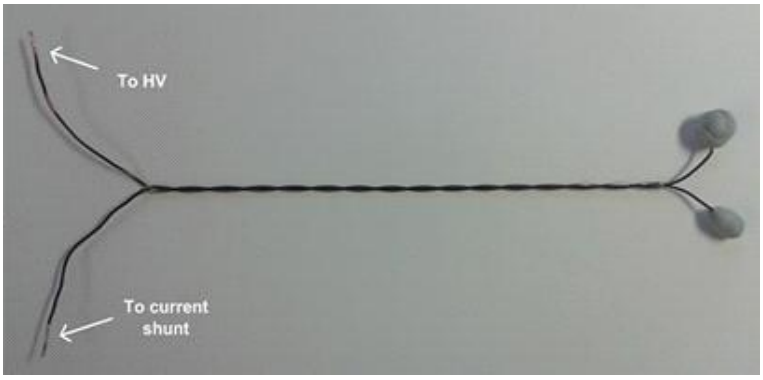

Figure 4.2. Twisted-pair test object used in the measurements.

4.1.3 Cavity

The tested cavity specimens consist of three layers of dielectric sheets with a hole drilled in the middle layer. The detailed dielectric materials information and cavity dimensions are provided in the context of each experiment presentation. To avoid PDs from the electrodes edges, they are embedded in epoxy resin. Figure 4.3 illustrates a cross section of the used electrode system.

The cavity specimens were also tested under various voltage waveforms. The following table shows the parameters of current sensing shunts as well as the values of front resistors used for the testing.

Voltage waveform	Current shunt	Front resistor	Section
Sinusoidal 500 Hz	2 kΩ // 3.3 nF	50 kΩ	6.1.2
Semi-square 500 Hz	1 kΩ // 3.3 nF	50 kΩ	6.2 and 7.4

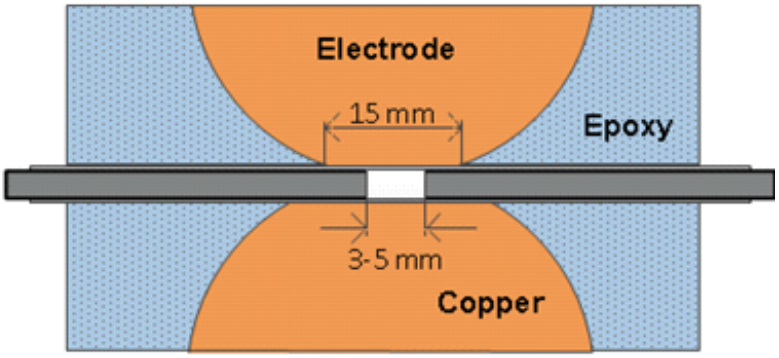

Figure 4.3. Illustration of electrode system used for the cavity specimen.

4.1.4 Test environment

During most measurements, specimens were tested in a closed plastic box to reduce the influence of external environmental conditions and air circulation, in this way securing repeatability and stability of the obtained results.

It was found that the box significantly increased repeatability of measurements. In contrast, measurements with blowing air on the objects were also performed. This is of course only effective in case of twisted pair specimens where the PDs occur in contact with the surrounding air. An air tunnel made out of a polystyrene tube with the possibility of a controllable air blowing from one side with the other side open was utilized, as illustrated in Figure 4.4.

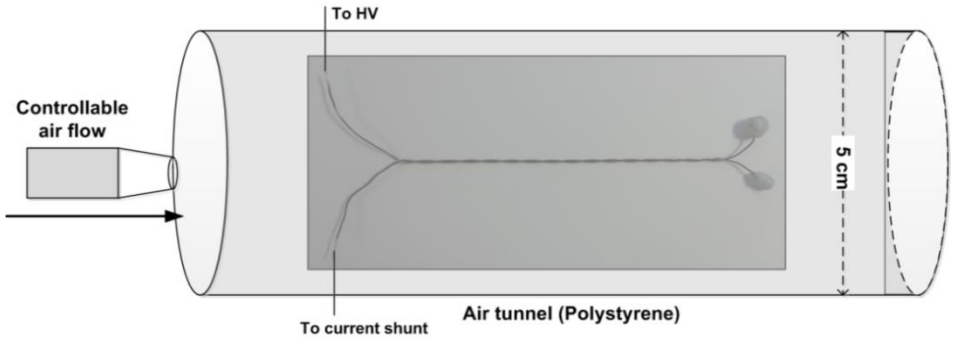

Figure 4.4. Test setup used for twisted-pair specimens to allow a strong air flow during PD activity.

4.2 Test voltage waveforms

To demonstrate the excess current measurements under different voltage waveforms, three different voltage sources were implemented. Two of which were used to generate sinusoidal waveforms of different base frequency and harmonics content by means of a step up transformer. The third one employs high voltage switch circuit to generate semi-square wave voltage of various base frequencies and rise times.

4.2.1 Sinusoidal waveform

To generate high voltage sinusoidal waveform directly from the power mains, two series connected transformers are used to adjust and boost voltage levels as shown in Figure 4.5. The regulating transformer (0～260 V, 1040 VA) fed directly by a power outlet, is used for adjusting the output voltage level. The other one is a voltage transformer, 110 VA, up to 22 kV, with ratio of 1:200.

The voltage waveform obtained from power outlets often contains harmonic distortion. The total harmonic distortion (THD) for the waveforms can be as high as several percent. Figures 4.6 and 4.7 show a trace of a voltage waveform from the power outlet as well as the corresponding frequency spectrum. The use of such a waveform is dictated by the fact that the tested objects are exposed to service-like conditions. Waveforms with high harmonic distortion will not be any issue for testing with the AWIS technique and a varying voltage harmonic contribution can be accommodated via a frequency domain analysis as discussed in section 3.3.3.

The general stability of the test voltage is however important in measurements utilizing a reference determined at another time instant than the actual measurement. The frequency and voltage in the power system is allowed to vary up to the order of a percent or more, making high-precision tests impossible or unreliable.

To generate a stable sinusoidal voltage with adjustable base frequency, another voltage setup was applied. It consists of a function generator (HP 33120A), a power amplifier (Brüel & Kjær, type 2706, 75VA, frequency response 10 Hz to 20 kHz) as well as the voltage transformer (110 VA, up to 22 kV; 1:200). An illustration of the setup is shown in Figure 4.8.

The voltage waveforms generated by function generator and power amplifier solution

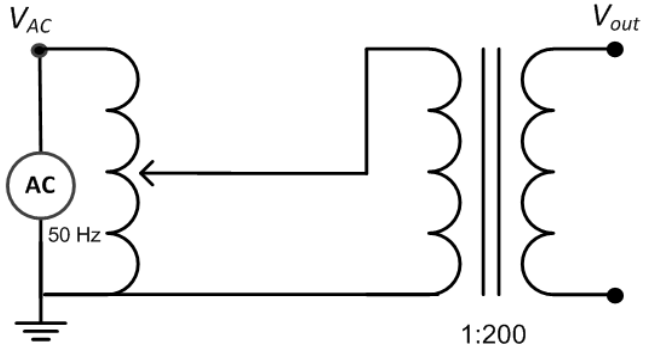

Figure 4.5. Illustration of circuit used for generating high voltage sinusoidal waveform directly from power outlets.

have much lower THD (≈ 0.5%) and can be easily adjusted both in the voltage amplitude as well as the base frequency by meanings of digital control. Further, the waveshape generated is considerably more stable than the waveshape from the power system. This setup is therefore more appropriate for precision tests under repeatable voltage levels and various frequencies.

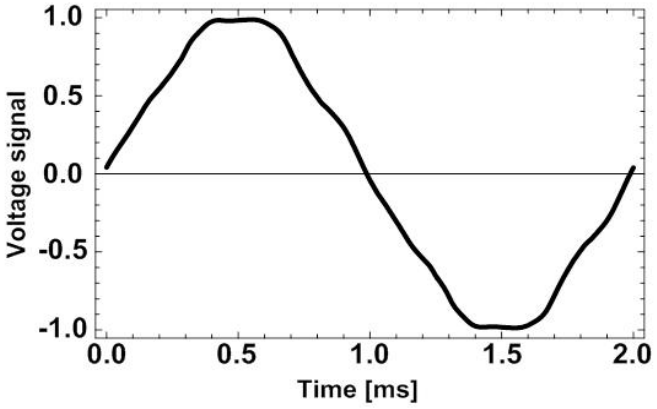

Figure 4.6. Voltage waveform generated from the power outlet.

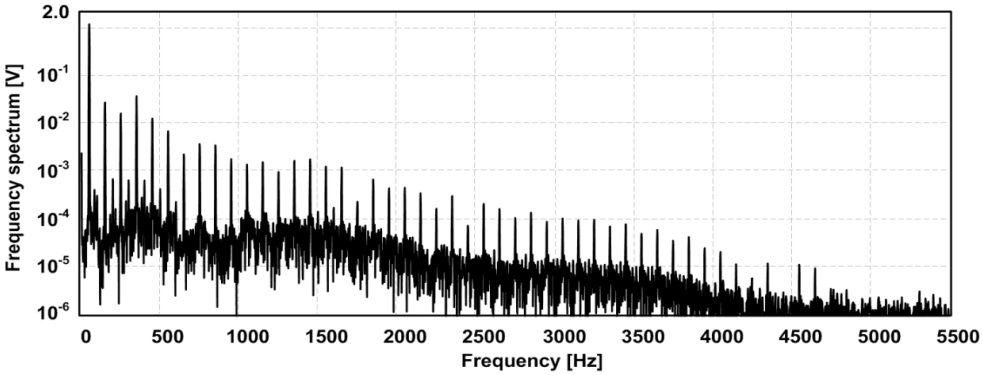

Figure 4.7. Frequency spectrum of the waveform shown in Figure 4.6.

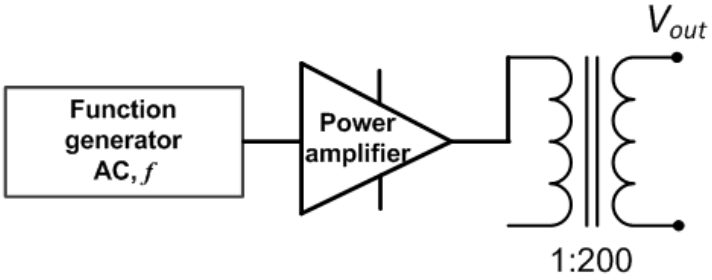

Figure 4.8. Illustration of circuit used for generating sinusoidal voltage waveform with variable frequency.

4.2.2 Semi-square waveform

A semi-square wave bipolar voltage is repetitively varying between positive and negative DC levels as shown in Figure 4.9. Its rise time can be varied independently from the frequency and the capacitive current response is only present at the polarity shifts. Therefore, this wave shape is considered the most suitable for PD excess current studies.

The time required to change voltage polarity is the rise time t_r, which is the measured time between 10% to 90% of the peak to peak voltage change. The frequency of the semi-square wave waveform is defined by the function generator that controls the operation of the high voltage switch.

Figure 4.10 shows the circuit used to generate a semi-square wave bipolar voltage waveform. A Spellman high voltage supply (RMP60N300/220) with modified voltage control was used to ensure repeatable DC supply voltage levels. In addition, the capacitor C_{DC} of 150 nF was employed for stabilizing the DC voltage. The used high voltage transistor switch, Behlke HTS 301-03-GSM, could operate at voltages up to 30 kV with maximum continuous current of 0.33 A. The series resistors R_s (800 Ω) are required for proper function of the switch. A high pass filter C_{HP} and R_{HP} (30 nF, 100 MΩ) is used to create a bipolar voltage. The time constant of the high pass filter was chosen much longer than a switching cycle to allow a constant voltage level during each half cycle. The rise time of the voltage waveform can be adjusted by the resistor R_r. In the presented studies, R_r varied from 0 Ω up to 300 kΩ and provided rise times of 5 µs up to 200 µs, dependent also on the capacitance of the test object. The switching frequency (Max. 2 kHz) of the high voltage switch is controlled by the control signal from a function generator (HP 33120A).

Switch jitter is a factor worth attention when high voltage switches are used. At least in the employed switch, there is about 10 µs delay from a control signal change to the actual switch operation. The jitter appears because this delay is not constant and can vary up to 3 µs. Thus the jitter is not detectable at all if the sample rate is lower than 200 kS/s, for the most commonly used sample rate in this work, 400 kS/s, it is barely visible and induces no observable degradation of the excess current results. At sample rates above 1 MS/s, however, the jitter becomes more and more of a concern, as discussed in section 3.3.3. This applies to both time and frequency domain analysis but it may be possible to accommodate the jitter deficiency more easily in the time domain.

To study waveforms with a fast rise time (< 10 µs), a high sampling rate is required. This is unfortunately not possible with the present frequency domain approach due to the switch jitter. A time domain approach should be more suitable, if all the switch operations are aligned in time.

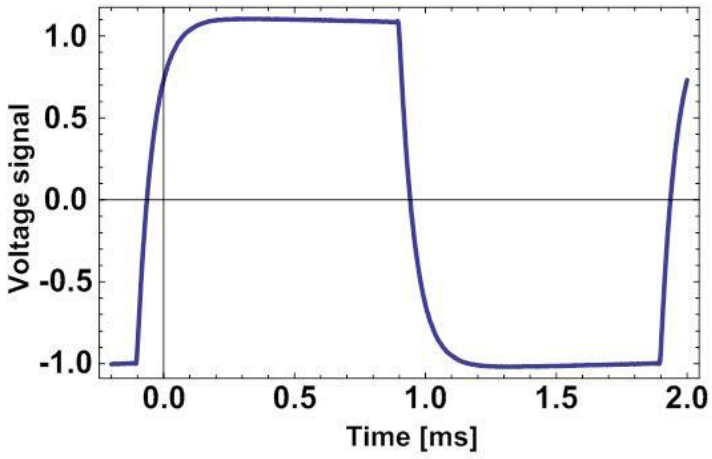

Figure 4.9. Semi-square wave voltage waveform with rise time of 200 μs and 500 Hz base frequency.

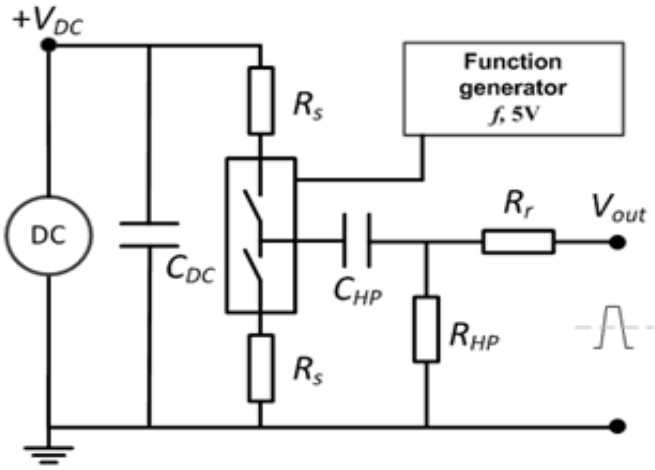

Figure 4.10. Circuit used for generating semi-square wave bipolar voltage waveform.

4.3 Final test setup

The full test setup for simultaneous excess current and pulse PD measurements is illustrated in Figure 4.11. Both the AWIS technique and the stochastic PD detection technique are LabVIEW based and all calculations were performed on the same computer to ensure synchronization of the measurements.

The AWIS technique implemented for the excess current measurements is basically the same as the one used in the dielectric response characterization [15] but with some additional functionality to enable "on-line" reconstruction of the excess current waveforms as well as integration of the waveforms. The "real-time" current waveforms facilitate easy handing of the measurements procedure and monitoring of possible changes. The integration over half cycles condenses the excess current information, which provides an overview of long time measurements of PD activity.

The NI USB-6251 multiplexing DAQ card is used for recording data and only two channels are used for data acquisition, which allows a sampling rate of 400 kS/s for excess current studies.

Crosstalk in electrical measurement is the phenomenon by which a signal in one measurement channel creates an undesired effect in another channel. Crosstalk is usually caused by capacitive or inductive coupling from one channel to another. The AWIS setup is subject to crosstalk interference due to high impedance signal sources [49]. One effective way to reduce the input impedance of the DAQ card is to employ an operational amplifier before the input channel. Therefore, amplifiers (OP42GP) [72] are installed in both input channels of the DAQ card. Apart from reducing the crosstalk, the amplifiers also serve as "safety fuses" for the DAQ card as they are relatively cheap and easy to replace in case of breakdown in the test object. In addition

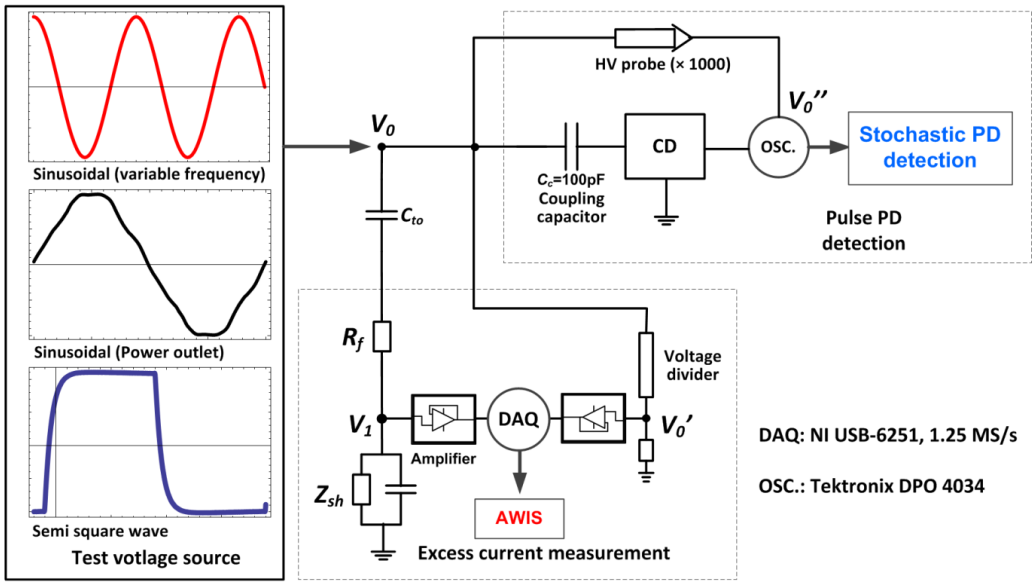

Figure 4.11. Schematic diagram of the experimental setup for simultaneous excess current measurement and pulse PD detection.

to these “fuses”, gas discharge tube arresters with a breakdown surge voltage of 90 V are connected to ground in front of the amplifiers, to further secure the DAQ system. All amplifiers have however a frequency dependent voltage response. This can either be handled by complex polynomial curve fitting [49] or it can be taken into account as a part of the shunt characteristics and normalized by the whole measurement circuit calibration. The bandwidth of the used amplifier is 10 MHz, which is much larger than the sampling rate of the DAQ card.

To generate PDs in the used test objects, the voltage levels required are generally in the range of few kV up to 10 kV. In the excess current measurement, the two measured signals (V_1 and V_0') should preferably be in the same order of amplitude to facilitate the best possible accuracy of the DAQ card. Therefore a resistive high voltage divider that consists of two series connected resistors (100 MΩ and 33 kΩ) was used to measure the applied voltage. As only voltage amplitude ratios are used in the excess current measurements to estimate the capacitive currents by scaling, a precision calibration of the voltage divider is not required. Nevertheless, calibration against a standard high voltage probe, Tektronix P6015A, has been performed, as this facilitates a correction for the frequency response of this divider. The standard high

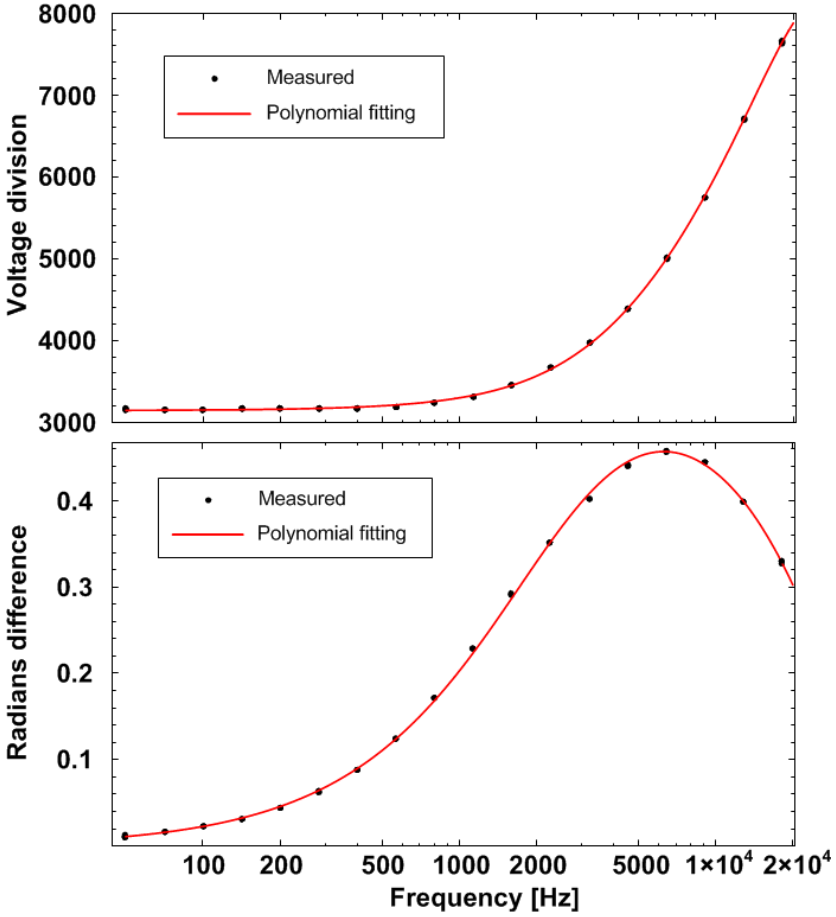

Figure 4.12. The voltage division and the radians difference of the voltage divider determined in comparison to a TEKTRONIX P6015A high voltage probe.

voltage probe is known to have a very constant response up to above 10 MHz. Figure 4.12 show the relative frequency responses of the voltage divider and it is seen that its high frequency characteristics are poor, so poor that the direct signal does not even properly reflect the used voltage rise times.

The poor high frequency response of this divider is however fully acceptable for the excess current measurements as it is mainly used to measure relative amplitudes of the same wave shape. To illustrate the true wave shape from the divider signal, it can be corrected with the measured transfer function shown in Figure 4.12 by Fourier transformation, correction and then reconstruction, as mentioned in section 3.3.2. This is how the reference wave shapes shown in many plots of this thesis are obtained.

In the used pulse PD detection system, signals are recorded by an oscilloscope (Tektronix DPO 4034) with sampling rate of 100 MS/s and a high voltage probe (TEKTRONIX P6015A, 1000x) is used to scale down the applied voltage amplitude. To amplify the pulse PD signals and suppress the low frequencies, a resonant PD decoupler is realized. It consists of a coupling capacitor (C_c), a decoupling circuit (CD), a coaxial cable and the input impedance of the oscilloscope (1 MΩ // 20 pF) as illustrated in Figure 4.11. A detailed discussion of the resonant PD decoupler circuit can be found in [6].

To avoid the noise from any external sources as much as possible, all the connections in the low voltage part are realized via BNC cables and the low voltage components are all shielded within grounded metal boxes. As a result, a noise level of 10^{-5} is reached when the AWIS averaging technique via Fourier analysis of long records is used, as illustrated in Figure 4.13.

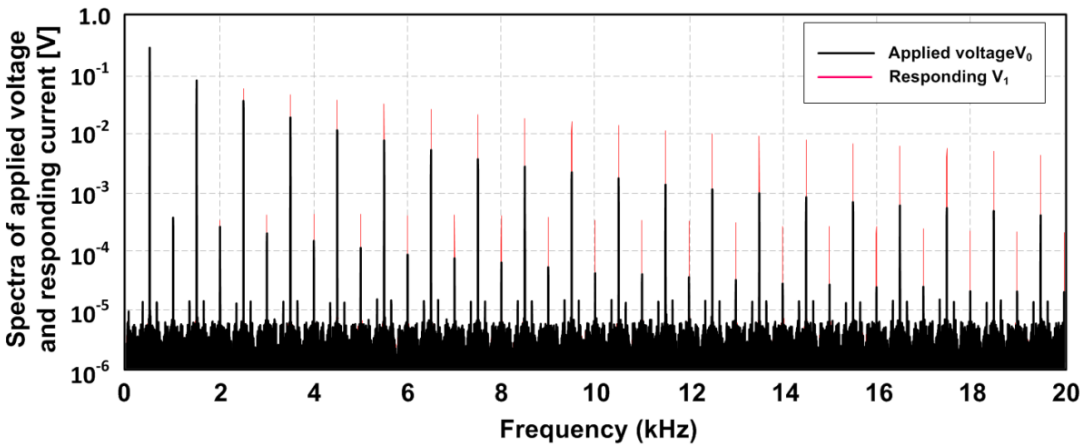

Figure 4.13. Spectra from the two recorded voltage signals, V_0 and V_1, when testing a twisted pair object under a semi-square wave waveform with rise time of 200 μs. The applied voltage is 1.57 kV and 500 Hz. The noise level is generally below 10^{-5} for an object without PD activity. PDIV is about 1.6 kV for this test object.

5 Verification of PD excess current measurement

The PD excess current measurement technique introduced in chapter 3 provides an opportunity to study PD activity by its resulting current. This measurement is independent from the conventional pulse PD measurement, stochastic PD detection, which detects PDs as very fast signals. It is therefore a natural requirement that the excess current measurement is verified against simultaneously performed pulse PD detection.

The verification measurements start with sinusoidal voltage waveforms applied to the needle-plate and twisted pair specimens for illustrating basic correlations between pulse PD and excess current measurements. Semi-square wave voltage waveforms were also employed to demonstrate PD excess current measurement of a twisted pair test object under such voltages.

The word “verification” in the title of this section should be understood in broad terms. As the excess current and the pulse PD measurements provide different results, the issue is rather to understand how PD activity is represented in the two types of measurements. This provides a qualitative verification. A more quantitative verification is obtained by calculating the current implicit from the detected PD pulses and comparing it with the excess current. Both approaches are used here with the aim of elucidating the excess current properties under PD activity.

5.1 Corona discharge

Corona discharges have a well-known non-symmetrical discharge pattern with many discharges of similar amplitudes and with almost fixed time difference appearing in the negative half periods. Only at higher voltages can discharges be observed in the positive half periods. This characteristic pattern is illustrated for three voltage levels in Figure 5.1. To resolve PD excess current from non-symmetrical discharge patterns, it is important to include both even and odd harmonics as well as the DC component if the analysis is performed via the frequency domain. Without even harmonics, the reconstructed current would be forced to be symmetrical for both half periods and a DC component would appear to reflect the integrated asymmetry of the half periods.

The needle-plate test object with 3 mm gap distance as described in section 4.1.1, for which PDIV is about 4.5 kV, was used. Before the PD measurements, one reference measurement was performed at 4 kV to estimate the capacitive current. Figure 5.2 shows three PD excess current waveforms of corona discharges obtained at 4.9, 5.4 and 6.3 kV. With the voltage increase, PD excess current amplitudes in the negative half-period increase. At higher voltage level, discharges also start in the positive half-

period, which well agrees with PD signals obtained from pulse PD detection illustrated in Figure 5.1.

An interesting observation is that the pulse PD amplitudes during the negative half period decrease for the highest applied voltage of 6.3 kV, as seen in Figure 5.1. This is in contrast to the result of PD excess current measurement shown in Figure 5.2, where the current amplitude continues to increase with the voltage. The duration of PD activity at the negative half period, t_1, is the same for both measurements. The explanation of this observation is that with increasing voltage, the density of PDs increases significantly, as shown in Figure 5.3, where three PD signal traces are zoomed in to illustrate the discharge density and amplitudes in a 0.1 ms time frame. Further, one should also notice that each of the PD excess current waveforms shown

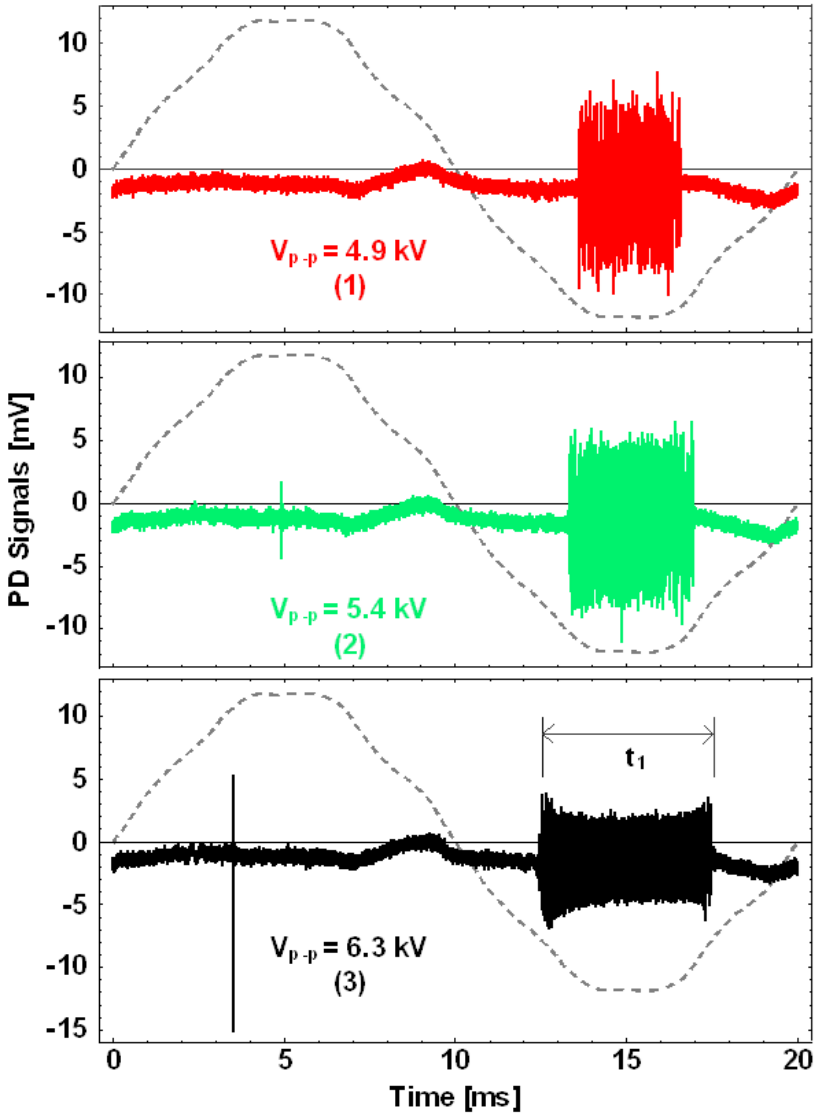

Figure 5.1. PD signal traces of corona discharges from 3 mm gap needle-plate object as measured by pulse PD detection at three different voltage levels.

in Figure 5.2 is an average of a 2 s long measurement, providing an average from about 100 periods. For the pulse PD detection, a statistical study of corona discharge activity is rather difficult as each PD signal trace may contain thousands of discharges. For example, over 2000 PDs are detected in one period at 6.3 kV, which makes it difficult to resolve and account for all individual PD events of over 100 periods.

In the positive half period, some weak discharges are detected at 5.4 kV, whereas they

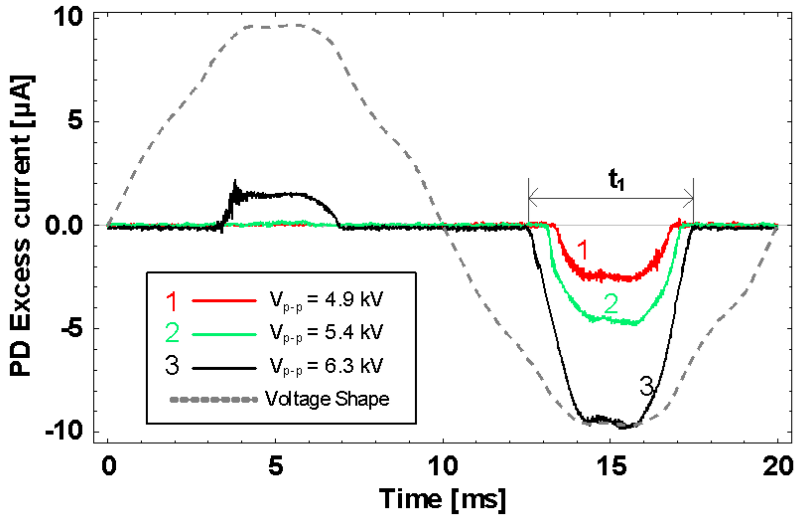

Figure 5.2. PD excess current waveforms of corona discharges from a 3 mm gap needle-plate object acquired simultaneously as the pulse PD traces shown in Figure 5.1. Each waveform is averaged from 100 cycles.

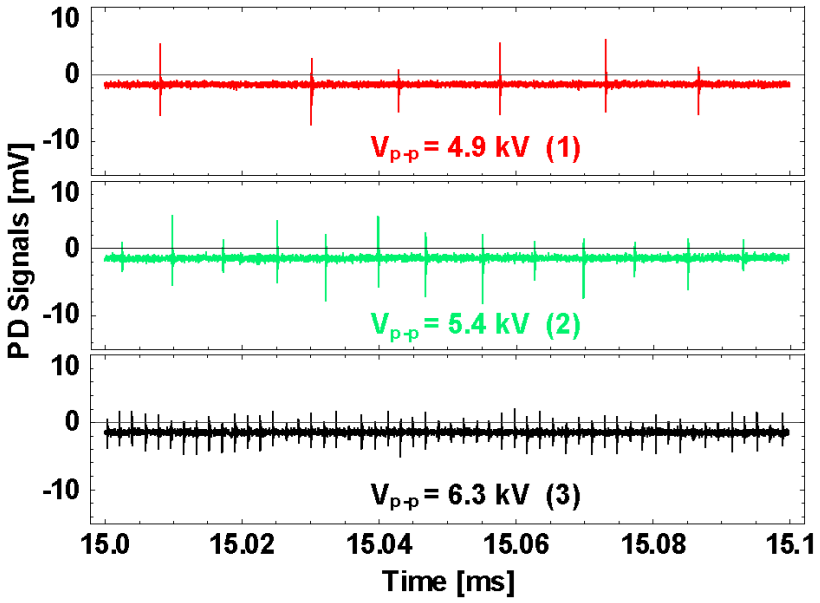

Figure 5.3. The PD signal traces shown in Figure 5.2, shown with a higher time resolution to illustrate the density and amplitudes of the discharge pulses appearing in the negative half cycle.

are hardly noticeable in the excess current, at least in the scale of Figure 5.2. This is because discharges in the positive half period do not occur in every cycle at this voltage level. A closer inspection of the excess current reveals however a positive current around the positive voltage peak as compared to the result from the measurement at 4.9 kV. The positive half period discharges become more frequent and larger at the highest voltage used and this is reflected in the excess current. It is of interest to note that, even though the discharges in the positive half period may be substantially larger than those in the negative one, they are represented by a weaker excess current because they are much fewer.

This example illustrates how a well-known PD source is seen by the excess current measurements. As intended in the design, the excess current accounts for both number and amplitude of discharges and can thus be utilized to evaluate many small against few large ones.

5.2 Twisted pair under sinusoidal voltage

The PD excess current measurement was additionally verified with a symmetrical test object, a twisted pair specimen. Details of the test object and the current shunt are presented in section 4.1.2. The test object was exposed to sinusoidal voltages and the obtained PD excess current waveforms are compared with both distributions of detected PD events as well as PD currents from pulse PD detection. The PD currents were averaged from the detected PD events according to equation (3.8). Similarities and differences in the results are discussed in the following.

Figure 5.4 shows two reconstructed current waveforms, both obtained after energizing by voltage waveforms similar in shape but of different amplitude, below and above the PD inception voltage. To better illustrate the capacitive current part of the total

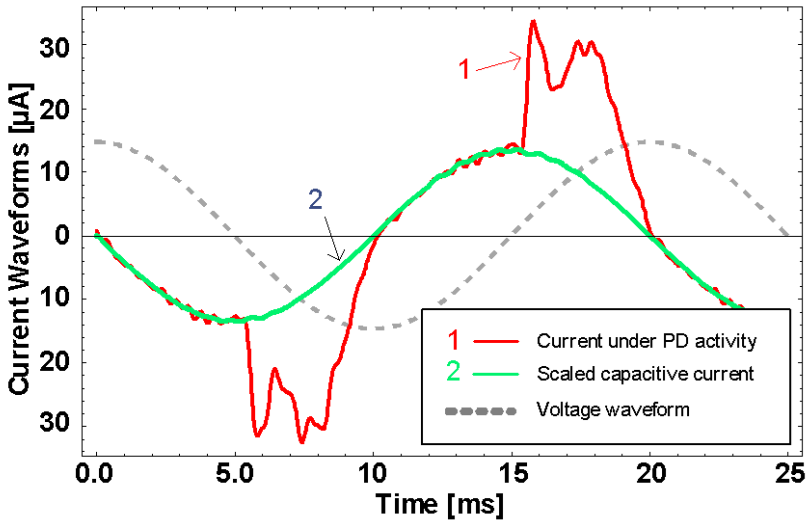

Figure 5.4. Two reconstructed current waveforms under a 50 Hz sinusoidal voltage, (1) is measured under PD activity at 3.1 kV and (2) is measured at voltage 1.5 kV and scaled with the voltage ratio 3.1/1.5. PDIV is about 2 kV.

current measured with PD, the waveform without PD is scaled with the ratio of the two voltage levels. In Figure 5.5, the PD excess current is compared with the distribution of the detected PD events from the pulse PD detection. These PD events were accumulated from 5 continuous cycles. In Figure 5.6, the comparison is also done with the averaged PD current acquired from the pulse PD detection.

In Figure 5.5, the PD excess current for a complete cycle is shown. The detected PD events are also included. The first peaks of both polarities in the signal correspond to appearance of a few but strong PDs. The second peaks result from many but weaker PD pulses. The amplitude of the second peak appears to be even larger than the first

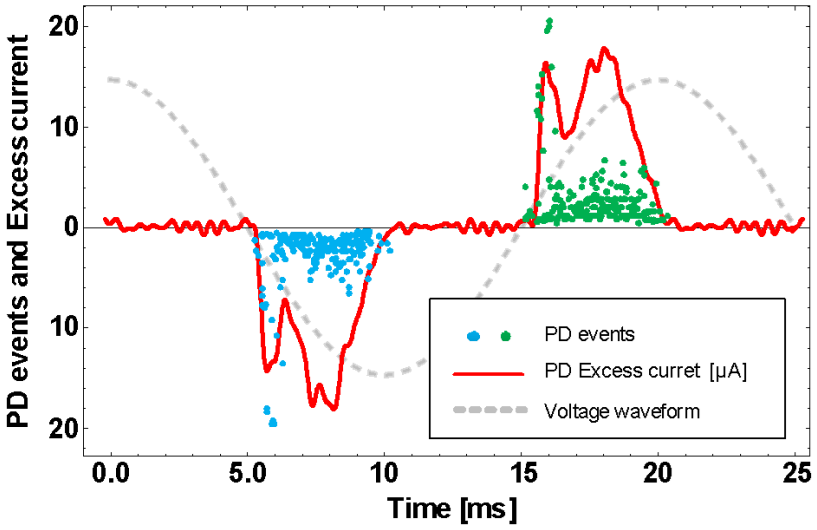

Figure 5.5. PD excess current waveforms extracted from the waveforms shown in Figure 5.4 compared to the simultaneously recorded PD events from pulse PD detection.

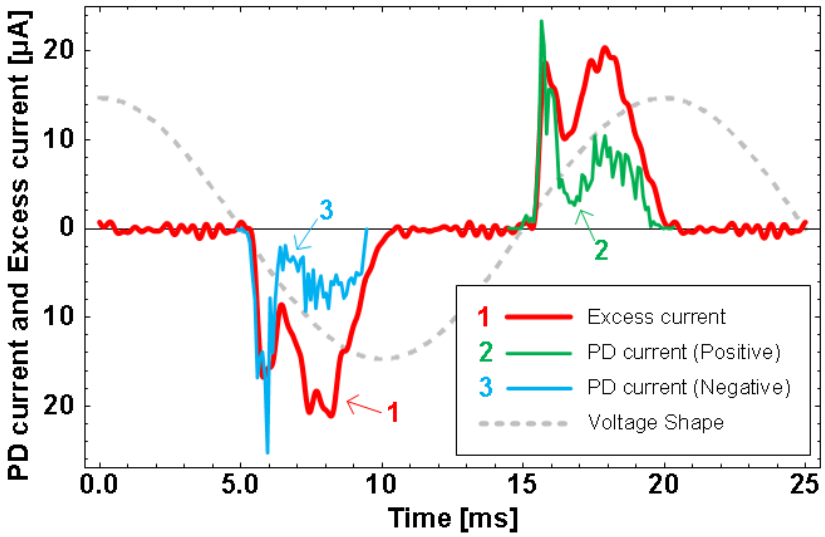

Figure 5.6. PD excess current waveforms extracted from waveforms shown in Figure 5.4 compared with the PD current calculated from the simultaneously detected PD events by equation 3.8.

one as seen in the negative half cycle.

In Figure 5.6 the main difference between the excess current and the PD current is additionally elucidated. At time intervals between 6 ~ 10 ms and 16 ~ 20 ms, the PD excess current amplitude is larger than the averaged PD amplitude. A plausible explanation is that many discharges with amplitudes lower than the PD trigger level are not detected by the pulse PD detection system. Further, PDs may also occur within a short time interval, causing the recorded signals to overlap. These possibilities are supported by the PD trace presented in Figure 5.7, which shows numerous small and possibly overlapping discharges between 2 and 6 ms, whereas the PD excess current measurement integrates and measures all the PDs whatever the amplitude. In contrary, the pulse PD detection system finds only pulses above the trigger threshold. A too low PD trigger level will falsely detect noise and corrupt the result. The trigger level is therefore an important limiting factor in pulse PD detection. In addition, the used stochastic PD detection utilizes a resonant circuit to enhance the PD signals and measures the PD peak amplitude. Therefore several PDs appearing within a short time period, so that their signals are overlapping, will be counted as one PD with the amplitude of the largest. This is in contrast to conventional pulse PD detection techniques where small overlapping PDs are integrated to one larger PD event.

In this example we showed how detected PD pulses can be represented as a current signal and compared with the excess current. It was observed that, due to the trigger threshold required in pulse PD detections, the summed amplitude of all detected PD events cannot properly account for the total discharge current if there appear many small PDs.

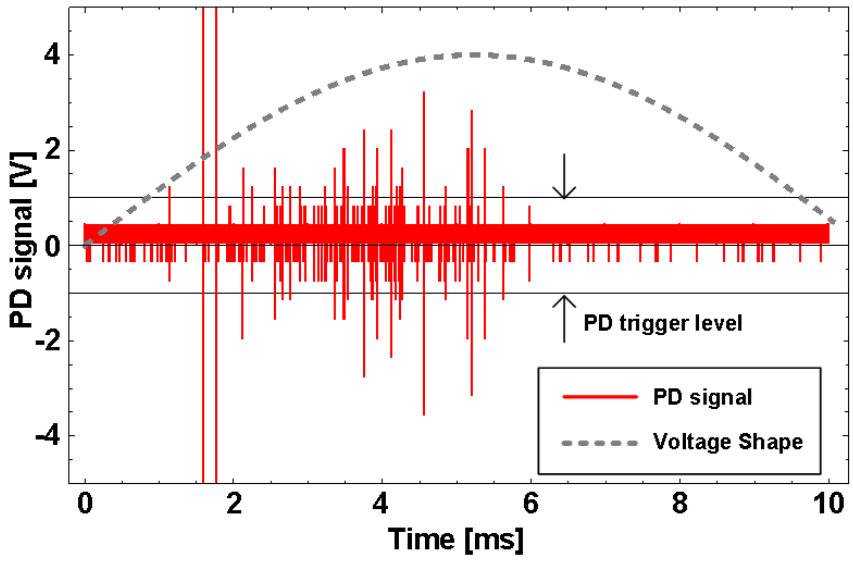

Figure 5.7. One trace of a pulse PD signal, the used PD trigger level is 1 V. Note that some PDs are below the PD trigger level.

5.3 Twisted pair under semi-square wave voltage

To compare PD excess current behaviour under different waveshapes, a semi-square voltage is applied to the same type of test object as above. In addition, several voltage levels are studied.

The twisted pair specimen was measured at different amplitudes of the same semi-square wave shape. The PDIV of this test object is about 1.6 kV. Figure 5.8 presents three PD excess current waveforms obtained at 2123 V, 2241 V and 2430 V peak-to-peak voltage levels of 105.7 Hz. As the twisted pair object is of symmetric

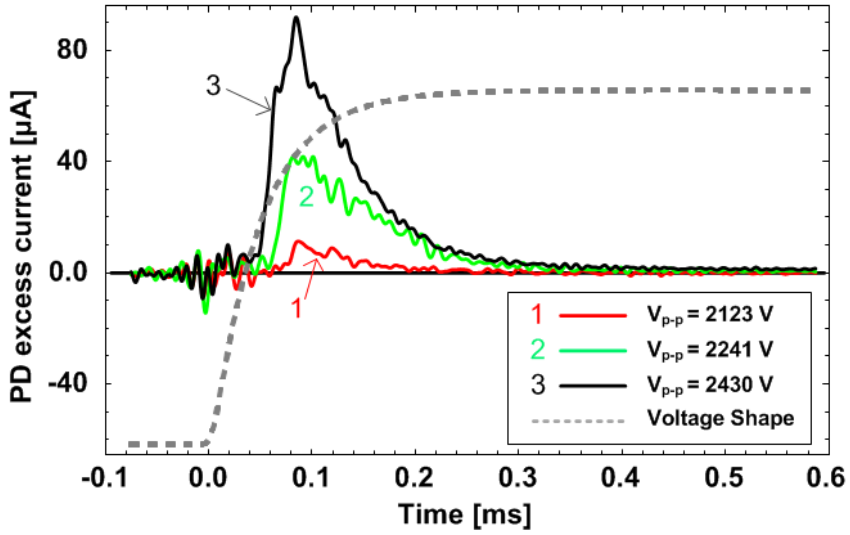

Figure 5.8. PD excess current waveforms measured with 105.7 Hz semi-square wave waveforms of different voltage amplitudes. 800 harmonics are used to reconstruct these waveforms.

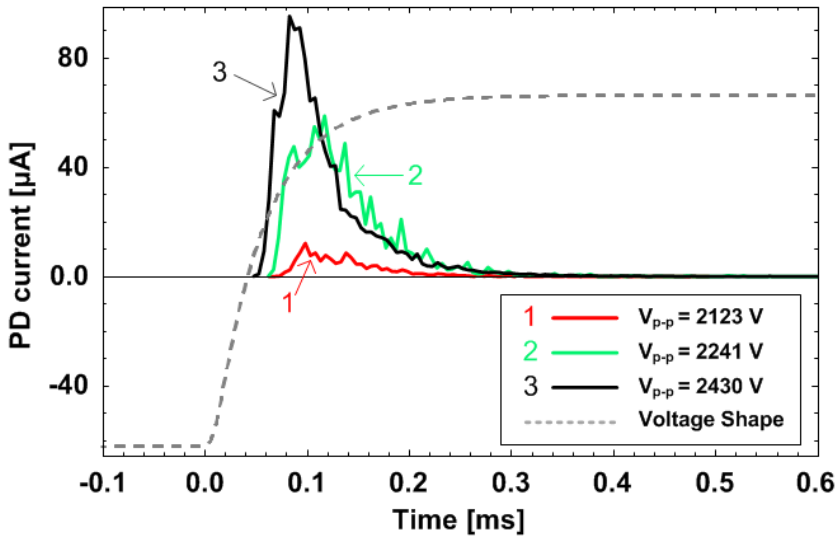

Figure 5.9. PD current waveforms obtained from pulse PD detection, measured simultaneously with the results shown in Figure 5.8.

configuration, the discharge patterns for positive and negative half periods are very similar and therefore only results from the positive half period are plotted. The results indicate that for higher voltage levels, the first discharges occur earlier and their amplitudes become larger, which is very similar to observations using pulse PD detection, the latter shown in Figure 5.9. The peak amplitude of both currents are definitely within the 15 % pulse PD calibration uncertainty reported in section 3.5.

Figure 5.10 plots the three PD excess current waveforms shown in Figure 5.8, but with a different scaling. A slowly decaying current component appears in the time range 0.6 ~ 4.6 ms, where there is no significant discharge activity. In addition, the amplitude of this current component seems to increase with the applied voltage. One possible explanation is that the current appears as a result of solid material charging during the fast discharge activity.

Further, the integrated "slow" currents are plotted as the bottom curve in Figure 5.11. This is obtained by integrating the current traces for time interval 0.6 ~ 4.6 ms in Figure 5.10, i.e. after the fast discharges has ceased. In contrast, the other two curves in the figure present integrated charges of PD activity based on the results of PD excess current and pulse PD detection methods. In this case the integration is done for the current traces shown in Figures 5.8 and 5.9 in the time range 0 ~ 0.6 ms.

As observed in the two upper curves at the lower voltage levels, the integrated currents from both methods are similar. However, when further increasing the voltage level, the integrated current from the excess current measurement becomes larger than the one obtained from the pulse PD detection. This is similar to the result presented in section 5.1 for corona discharges, where undetected PD pulses with amplitudes lower than the trigger level or overlapping pulses occur. These cannot be properly resolved by pulse PD detection, yielding a lower integrated current. It can be also noticed that the slow currents value for the time range 0.6 ~ 4.6 ms, is comparable in magnitude to the current caused by fast PD events. The existence of slow currents may thus have an impact on PD activity, as will be clear from in the following.

Until this stage of the measuring setup development, the front resistor R_f was not introduced. The observations related to the data presented in Figure 5.10 prompted a desire to improve the measurement resolution for studying the slow current component in more detail.

This example verifies that, by relatively precise calibration of a pulse PD detection system and counting all detectable PD pulses, the currents observed by both detection systems is consistent. It has again been illustrated that the excess current measurement has the advantantage of not requiring a detection limit and the observation of the "slow" current shows the ability to detect all currents, not only fast pulses.

5.4 Summary

In this chapter, through measurements of a well-known PD source, corona discharges, it has been illustrated that excess current accounts for both number and amplitude of discharges and can thus evaluate many small against few large PDs.

By measurements of the twisted pair specimens under different voltage waveforms, the measured excess current waveforms were compared with the currents interpreted from detected PD pulses. It was observed that, due to the pulse threshold required in

pulse PD detections, the summed amplitude of all PD events could not properly reflect the total current in case of appearance of many small discharges. Similarly, the slow current contributions cannot be seen through pulse PD detection as they are below the detection frequency range.

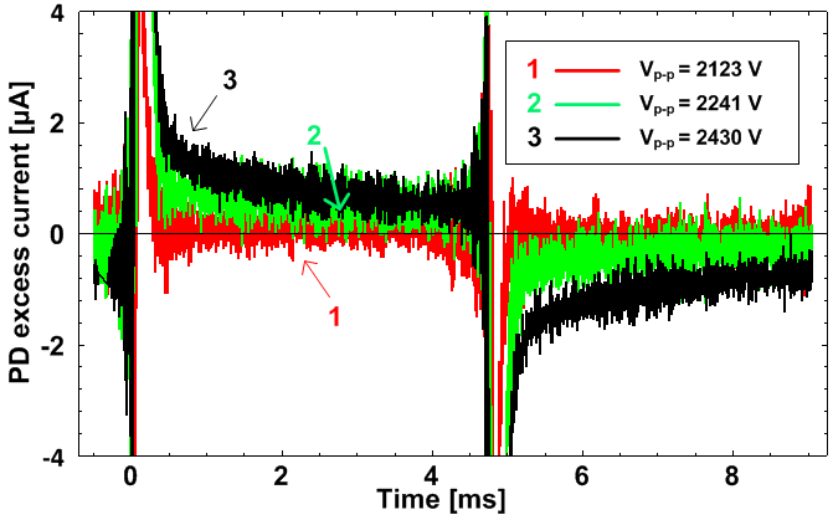

Figure 5.10. PD excess current waveforms as shown in Figure 5.8 in another scale to emphasize the existence of slow currents at times where there is no PD activity detected.

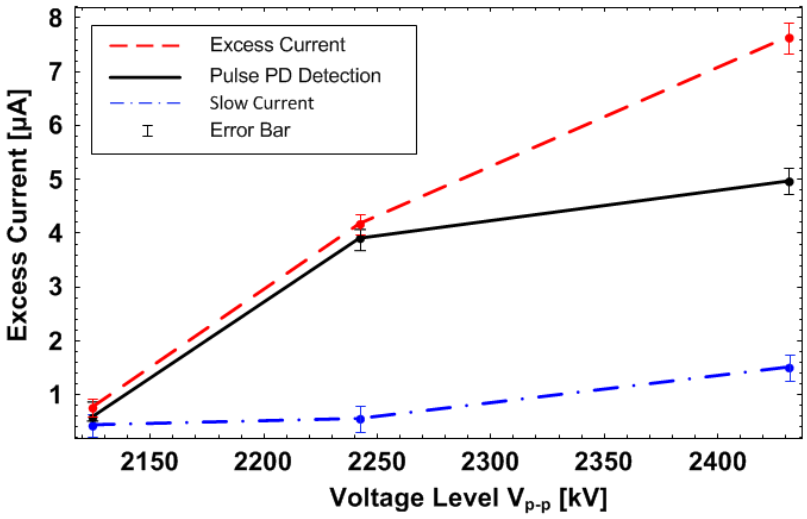

Figure 5.11. Integrated current components as function of the applied voltage levels. The components measured during PD activity by excess current measurement (Figure 5.8) and pulse PD detection (Figure 5.9) are integrated between 0.0 ~ 0.6 ms, whereas the slow current component (Figure 5.10) is integrated between 0.6 ~ 4.6 ms.

6 PD activity variation

Investigations presented in chapter 5 gives an understanding of how various aspects of PD properties are reflected in the excess currents. Indeed, both measurements are complementary to each other as they elucidate different properties of PD activity. Therefore it is very informative to apply both techniques simultaneously when studying of PD activity variations over time. However, based on the results presented above, it had been realized that a further improvement of the measurement resolution was still needed. This task could be achieved by introducing into AWIS measuring circuit the front resistor R_f, as discussed earlier in chapter 3. This concept is utilized in this chapter by presenting measurements performed on twisted pair and cavity specimens over time.

6.1 PD activity decay

The PD activity variation can be studied under different scenarios, such as different voltage levels, different environmental conditions, PD exposure time and so on. In this study we mainly focus on PD development with time, where the activity changes under a constant voltage level. Two types of voltage waveforms, sinusoidal and semi-square wave shapes are used.

6.1.1 Twisted pair under semi-square wave voltage

As a first step in the investigation of PD development over time, one reference measurement was made on virgin twisted pair specimen exposed to a voltage of 1.55 kV to estimate the capacitive current. PDIV is about 1.6 kV for the twisted pair specimens used in the study. It was also checked that the excess current was non-existing at this voltage level. Thereafter the voltage level was increased to 2.2 kV, at which PD activity started and the excess current appeared. The obtained excess current waveforms were further condensed by integrating each half cycle into an average excess current value, as for symmetric test objects, the integrated excess currents from positive and the negative half cycles are very similar. In addition, the simultaneously detected PD pulse amplitudes were also summed in each half cycle and averaged over 10 cycles. This was calculated by applying equation (3.8) with a time step (Δt) equal to a half cycle.

In Figure 6.1, the integrated excess current is compared with the sum of PDs amplitudes for the simultaneous measurements. After the voltage increase, a strong PD activity was detected for the first 100 s and both measurements could follow this activity. However, after 100 s, the detectable pulse PDs almost disappeared while the excess current continued to increase until reaching a stabilized level after 500 s.

To better understand the observed disappearance of the initially strong PD pulses, the excess current waveforms as well as the distribution of individual PD events were further analysed. Figure 6.2 summarizes seven excess current waveforms, selected at

different times during the measurement, marked by the grid lines in Figure 6.1. For the first two occasions, at 64 s and 103 s, relatively strong PD events were detected. These two waveforms are plotted separately, together with the detected PD events. At the other five occasions no PDs were detected, but the excess current waveforms could be measured. It is important to stress that the lack of detectable PDs mainly result from the used trigger level.

At 64 s, the distribution of PD events matches the excess current waveform well and no other contributions are noticeable. However, at 103 s, when PDs are reduced both in number and in amplitude, additional contributions appear in the current in other parts of its waveform, for example before the PDs start, <0.1 ms, and after 0.3 ms.

When comparing the five later excess current waveforms, even though no PDs were detected, the excess current continuously increased with a similar shape of the waveform until it is stabilized. It is also seen that all the excess current waveforms have a significant peak between 0.1 ~ 0.2 ms, where the PDs used to be detected at the first two occasions. This might be due to the existence of weak discharges, possibly similar to glow- [13, 73] or micro-discharges [74].

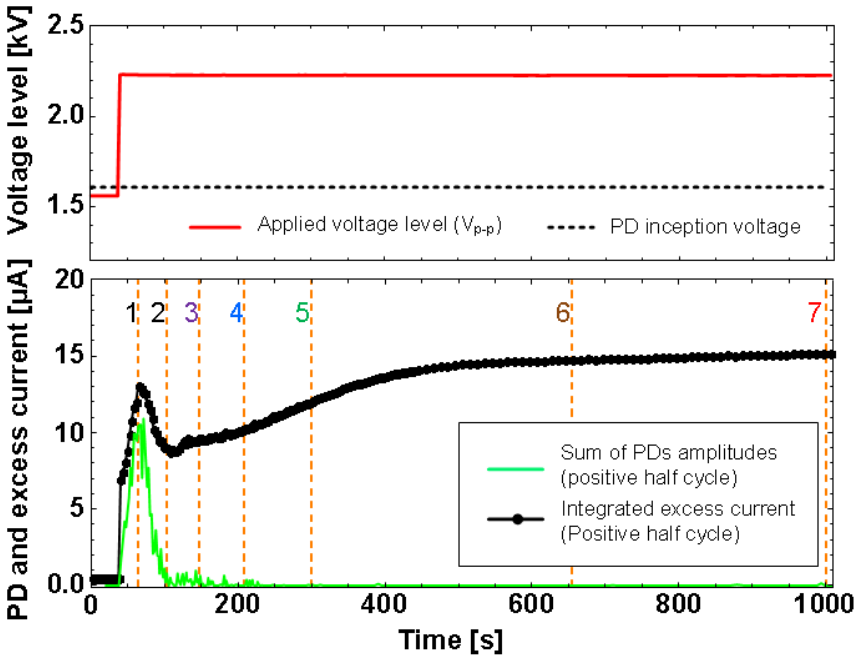

Figure 6.1. Long-time development of PD activity (sum of PDs amplitudes) and integrated excess current from positive half cycles under a bipolar semi-square wave voltage with base frequency of 500 Hz. In twisted pairs, positive and negative PD properties are very similar. The grid lines in the x-axis show the times selected for the waveforms presented in Figure 6.2.

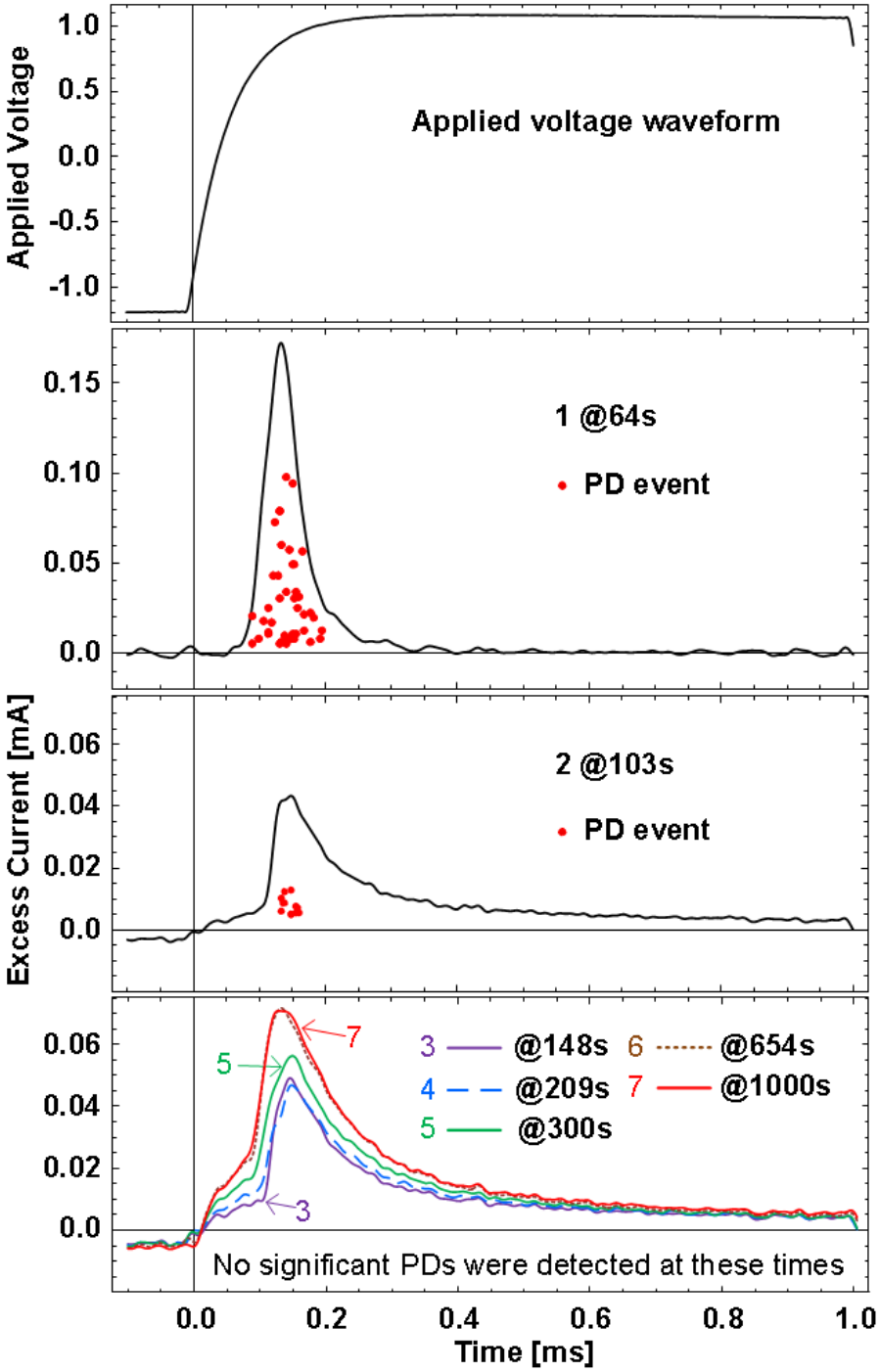

Figure 6.2. Excess current waveforms as well as detected PD events at the different times indicated in Figure 6.1. The applied voltage waveform is shown for a reference in the top graph.

To evaluate the possible existence of small undetected discharges, traces of the PD signals from the time events at 64 s and 654 s are shown in Figure 6.3 with the trigger level indicated. The used vertical range is selected to be just enough to accommodate the large PDs detected in the beginning of the test (top figure at 64 s). In the PD trace at 654 s, there are a few small peaks sticking slightly above the average noise level but smaller than the PD trigger level. Detection of such small discharges may be possible by decreasing the measurement vertical range but there may always appear some PDs with amplitudes lower than the noise level of the measurement setup. Therefore, absolute detection of all the small PDs is not possible for a conventional pulse PD detection system as seen in section 5.2. In contrast, the presence of the small discharges may be detected and quantified with the employed excess current measurement system.

Here we have observed a disappearance of PD activity after some time and a relation to the excess current seems to be apparent, at least in this case. The excess current measurements indicate a continued PD activity with many small discharges. By considering the pulse PD trigger level, it can be estimated that at least 50 small discharges occur in the time range 0.1 to 0.3 ms of each half period. In addition we have noted another current contribution which is to be studied in more detail later.

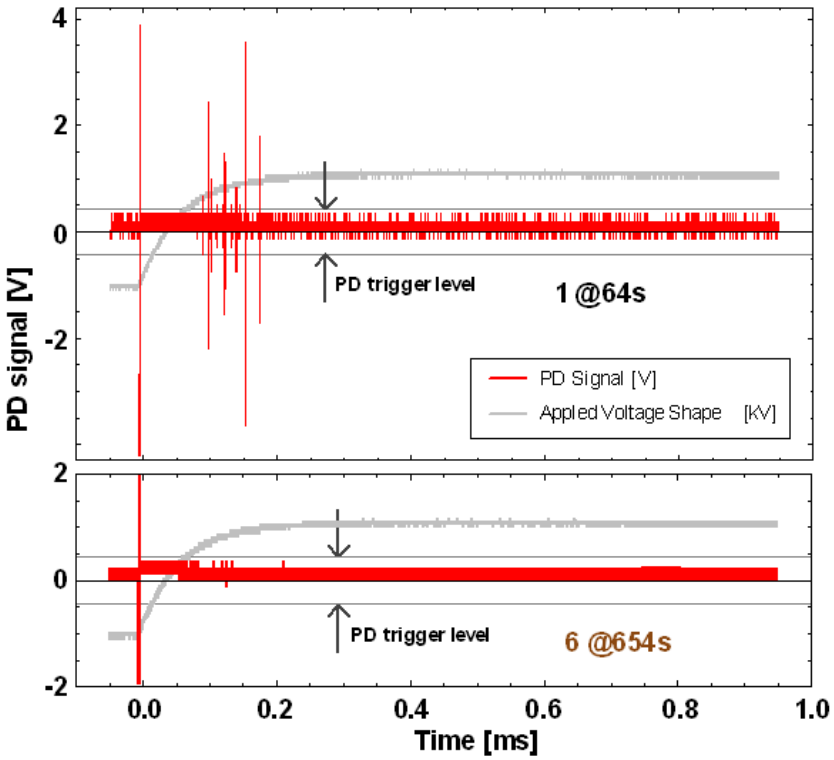

Figure 6.3. Pulse PD traces at peak PD activity (64s) and at stable excess current condition (654s).

6.1.2 Dielectric cavity under sinusoidal voltage

To get an indication if the observations presented in the previous section are a general phenomenon, the PD time development measurement was repeated on a dielectric cavity specimen with excitation of 500 Hz sinusoidal voltage. Thus both the PD source and the test voltage type is different from the previous example.

The used cavity specimen has one layer of 0.8 mm thick Epoxy sheet sandwiched by two layers of 0.1 mm polyamide (PA) films, where the Epoxy sheet has a drilled hole with 5 mm diameter. The detailed description of the cavity setup is provided in section 4.1.3.

The time development of PD activity and the integrated excess current are shown in Figure 6.4. The characteristic of PDs amplitudes is similar to those presented in Figure 6.1 for a twisted pair specimen. The reduction in PD amplitude of the cavity specimen is very significant during the first 100 s. However, around 140 s and 175 s, the sum of PD amplitudes exhibits temporarily some stronger pulses. The integrated excess current, after decaying during the initial 100 s, also exhibits some oscillations and stabilize afterwards. Therefore, the effects of reduction of the PD amplitude as well as stabilization of the excess current are observed in the cavity specimen. Some additional phenomena related to PD activity in the cavity specimen are explored in section 6.2.

The excess current waveforms at two different exposure times, 41 s and 216 s marked as grid lines in Figure 6.4, are plotted in Figure 6.5. In addition, the detected PD events that are accumulated from 10 continuous cycles at the same times are shown for reference. The peak value of the waveform at 41 s is nearly 10 times larger than the waveform recorded at 216 s, however the difference in the total integrated excess

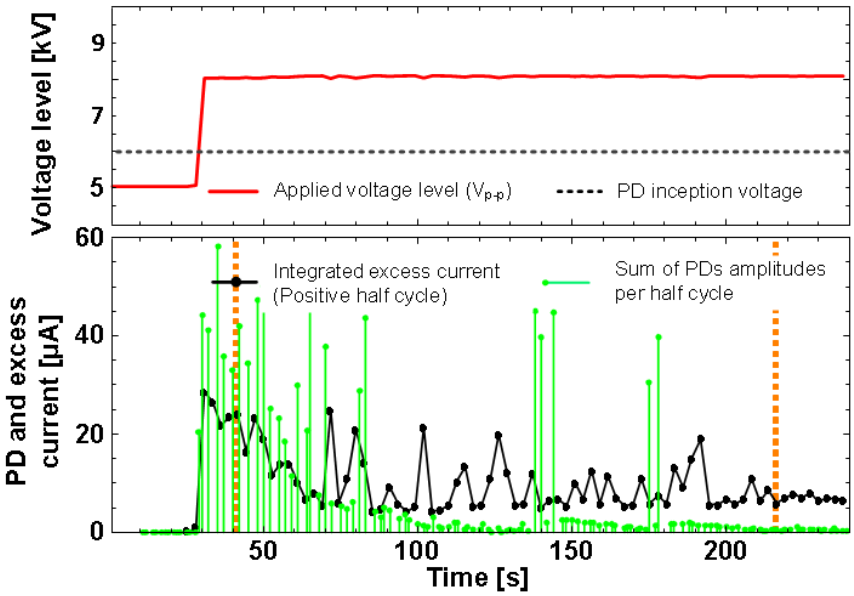

Figure 6.4. Time development of PD activity in Epoxy-PA cavity specimen, integrated excess current and sum of PDs amplitudes at positive half cycle are compared. PDIV is about 6 kV. The grid lines in the x-axis illustrate the time of waveforms shown in Figure 6.5.

currents is only about 3 times. This is a result of the contribution from an additional current component and can be well observed in the waveform recorded at 216 s (before and after the detected PD events). A similar phenomenon was also observed for the twisted pair specimen, see Figure 6.2.

One important common observation from this and the previous example is the appearance of an additional current contribution when both the PD amplitudes and their numbers are reduced. This additional current contribution does not seem to be directly related to the simultaneously recorded PD events as it appears in a much wider phase range. We have chosen to name this current contribution non-PD excess current and more detailed investigations are presented in chapter 7.

This example shows that the observations with a twisted pair under semi-square voltages are not unique to that type of test object. Most of the properties observed are qualitatively repeated in a cavity under sinusoidal voltage. The observations must therefore have some general relevance.

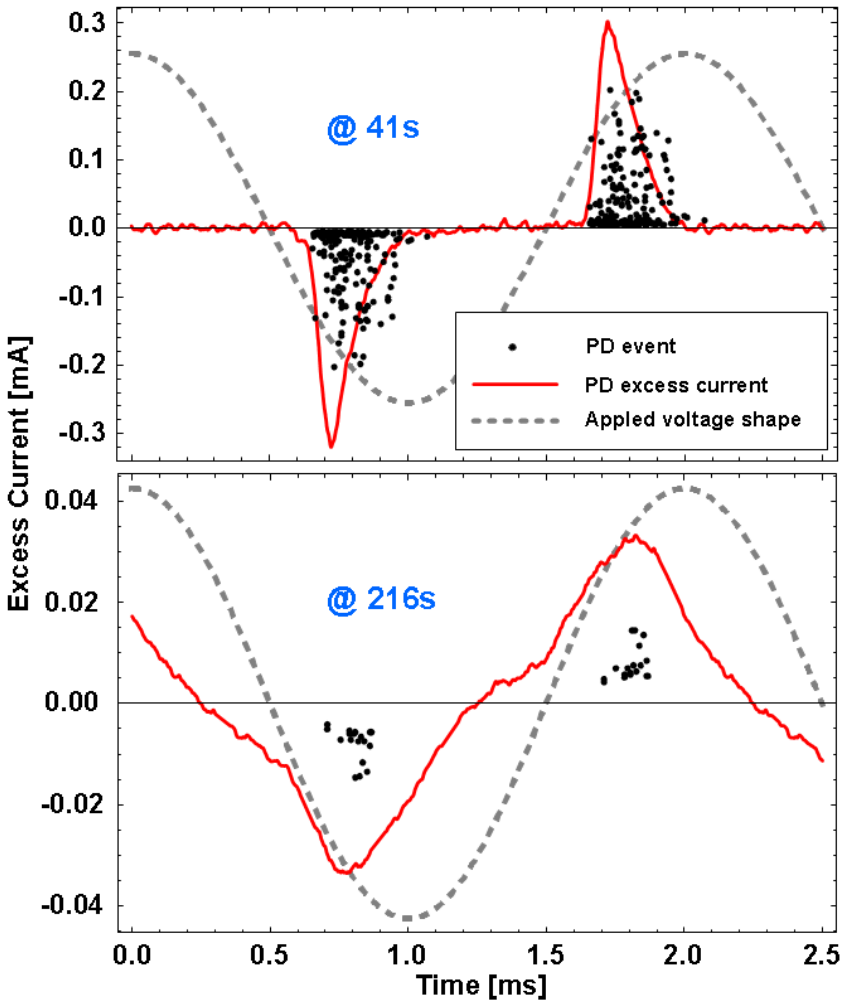

Figure 6.5. Excess current waveforms as well as detected PD events at the different time points indicated in Figure 6.4

6.2 PD activity oscillation

As some occasional significant PD activities were observed after the initial decay of the PD activity in the cavity specimen test presented in section 6.1.2, three more cavity specimens made of different dielectrics were tested by applying the same test procedure but with a longer testing time. As a result, PD activity oscillations with varying properties are revealed. Such oscillations are a hitherto unknown but striking phenomenon where the excess current seem to play an important role.

6.2.1 Epoxy-polyamide cavity

A measurement was performed on virgin cavity specimen (no previous PD exposure), made of a 0.75 mm thick epoxy resin board with a 5 mm diameter hole sandwiched by two layers of 0.1 mm thick polyamide (PA) films. Detailed dimensions of the test setup are presented in section 4.1.3.

At the beginning, a reference measurement was made at 5.6 kV to estimate the capacitive current, where the excess current was defined to be zero (PDIV is about 6 kV). Later, the voltage was increased to 8.03 kV, where PD starts and the excess current appears. The integrated excess current over the positive half cycle and simultaneous measured sum of PDs amplitudes by pulse PD detection are compared in Figure 6.6.

The results indicate that a strong PD activity started right after the voltage increase and both measurement results seem to agree only initially. Thereafter, the PD activity starts to decrease whereas the excess current increases for the next 400 s. This is very similar to the observations presented in section 6.1.1. More surprisingly, additional activities occur here. The excess current behaves periodically – after reaching a certain level it suddenly drops, being accompanied by simultaneous increase in the sum of PD amplitudes. Shortly after, the excess current is restoring while the PD activity decreases. This oscillation-like dynamic phenomenon seems to be repeatable and its periodicity varies slightly. Finally, when the voltage was reduced below PDEV to cease the PD activity, the excess current can still be sensed showing a decay in amplitude.

Several excess current waveforms at times marked by grid lines in Figure 6.6 are plotted in Figures 6.7 and 6.8 for a detailed analysis of both initial stage of PD excess current as well as excess current without PD activity. Figure 6.7 contains additionally information about the PD events acquired from 5 positive half cycles at the same time as the indicated current traces. In addition, a trace of the integrated excess current between 900 s and 1100 s is zoomed in Figure 6.9 for a detailed study of the oscillation.

Figure 6.7 shows three excess current waveforms obtained at the beginning of the test, where the excess current continuously increase. It is seen that the peak phases are corresponding well with the detected pulse PD events. The peak amplitudes do however not follow the increasing trend of the total integrated excess current. This may perhaps result from a combination of PD number, PD amplitude as well as their occurrence time. The other parts of the excess current waveforms (0.0 ~ 0.08 ms and 0.14 ~ 0.5 ms), where no significant PD events were detected, shown an increase with the PD exposure time. This is due to the existence of a non-PD excess current and

increase with time. In addition, the detected PD events at 396 s (highest integrated excess current) show a decrease in amplitude but spread in a wider phase range as compared to the other two occasions at 175 s and 286 s.

Figure 6.8 plots four excess current waveforms obtained after the voltage reduction below PDEV. A clear decay in waveform amplitude is shown with time. In addition, the shapes of these excess current waveforms are seen to be similar and all follows the front of the applied voltage waveform. The observed behaviour provides additional evidence for the existence of the non-PD excess current, which is very similar to the one observed from twisted pair and cavity specimens as discussed in section 6.1.

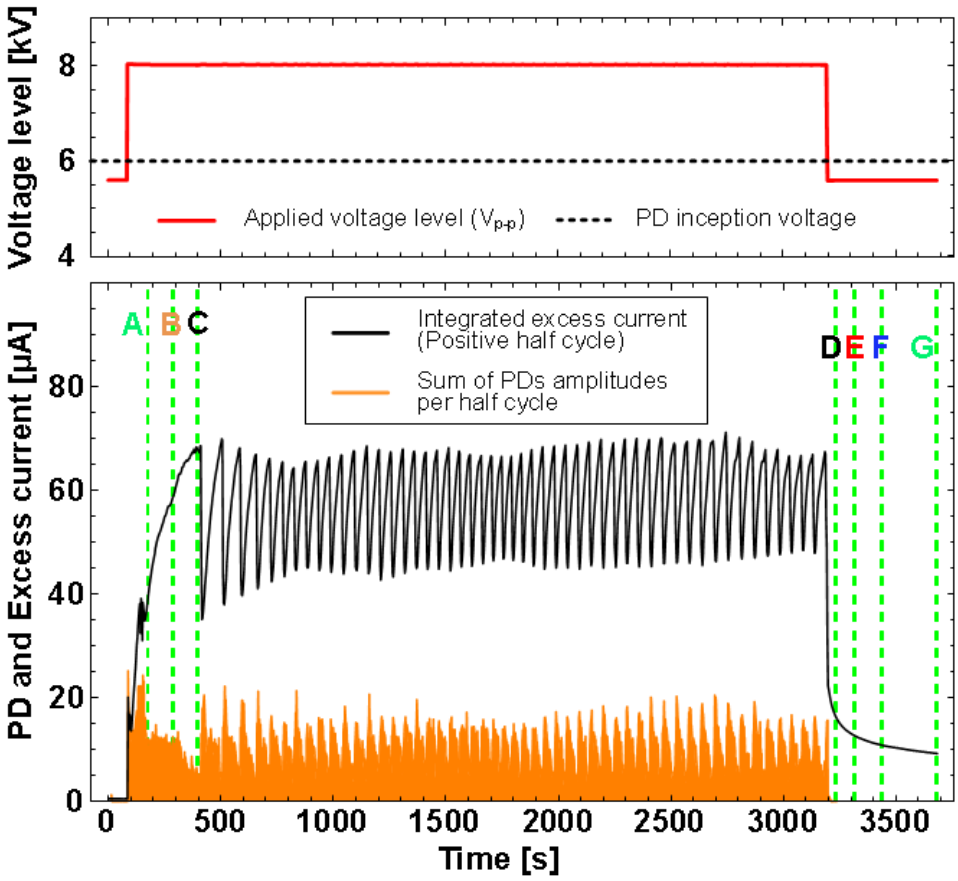

Figure 6.6. Time development of PD activity and integrated excess current from positive half cycles. The grid lines in the x-axis show the times selected for the waveforms presented in Figures 6.7 and 6.8.

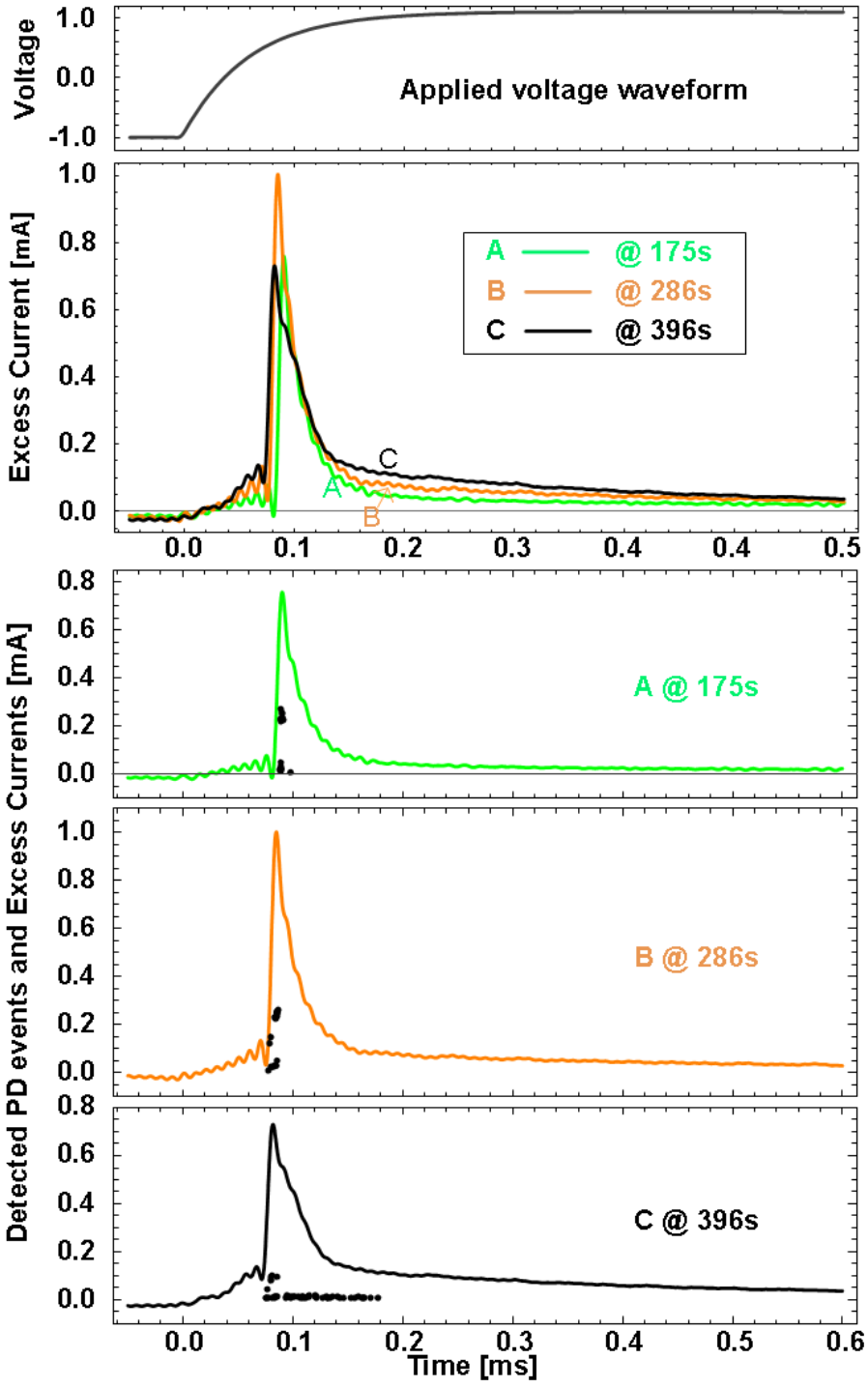

Figure 6.7. Three PD excess currents waveforms at initial stage of the measurement (at times marked as gridlines in Figure 6.6). The bottom three plots show the individual current waveforms together with detected PD events accumulated from 5 positive half cycles at the same time instants.

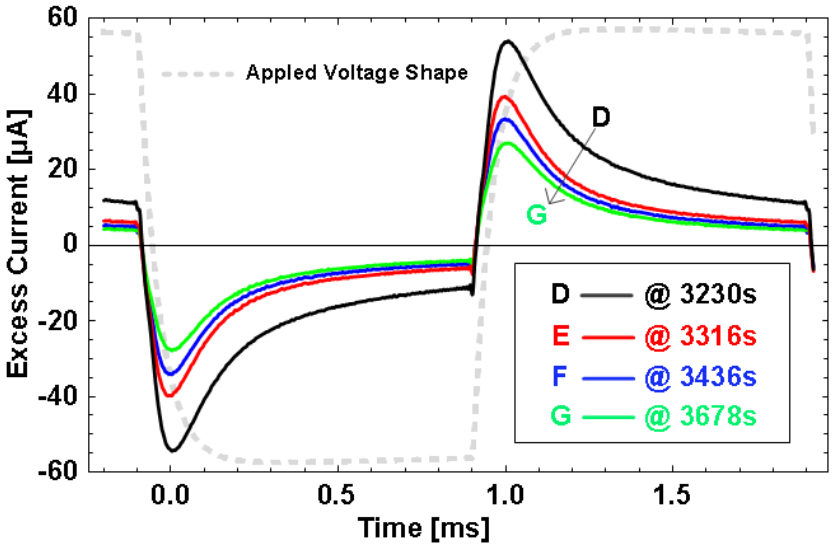

Figure 6.8. Excess currents waveforms measured with voltage below PDEV after 3000s PD exposure at times marked as gridlines in Figure 6.6.

To further understand the oscillation behaviour, a short trace of the integrated excess current is plotted in Figure 6.9 and compared with the sum of PD amplitudes, PD numbers, and average PD amplitude. The amplitude of the excess current is scaled down 4 times for a better illustration. The figure indicates that the excess current oscillation is closely correlated to the sum of PD amplitudes. Additionally, the number of PDs also varies during the oscillation and so does the average PD amplitude. Three excess current waveforms recorded at different stages of the oscillation presented in Figure 6.9 are further studied in Figure 6.10 together with PD events accumulated at the same time during 5 periods.

The results shown in Figure 6.10 are very similar to the plots in Figure 6.7. However, the peak amplitudes of the excess current waveforms do not follow the integrated excess current amplitudes or the sum of PD amplitude. They seem to be more dependent on the averaged PD levels, as compared to the averaged PD amplitude shown in Figure 6.9. This also indicates that the integrated excess current should be dependent on the current level at times in the period where no significant PDs are detected. Two such PD free times can be identified in Figures 6.7 and 6.10, indicating again existence of slower contribution to the excess current. This contribution seems to last for almost the entire half period and decay when the voltage amplitude stabilizes. It is very similar to the waveforms shown in Figure 6.8, where the voltage level was below PDEV. A possible origin of the observed current may be caused by movements of PD generated charges in the cavity.

As seen in Figures 6.7 and 6.10, the non-PD excess current is also sensed before PD restart and show an increasing tendency with time. Simultaneously, as seen in Figures 6.6 and 6.9, the sum of PD amplitudes is reduced. The decrease in PD activity is presumably caused by reduction of electric field in the cavity. This can be a result from dynamic behaviour of charge movement in the cavity. On the other hand, the

oscillations, a quick and repeated cyclic transformation from the excess current waveforms 3 to 1 in Figure 6.10, might result from a sudden creation of temporary conductive channel on the cavity wall, when the excess current reaches high enough level. However, the understanding of this phenomenon demands further exploration.

To exemplify that the observation of the excess current oscillation that appeared in the studied cavity specimen is not a unique and uncommon phenomenon, two other cavity specimens were further tested. One is made out of three polyethylene (PE) sheets with thickness of 1 mm in the middle and 0.1 mm at top and bottom. The middle layer has a drilled hole of 3 mm in diameter. The other one is made from Polycarbonate (PC) board sandwiched by two layers Polyamide (PA) sheets. This specimen has the same dimension as the Epoxy-PA specimen used in the previous test, 0.75 mm thick in the middle layer covered by two 0.1 mm thick PA films. The cavity has a 5 mm diameter drilled hole. Here, the only difference between the latter specimen and the one just presented is the middle layer dielectric.

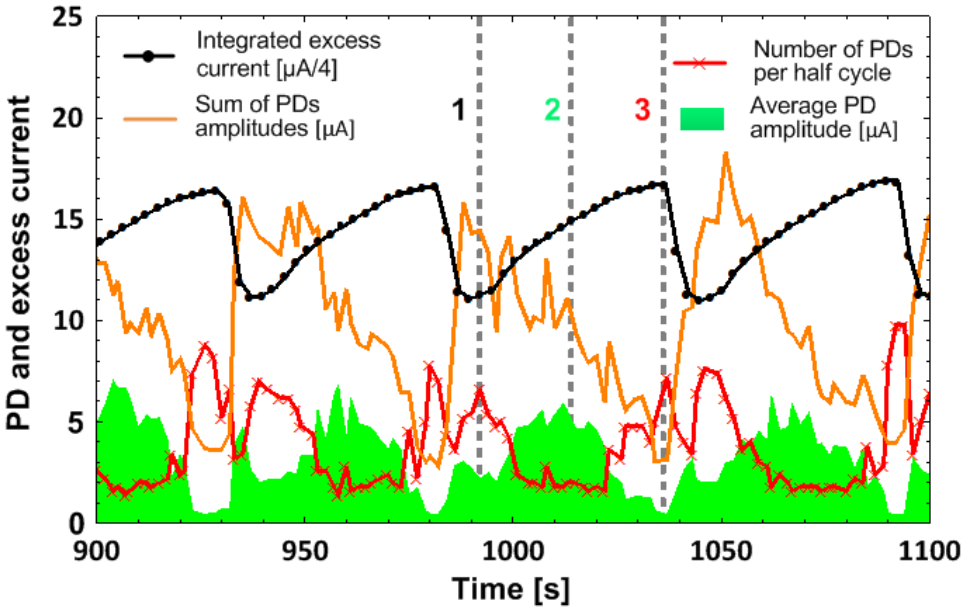

Figure 6.9. A detailed portion of the PD excess current (also shown in Figure 6.6) compared with sum of PD amplitude, PD numbers, and average PD amplitude. The dashed grid lines show the times selected for the excess current waveforms plotted in Figure 6.10.

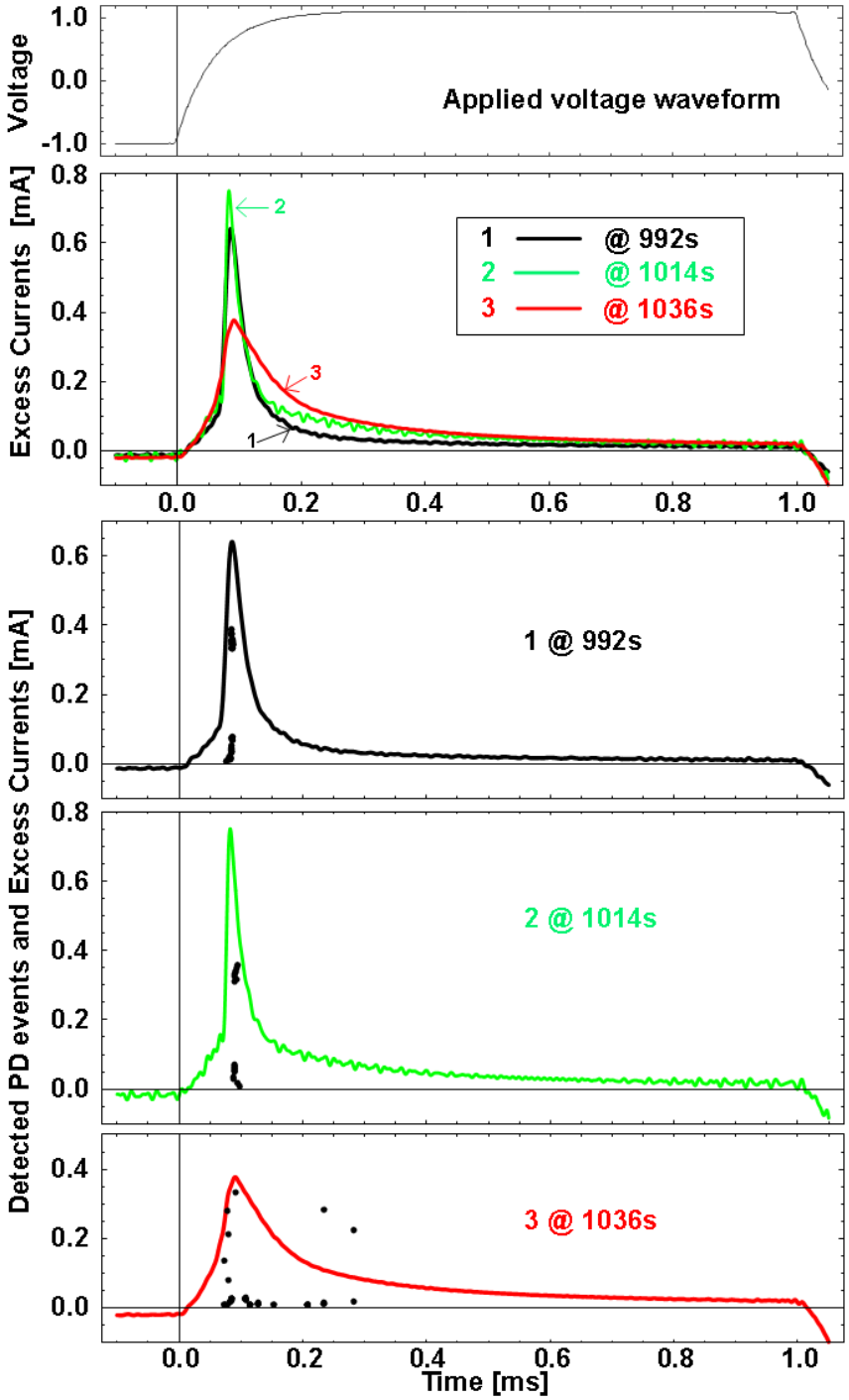

Figure 6.10. Three PD excess currents waveforms at times marked as gridlines in Figure 6.9. The bottom three plots show the individual current waveforms together with detected PD events accumulated from 5 cycles.

6.2.2 Polyethylene cavity

The same test procedure but at different voltage levels, 8 kV for reference measurement and 10 kV for PD exposure, was performed on the PE cavity. The obtained integrated excess current and sum of PD amplitudes are shown in Figure 6.11. As seen from the figure, both the initial stage and the oscillation were qualitatively repeated, similarly to the data from Figure 6.6. The main differences between the two specimens, Epoxy-PA and PE, are the time scale and the amplitudes of both the excess current and the PD events. In addition, the results obtained from the PE specimen also show a trend of amplitude decrease in the excess current. These similarities and differences need to be further investigated, as they might shine new light on the processes responsible for PD behaviour in dielectrically isolated cavities.

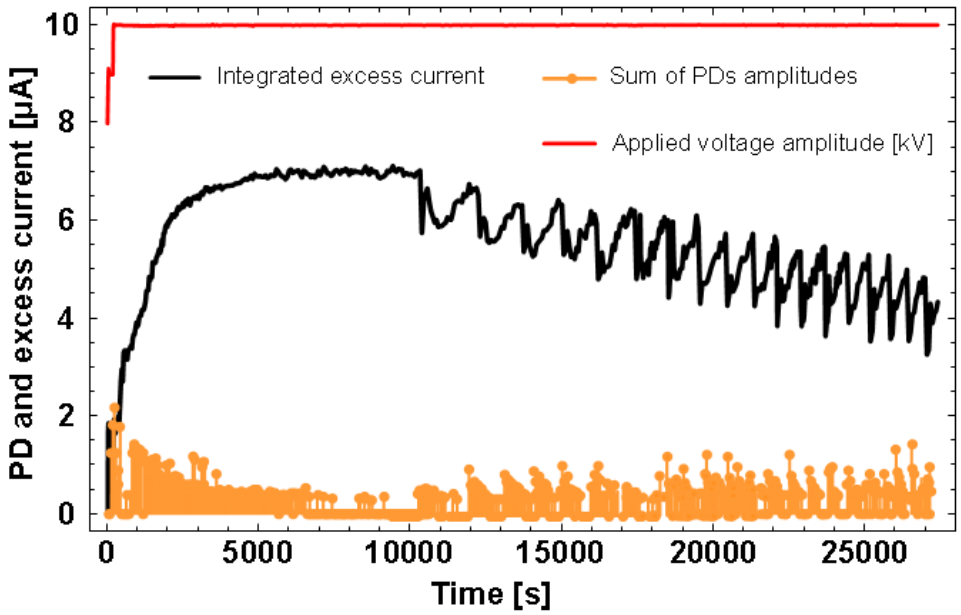

Figure 6.11. Integrated PD excess current and summed PD amplitude for the PE specimen at 10 kV.

6.2.3 Polycarbonate-polyamide cavity

In addition to the qualitative confirmation from the PE cavity specimen measurement, the PC-PA cavity specimen was measured with the same test procedure and even the same voltage levels as used in the Epoxy-PA cavity specimen. The results are presented in Figure 6.12. Surprisingly, another type of PD "oscillation" is revealed in this case. The detected PD amplitudes were relatively strong but with very few PDs appeared within short time intervals, so short that they were sometimes missed by the pulse PD detection. The miss is a consequence of a need for detection dead time between two consecutive measurements for data processing. However, evidences of single or a few concentrated PD events were perceived by the sudden increase in integrated excess current. This quick charging and long-time decay type oscillation is again repeatable, but the decay rates seem to be varying and deserve some further studies. The study of the 6 decay curves, marked by numbers in the figure, is postponed to section 7.5. However, few excess current waveforms marked as grid lines in Figure 6.12 are worth presenting for a better understanding of this excess current oscillation.

Only one excess current waveform, marked as A in Figure 6.12, is captured where a strong PD activity is present and is plotted in Figure 6.13. All other waveforms are more or less similar to the three excess current waveforms shown in Figure 6.14. Their recording times are marked by a, b and c in Figure 6.12.

The PD excess current measured during strong PD activity shown in Figure 6.13 is

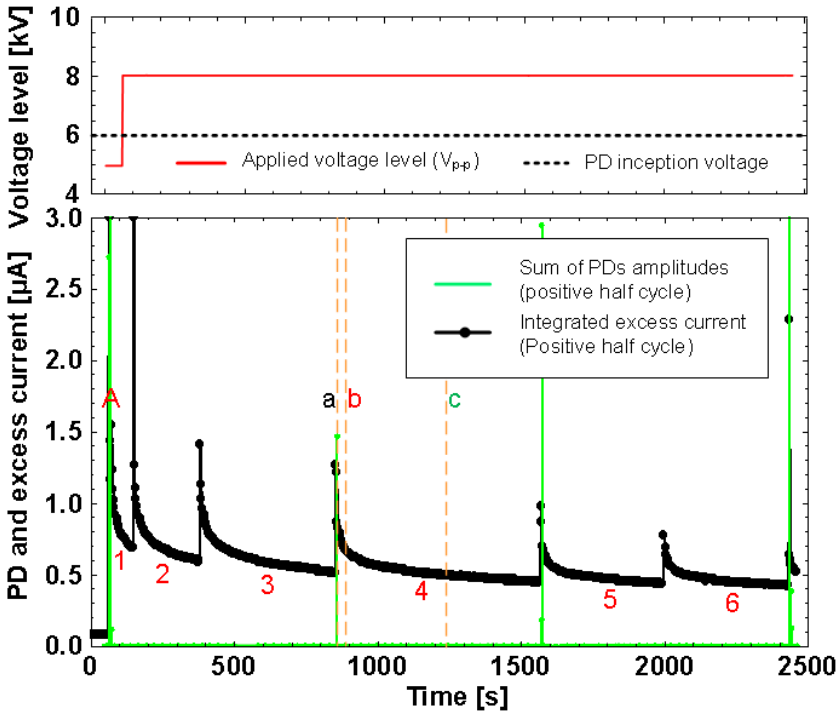

Figure 6.12. Integrated PD excess current and summed PD amplitude measured in a cavity specimen made of one layer of PC sandwiched by two layers of PA at 8 kV semi-square wave voltage. The numbered sections are used for decay studies in section 7.5.

very similar in shape as the one recorded from the Epoxy-PA specimen, presented earlier in Figure 6.7 at 175s, but having different peak amplitudes. The current is nearly 10 times smaller than in the Epoxy-PA specimen, though both tests were performed at the same applied voltage level. The excess current waveforms, shown in Figure 6.14, are similar to the non-PD excess current waveforms recorded from the Epoxy-PD cavity at the voltage level below PDEV, shown in Figure 6.8. The peak amplitudes differences between these excess currents are however about 20 times. In addition, some small differences observed between the two measurements are attributed to noise and possibility of some small PD activities. The latter can be seen from the small negative peak found at 0.5 ms in the recorded waveform "a" at 863s. The difference of non-PD excess current amplitude may reflect some property difference of the dielectrics of which the specimens are made, such as surface conductivity of the cavity wall, as the middle layer dielectric is the only different component.

To investigate the assumption above, volume conductivity measurements were performed using a Keithley electrometer (Model 6517B). The cavity middle layers with the drilled hole plus one layer of PA film were placed in a test cell (Model 8009) under ± 200 V DC to evaluate the relative difference in the conductivity. The results revealed that the average conductivity of the Epoxy wall is about 18.3 times higher than that of PC wall. This is of the same order of difference as found between the non-PD excess currents.

To conclude the studies of PD activity oscillations, which was detected at some surprise, it has been found that they can occur in cavity specimens after some time of PD exposure. The effect seems to be related to an interplay between PD activity and non-PD excess current. Times and amplitudes involved can apparently vary widely, which indicates that material properties, like surface conductivity, play an important role.

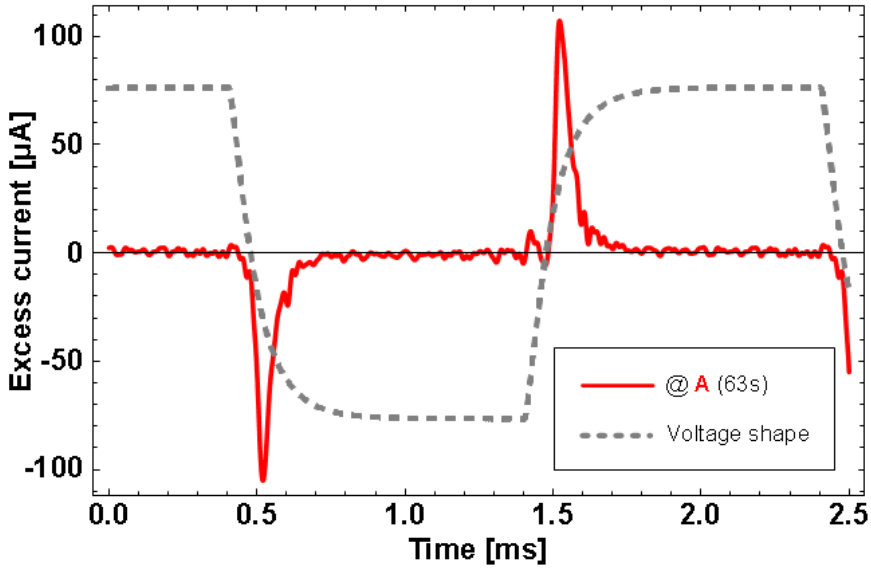

Figure 6.13. PD excess current waveform recorded at the beginning of the test indicated by grid line "A" in Figure 6.12 when PD activity recorded by pulse PD detection was strongest.

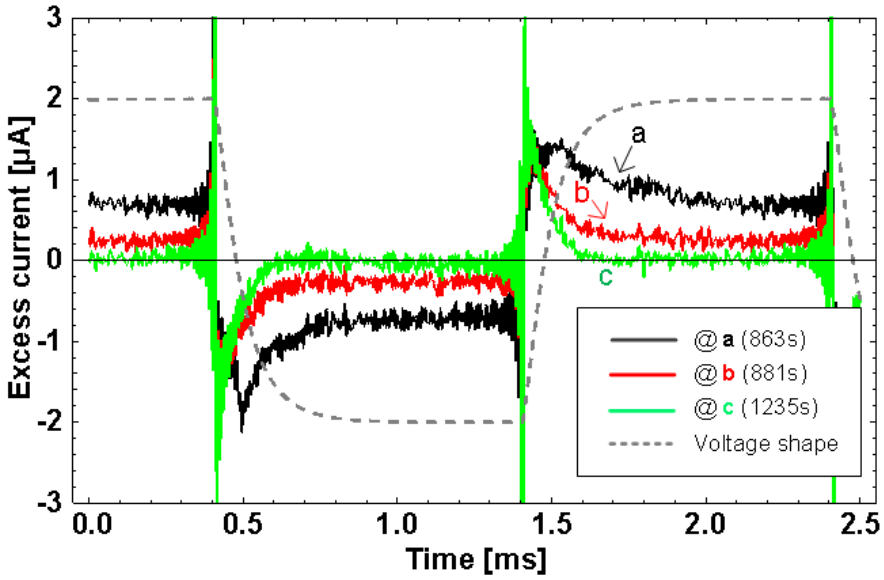

Figure 6.14. Three PD excess current waveforms at the times indicated in Figure 6.12, where no significant PD activity was detected.

7 Non-PD excess current studies

As seen from the results presented in chapter 6, PD activity variations in the form of decay or oscillations are closely related to changes in the measured excess current waveforms, where an additional current contribution, a non-PD excess current, has been observed. To verify the existence of the non-PD excess current and to investigate its properties, a few additional studies are presented below.

7.1 Existence of a non-PD excess current

To investigate the non-PD excess current contributions and to separate them from the effect of small discharges, a measurement was carried out with a virgin twisted pair specimen under similar conditions as described in section 6.1.1 (bipolar semi-square wave voltage with base frequency of 500 Hz). In this particular case, the applied voltage level was occasionally decreased below PDEV during the test. This way, the excess currents measured under the decreased voltage should be free from PD contributions and this seems to be confirmed by the results. In Figure 7.1, the integrated excess currents as well as the used voltage levels are shown and it can be

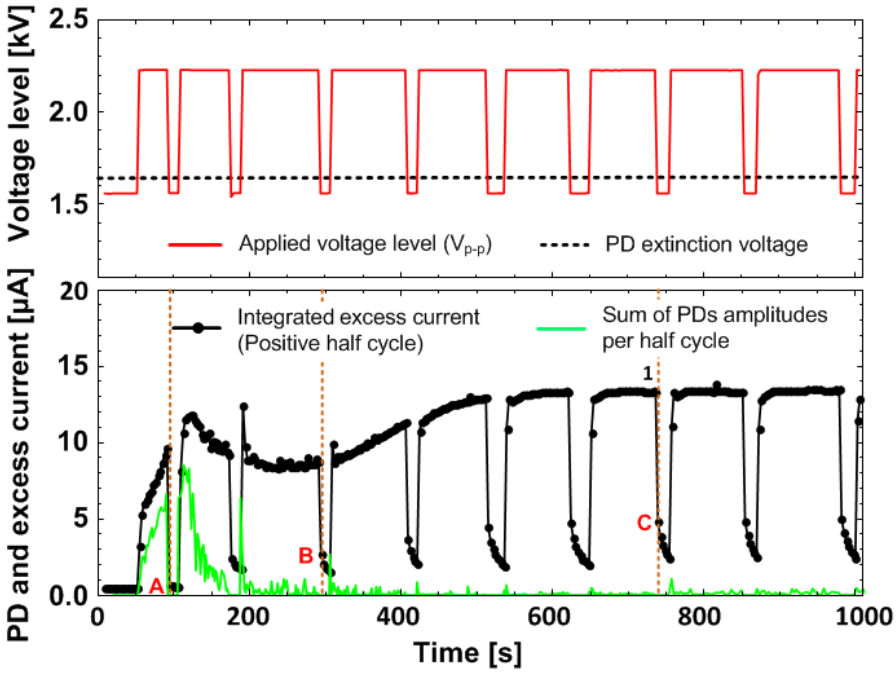

Figure 7.1. Time development of PD activity reflected by integrated excess current and sum of PDs amplitudes at positive half periods of a twisted pair specimen under 500 Hz semi-square wave voltage when the voltage amplitude is occasionally decreased as shown in the top frame.

noticed that the overall curve representing the excess current at voltage above PDIV is very similar to that shown in Figure 6.1. However, the integrated excess current below PDEV still remains measureable and exhibits a decaying tendency. The decay rate of this current is found to be varying as exemplified in section 7.5. Nevertheless, excess current waveforms, obtained right after the voltage is set below PDEV, are particularly interesting. Three such non-PD excess current waveforms, obtained at different stages marked as A, B and C in Figure 7.1, are plotted in Figure 7.2. In the figure, the top frame shows the actual current waveform. To compare the wave shapes, the waveforms are normalized to a common peak value and plotted together with the applied voltage shape in the bottom frame.

From Figure 7.2, it appears that the amplitude of the non-PD excess current increase with time, while the detected PD activity decreases. At the same time the shapes of all the non-PD waveforms remain the same, even though curve A contains much higher noise level, as the measured non-PD excess current is very low. The plots in Figure 7.2 also shows that the front of the current waveforms follow well the applied voltage shape up to its peak and start to decay when the voltage becomes stable. It may thus be suspected that the shape of non-PD excess current waveforms depends on the voltage waveform and material properties, but seems independent of PD activity. Therefore, it should also be linearly dependent on the voltage amplitude.

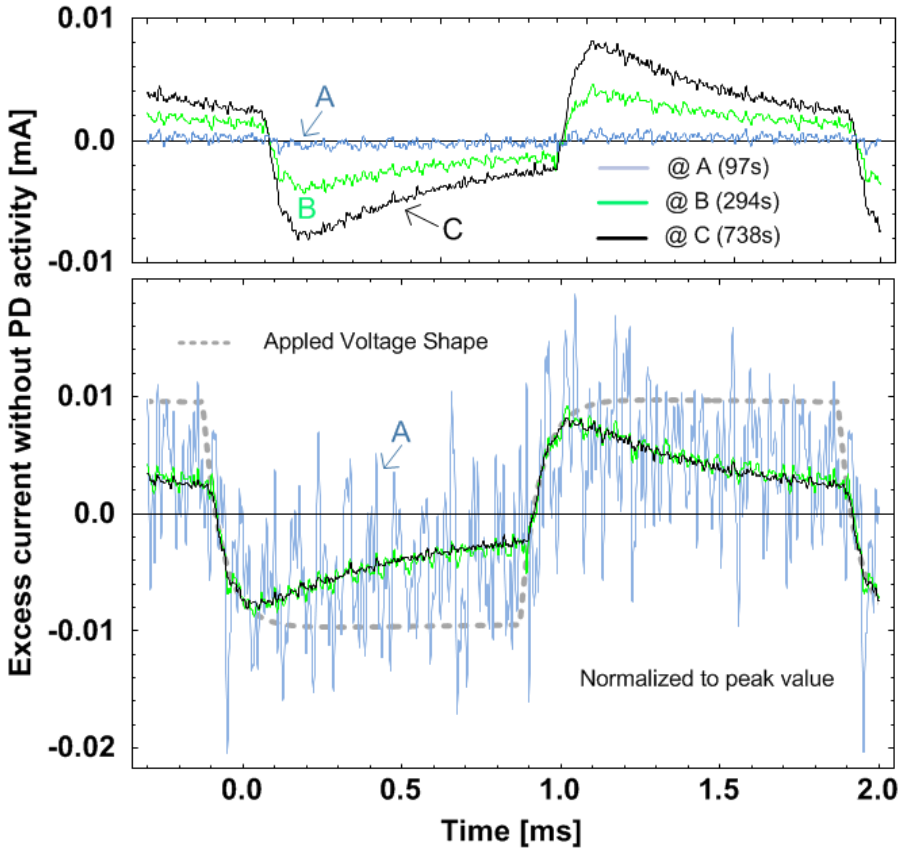

Figure 7.2. Non-PD excess currents waveforms, at time points marked A, B and C in Figure 7.1. The waveforms shown in the lower frame are normalized with reference to the strongest one.

To verify the later assumption, two excess current waveforms obtained before and after reducing the voltage amplitude below PDEV are compared in Figure 7.3. The one measured below PDEV is scaled with the voltage ratio as well as corrected for the difference in time, taking into consideration the decay characteristics right after the voltage reduction. The plots show a good match between the scaled non-PD excess current and the total excess current at the places where there should not be any PD activity. This is an indication that the non-PD excess current changes linearly with voltage amplitude. With this assumption in mind, the other contribution to the total excess current, marked in the figure as grey area of curve 1, should be a result of large or small PD activity. We choose to denote these contributions a pure PD excess current.

To additionally illustrate the behaviour of the pure PD excess current, the results presented in Figure 7.1 are further processed by removing the estimated non-PD excess current and the result is illustrated in Figure 7.4 together with the estimated non-PD excess current. The indicated level of non-PD excess current shown in the figure is estimated in the same way as the current presented in Figure 7.3. The pure PD excess current is then obtained by subtracting the obtained non-PD excess current from the total one.

The characteristics presented in Figure 7.4 show that initially the pure PD excess current fits the sum of PD amplitudes obtained by the pulse PD detection. They separate however after around 100 s and the pure PD current finally stabilize after 500 s, presumably as an effect of non-detectable discharge activity. At least 40 small PDs below the trigger level per half cycle are required to account for the observed current level. Figure 7.4 additionally indicates that the reduction of individual PD amplitudes is correlated with an increase of the non-PD excess current.

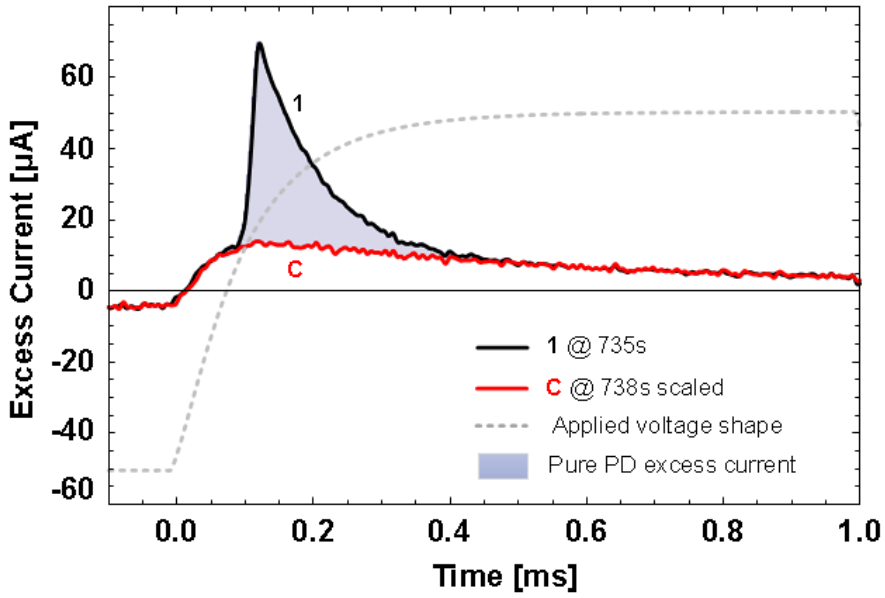

Figure 7.3. Fit of non-PD excess current below PDEV and excess current above PDIV. The non-PD excess current, scaled with the voltage ratio and the estimated decay rate, shows the same shape as the excess current in the regions where no PD activity takes place. The difference between the two curves defines the pure PD excess current.

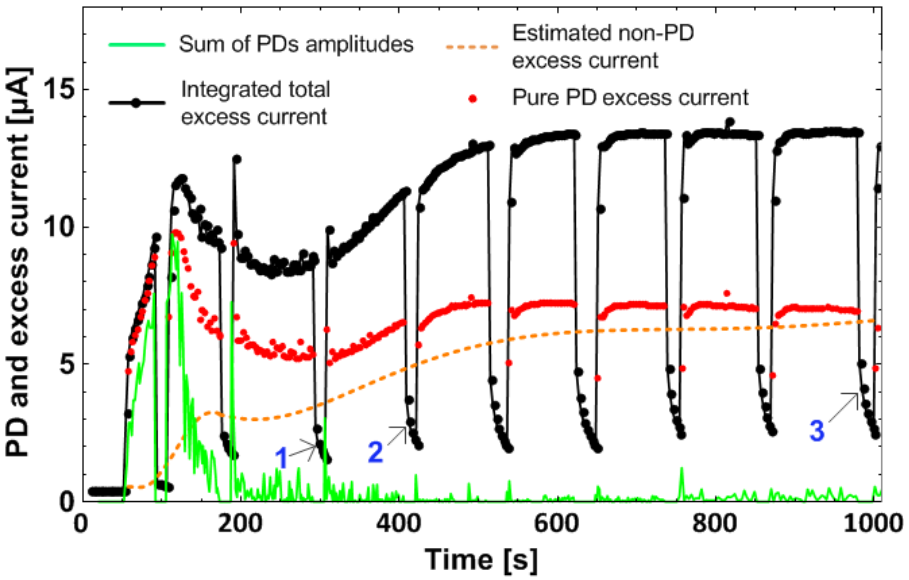

Figure 7.4. Time development of PD activity under a 500Hz semi-square wave voltage as shown in Figure 7.1 separated into the contributions from the estimated non-PD excess current and the pure PD excess current.

To verify that the non-PD excess current observations are not limited by the voltage type, i.e. semi-square voltage wave shape only, a similar measurement was repeated on a virgin twisted pair specimen excited by 500 Hz sinusoidal voltage and the results are illustrated in Figure 7.5.

Generally, the curves from voltage above PDIV are very similar to those reported earlier, in Figure 6.1 and Figure 7.1. One noticeable difference is that the PD events were still detectable after the integrated excess currents stabilized. This is possibly due to that the applied voltage level was about 200 V higher than in the semi-square wave measurements. The measurements below PDEV show an increase of non-PD excess current with time. Four such current waveforms, obtained at time points marked 1, 2, 3 and 4 in Figure 7.5, are plotted in Figure 7.6. The applied voltage and its responding capacitive current shapes are also presented in the figure for references. In addition, three PD excess current waveforms recorded at the times marked as A, B and C in Figure 7.5, are plotted in Figure 7.7 to study the time development in excess current shape under PD activity.

The amplitudes of non-PD excess currents in Figure 7.6 appear to increase with time while their shapes remain the same, similarly to the results presented in Figure 7.2. However, the phase of the non-PD excess current waveforms is shifted by about 40°, thus placed between the voltage and the current. At the same time, the PD excess current peaks shown in Figure 7.7 decrease with time. This behaviour is also confirmed by the measured sum of PDs amplitudes.

In addition, the peak phases are delayed with reference to voltage and contain additional current contributions around the zero crossing due to presence of the non-PD excess current.

Two excess current waveforms (C and 4) obtained before and after reducing the voltage amplitude below PDEV are compared in Figure 7.8. The one measured below PDEV is scaled with the voltage ratio as well as the estimated decay rate. The excess current behaviour presented in the figure is very similar to the one shown in Figure 7.3. A good match is shown between the scaled non-PD excess current and the total excess current at the times without any PD activity. The difference between two currents is the pure PD excess current and marked by the grey area.

A separation of the non-PD excess current from the total PD excess current is illustrated in Figure 7.9. It shows that similarly to the earlier discussed results (Figure 7.4), the pure PD excess current fits the sum of PD amplitudes at the very short initial stage, only a few seconds, thereafter they start to decrease and stabilize, but the non-PD excess current continuously increases.

Here we have seen that it is possible to separate the PD and non-PD excess currents by occasionally decreasing the voltage level below PDEV. As the non-PD excess current seem to be linear with voltage and follow the voltage wave shape, its contribution to the total excess current under PD activity can be estimated by scaling. There is however a phase shift or decay observed. Additionally, the total non-PD excess current decays slowly when the voltage is kept below the PDEV.

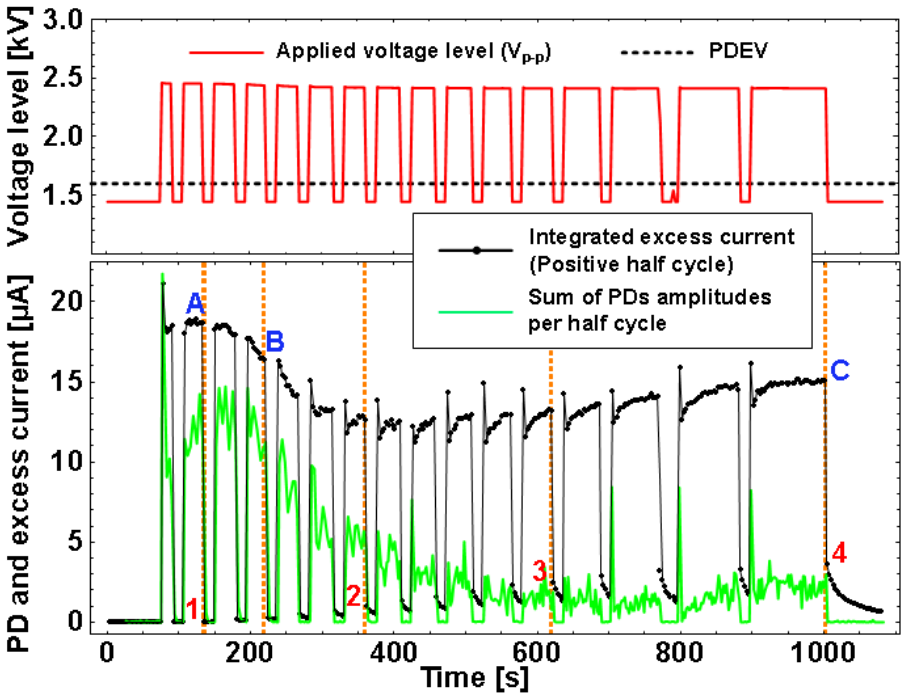

Figure 7.5. Long time development of PD activity reflected by integrated excess current and sum of PDs amplitudes at positive half periods of a twisted pair specimen under 500 Hz sinusoidal voltage when the voltage amplitude is occasionally decreased as shown in the top frame. PDIV is about 1.6 kV. The grid lines in the x-axis show the times selected for the waveforms presented in Figure 7.6 (1, 2, 3, 4) and Figure 7.7 (A, B, C).

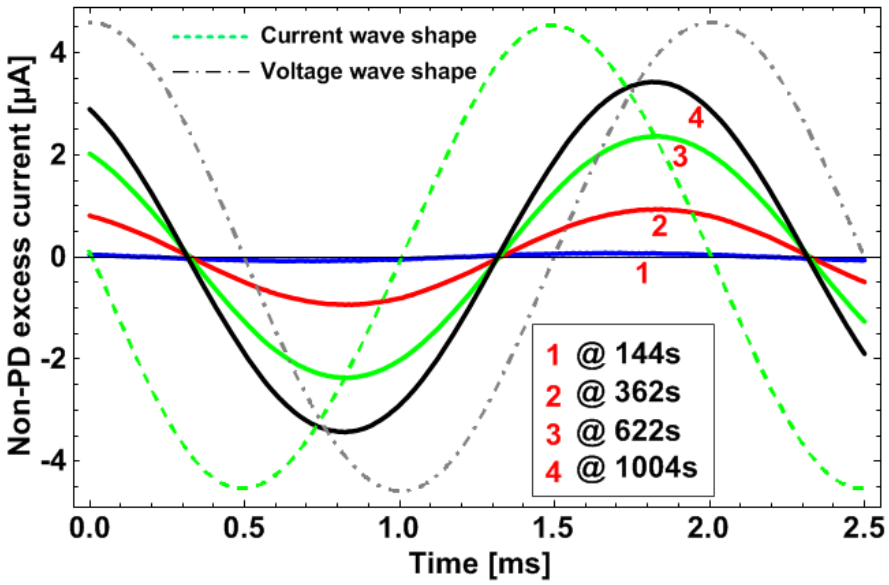

Figure 7.6. Three non-PD excess current waveforms, measured at the time points marked 1 - 4 in Figure 7.5.

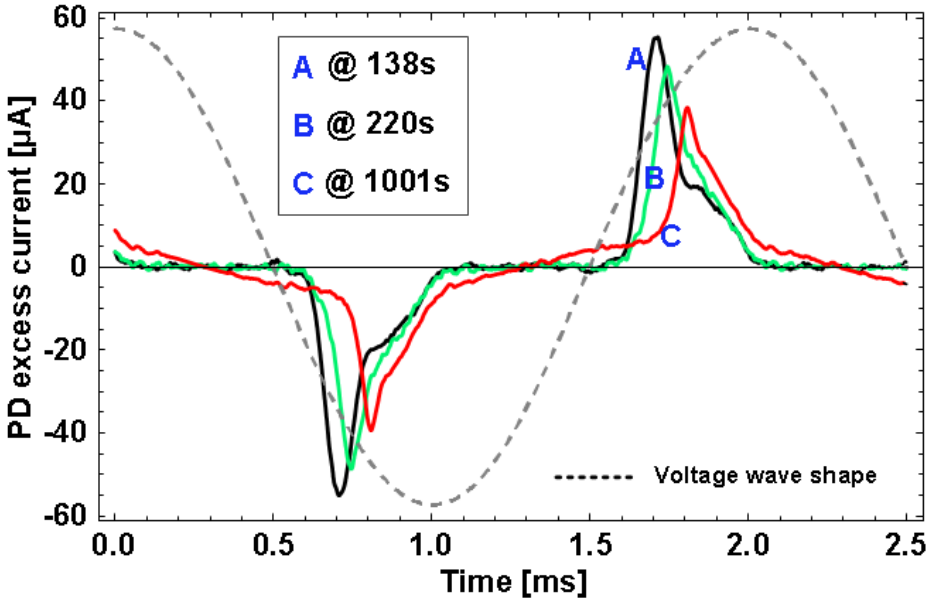

Figure 7.7. Three PD excess currents waveforms, recorded at time points marked A, B and C in Figure 7.5.

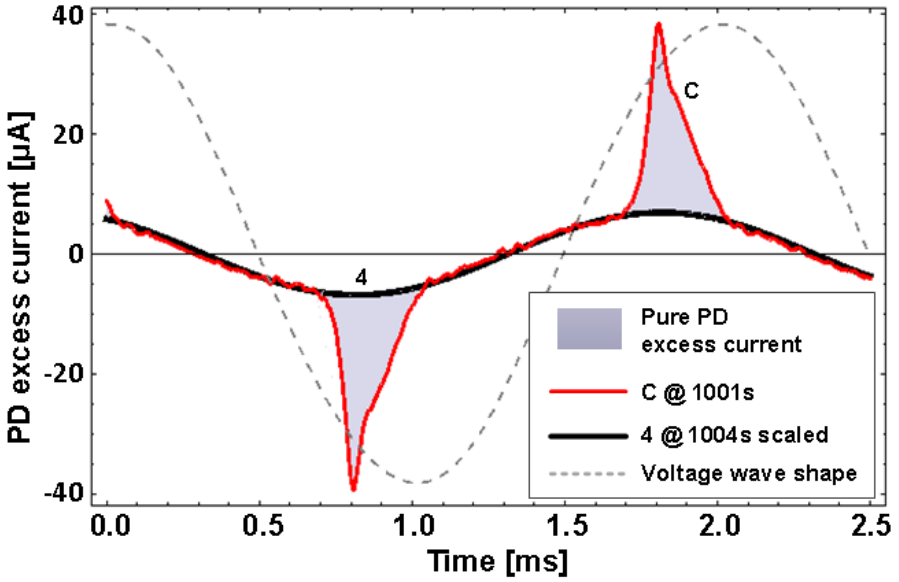

Figure 7.8. Fit of non-PD excess current below PDEV and excess current above PDIV under sinusoidal excitation. The non-PD excess current, scaled with the voltage ratio and the estimated decay rate, shows the same shape as the excess current in the regions where no PD activity takes place. The difference between the two curves defines the pure PD excess current.

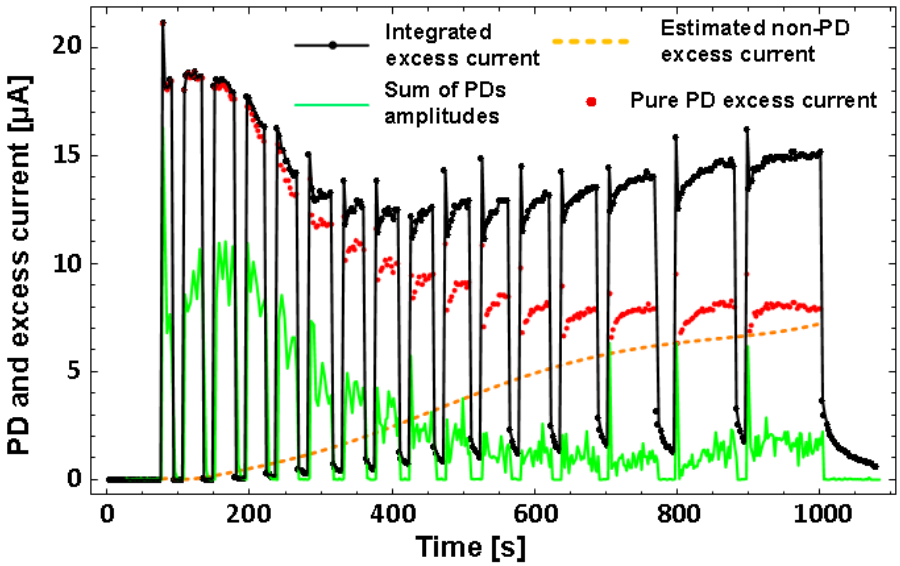

Figure 7.9. Time development of PD activity under a 500 Hz sinusoidal voltage as shown in Figure 7.5, separated into the contributions from the estimated non-PD excess current and the pure PD excess current.

7.2 Influence of air flow

The existence of a non-PD excess current has been confirmed by reducing the voltage level below PDEV. The obtained current shapes can even be fitted with parts of the PD excess current at a voltage level above PDIV, as seen from figures 7.3 and 7.8. The part of the non-PD excess current that appears before the pure PD excess current is of particular interest. One hypothesis is that the non-PD excess currents is resulting from remaining charge movement of preceding PD activity that can be moved fast enough to counteract parts of the electric field in the gas medium and yield the experimentally observed reduction of PD activity.

To verify the hypothesis, a special test setup, described in section 4.1.4, that allows a controllable air flow around the test object was adopted. The idea was to remove the charges generated around the specimen by air flow. Twisted pair specimens are the only useful for this type of verification as the discharge volume is in contact with the surrounding air.

A virgin twisted pair specimen was tested under 2.4 kV of 500 Hz sinusoidal voltage in the test tunnel in a similar way as described earlier in PD activity variation tests (section 6.1.1). The only difference is that the air flow was turned on and off during the measurement. Changes of obtained time dependences of the integrated excess current, the average PD amplitudes and the sum of PD amplitudes are presented in Figure 7.10. The shaded areas indicate times when air was flowing through the tunnel.

Before switching on the air flow, the behavior of the parameters presented in the figure is similar to what is presented earlier, discussed in sections 6.1.1 and 6.2, though a reduced PD activity is found to appear in a much shorter time. This is possibly due to effect of using the air tunnel instead of the larger plastic box. This reminds somehow the fast change of PD activity observed in the cavity specimens, as a small gas volume is involved.

After turning on the air flow, the PD activity changed. The sum of PDs amplitudes increased about 10 times, returning to the level when the PD just had started. The change is also noticeable from a dip appearing in the integrated excess current. Though the amplitudes of the excess current are quickly restored, its composition might be changed. As the amplitudes of the detected PD activity and integrated PD excess current are nearly the same during the air flow, the integrated excess current is believed to mainly come from the simultaneous PD activity. The non-PD excess current, which shared more than 90% of the excess current measured before the air flow, has disappeared. After stopping the air flow, the PD activity reduces and the excess current stabilizes. Later, with the voltage level reduced below PDEV, PD activity has stopped and the integrated excess current starts to decay. However, turning on the air flow again causes a quick reduction of the non-PD excess current level to zero.

The excess current waveforms as well as detected PD events recorded at 6 different times in sequence marked by gridlines in Figure 7.10 are plotted in Figure 7.11. Waveform number 3 was recorded with air flowing through the test object. It has very similar current wave shape as Waveform number 1 recorded at the beginning of the test. In addition, the distributions of the detected PD events match well with the excess current waveforms, indicating the excess current is mainly caused by the

simultaneously detected PD activity. This is in contrast to the other two waveforms, number 2 and 4, which were recorded when non-PD excess currents dominated. These are similar to the waveforms shown in Figures 6.5 and 7.8. Thus it is clear that the established non-PD excess current appearing in waveform 2 can be removed by air flow around the test object. After stopping the air flow, the non-PD excess current recovers again and the PD activity reduces accordingly as confirmed by results shown in Figure 7.10 between 800s and 1200s. With the nearly constant integrated excess current level, the recorded sum of PDs amplitudes reduces, which implies the non-PD excess currents are gradually increased.

Current waveforms number 5 and 6 shown in the bottom frame of Figure 7.11 further confirms that flowing air can remove the non-PD excess current. Waveform number 5 was recorded right after the voltage level reduction. It is very similar to the non-PD excess current waveforms presented in Figure 7.6. Waveform 6 was recorded with air flow. Despite the difference in current amplitudes, another clear difference is discovered from the phases. Waveform 6 has a 90° degree phase shift as compare to the applied voltage, i.e. identical as the capacitive current. It is therefore not a non-PD excess current but rather a component of the capacitive current, which presumably reflects the degradation of the test object after 1200 s PD exposure, the difference is about 0.5 μA in peak current as compared to the reference measurement performed at the beginning of the test. This provides us an indication of the accuracy in the measured PD excess currents. In this case, the absolute error due to changes in the test object is less than 1 %.

With the results presented above, it is confirmed that changes of the PD activity amplitude is closely related to the non-PD excess current. Further, as the non-PD excess current can be quickly removed by the air flow in the twisted pair tests, the non-PD excess current is presumably present in the gas medium, i.e. the charges are mainly concentrated in the surrounding air and can be quickly moved and locally reduce electric field strength, thus lowering the PD activity. It would be certainly interesting to know how fast these changes can be moved by the excitation voltage and measurements under different voltage rise times are further investigated in the following section.

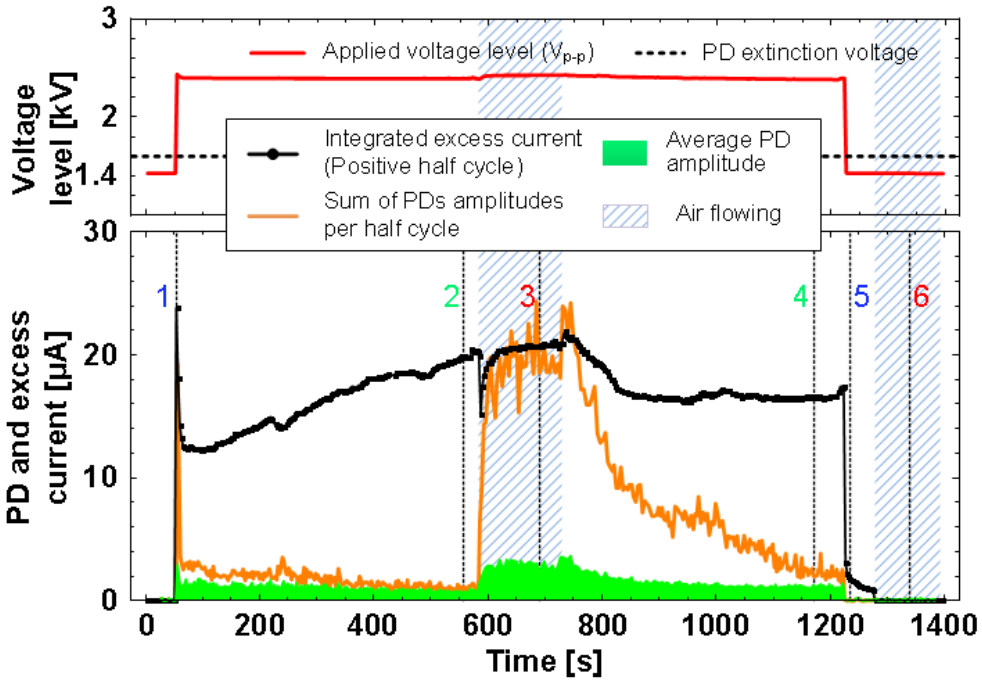

Figure 7.10. Time development of PD activity reflected by integrated excess current, average PD amplitude and sum of PDs amplitudes at positive half periods of 500 Hz sinusoidal voltage applied to twisted pair specimen in test air tunnel. The shaded areas indicate time slots when air was blown through the test tunnel. The excess current waveforms from times marked by gridlines are further presented in Figure 7.11.

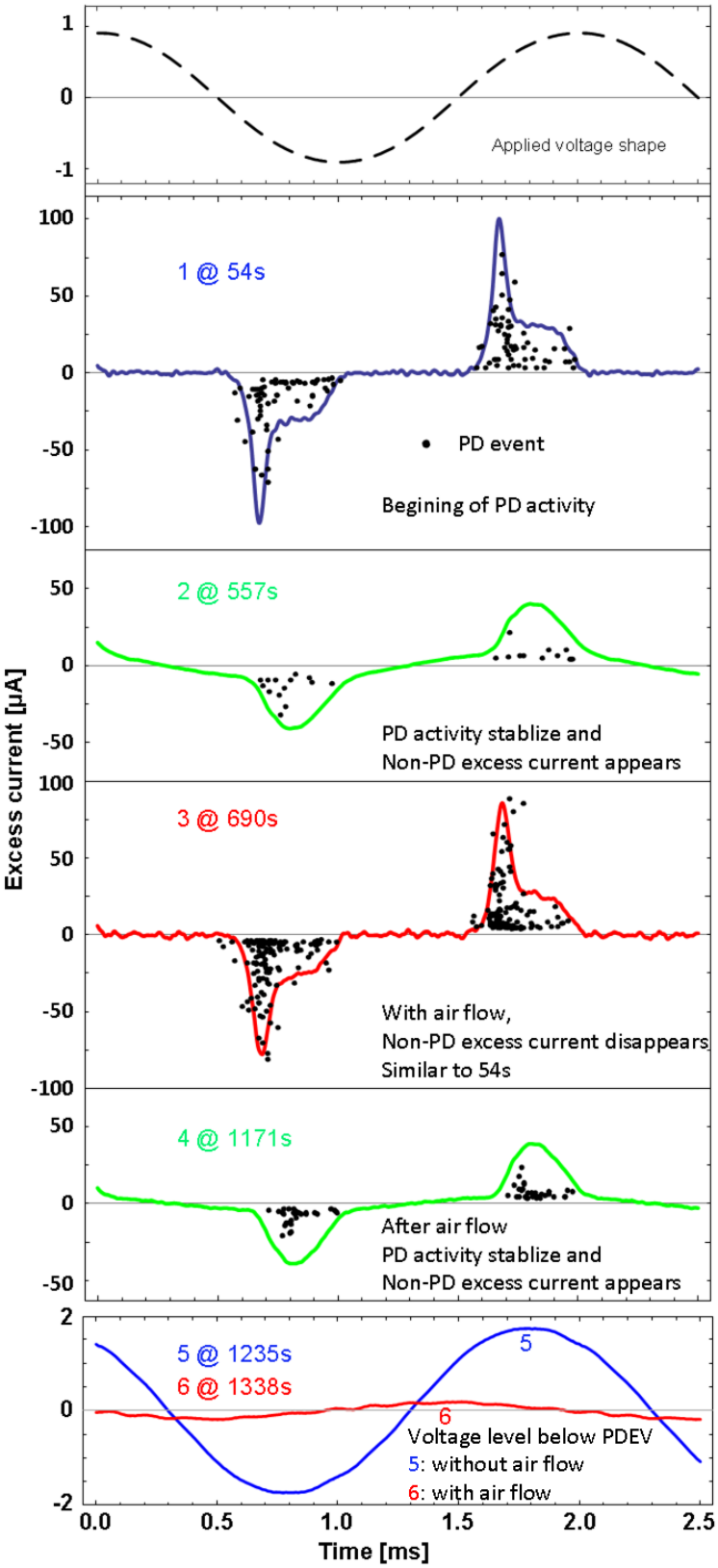

Figure 7.11. Excess current waveforms and PD events recorded at different times indicated by grid lines in Figure 7.10.

7.3 Influence of voltage rise time

Results presented in the previous section brought up a question on how fast the charges generated by PD activity around the test object can move. Therefore measurements under different voltage rise times are further investigated in this section. With the voltage shapes used hitherto in this work, we have seen that the non-PD excess current closely follows the voltage shape at the rising flank. In this section we report on measurements on twisted pair specimens under semi-square voltage waveforms with different rise times.

The used waveforms were of the same amplitude and frequency (500 Hz) but of different rise times: 40 μs, 200 μs and 700 μs. For each of the voltage waveforms, the specimen was first subjected to 2.7 kV for 200 s. The voltage was then decreased to 1.5 kV to evaluate the non-PD excess current waveforms. The PDEV of the specimen is about 1.6 kV for all the waveforms. Figure 7.12 shows the three non-PD excess current waveforms together with the voltage shapes.

The part of the non-PD excess current at the polarity shift follows the voltage variation, despite its rise time varies by a factor of 20. An interesting aspect is whether this tendency will continue for even shorter rise times. At present, the rise times possible to study are limited both by the sampling rate of the DAQ as well as the switching jitter, discussed in section 4.2.2. To enable studies of even faster rise times, resolving the excess current in the time domain as discussed in sections 3.3.1 and 3.3.3 might be a better solution.

The overall wave shape of the non-PD excess currents at different rise times show however a varying response to the applied voltage. This observation is an additional piece of information on the detailed nature of the non-PD excess current.

The amplitude of the non-PD excess current is found to be dependent on the rise time, possibly because of varying PD exposure. The part of the non-PD excess current at the polarity shift follows the voltage variation and at the fastest rise time and its peak level is twice as large comparing to the lowest one. Indeed, pulse PD measurements reported in [75] revealed an increase in summed PD amplitude in twisted pair specimens for rise times below 100 μs, being consistent with the present observation.

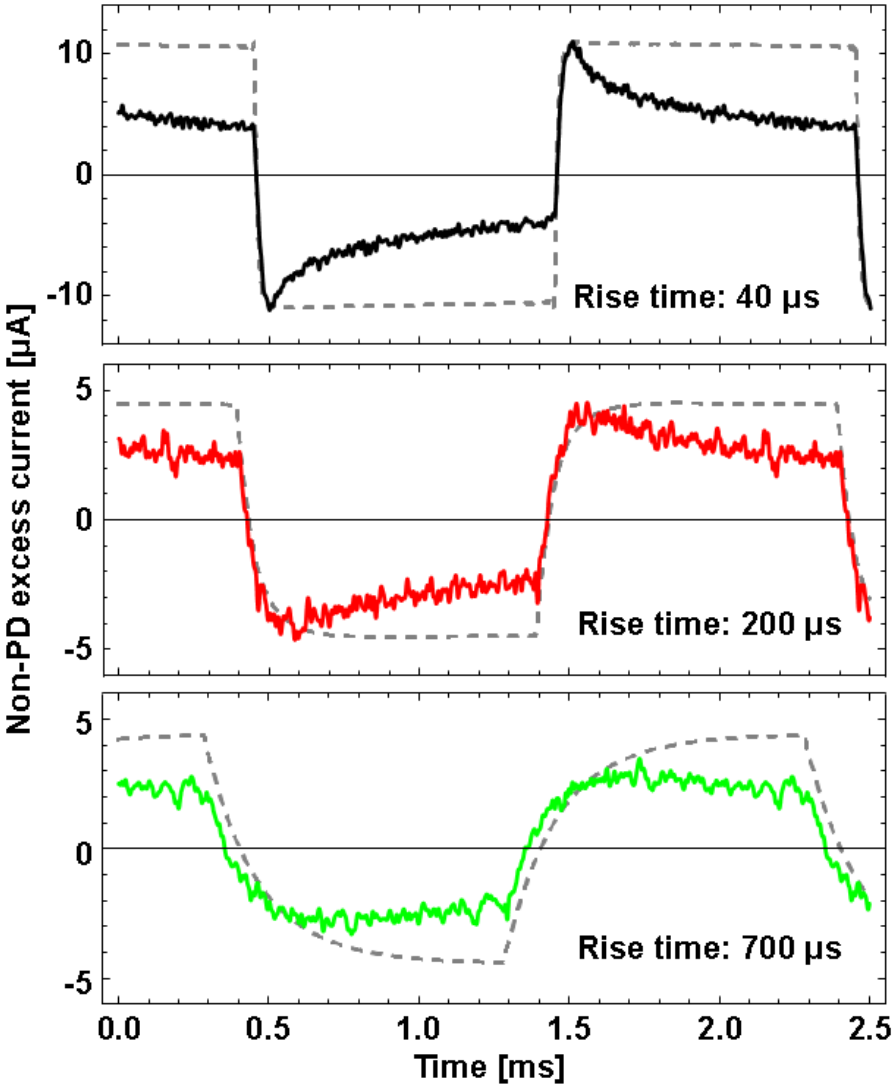

Figure 7.12. Three non-PD excess current waveforms that are measured with voltages of different rise times below PDEV, the waveforms are obtained right after the twisted pair specimens had been exposed to PD activity for about 200 s. The voltage shapes are scaled to fit the current waveforms as a reference.

7.4 Cavity wall influence

The results presented in section 6.2 showed different PD activity oscillations patterns in cavity specimens made out of different middle layer dielectrics. Thus, one cause of the difference could be attributed to the differences between the cavity wall conductivities. To verify this assumption, the test procedure was repeated on another PC-PA cavity, similar to the cavity used in section 6.2.3 but with the wall covered by a thin layer of graphite to increase its surface conductivity.

The measurement results from the modified PC-PA cavity specimen are presented in Figure 7.13. These appear to be similar to the results obtained on Epoxy-PA specimen, as shown in the Figures 6.6 and 6.9. To provide more details of measured excess current waveforms, the ones captured at time points marked as gridlines in Figure 7.13 are presented in Figures 7.14 and 7.15.

Figure 7.14 shows PD excess current waveforms from three different stages of one oscillation period. A distinct difference is observed between the non-PD excess current waveforms before 0.1 ms and the PD current peaks. In the present specimen, the PD activities appear to occur after the non-PD excess currents have reached their

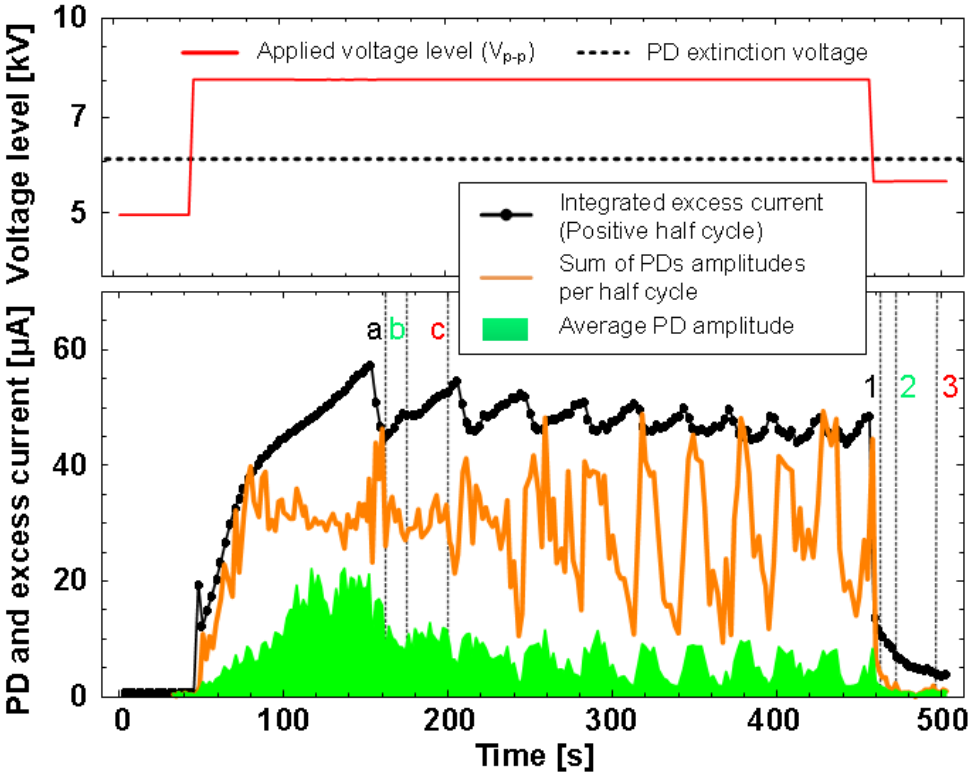

Figure 7.13. Integrated PD excess current and summed PD amplitude of a cavity PC-PA specimen with increased conductivity on the cavity wall. A similar PD oscillation is observed as in Epoxy-PA specimen (section 6.2.1). The excess current waveforms from times marked by gridlines are further presented in Figure 7.14 (a, b, c) and Figure 7.15 (1, 2, 3).

peak and start to decay. Similar to the Epoxy-PA specimen, shown in Figure 6.10, is that the decrease in the excess current PD peaks is accompanied with an increase of the non-PD excess currents, which is visible before and after the PD peak.

The observed non-PD excess currents at voltage level below PDEV, shown in Figure 7.15, have a similar shape and their amplitudes are decaying in time. This is similar to the observations found from the other tested specimens. However, compared to all other non-PD excess currents presented, the shape of the waveforms from the modified specimen does not follow the voltage shape. There are clear dips at the rising fronts, particularly at positive polarity. This is presumably due to the presence of different conduction paths in the cavity, the first current peak may result from the conducting wall followed with charge movements in the gas medium, or vice versa. At the same time the peaks at negative polarity are not identical to the positive ones.

Nevertheless, the PD oscillation pattern observed in both Epoxy-PA and PE cavity specimens as illustrated in section 6.2 is qualitatively reproduced in the PC-PA specimen with modified conductivity of cavity wall. It is therefore assumed that the dynamic behaviour of PD activity in dielectric cavities is related to the level of non-PD excess current amplitude. One of the reasons for the observed difference is presumably brought up by differences in conductivity of cavity walls.

With this experiment we have seen that cavity wall conductance is important for the non-PD excess current. The air flow experiment in section 7.2, showed that the charges involved are present in the gas phase. Thus we must conclude that there are several mechanisms possible.

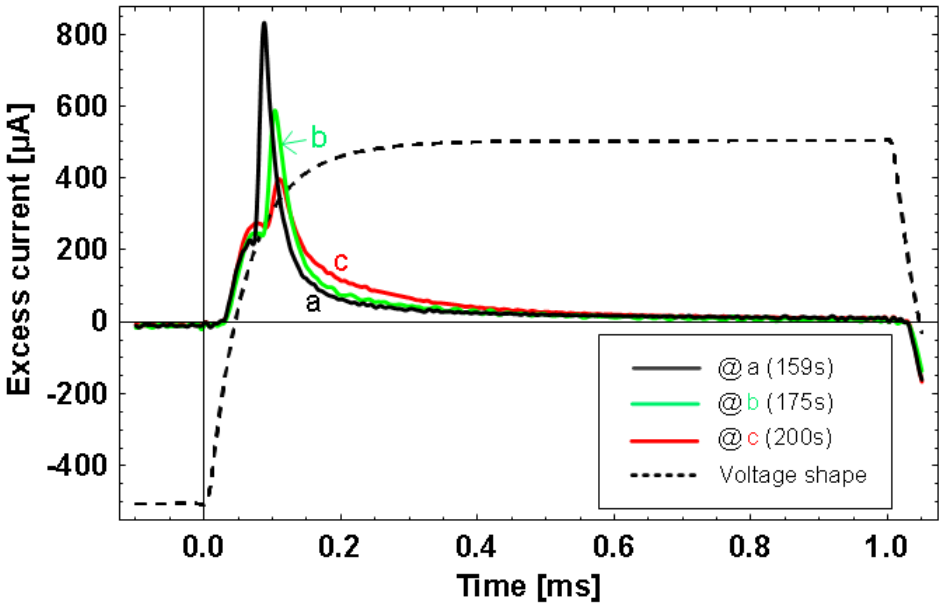

Figure 7.14. Three PD excess current waveforms at the different times indicated in Figure 7.13 at a voltage level above PDIV.

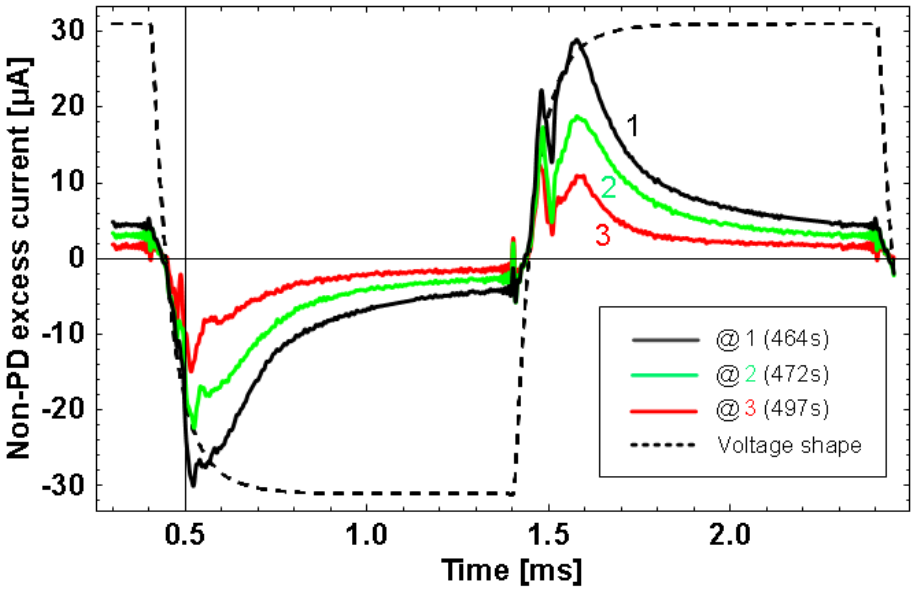

Figure 7.15. Three non-PD excess current waveforms at the different time points indicated in Figure 7.13 with applied voltage level below PDEV.

7.5 Decay of non-PD excess current

It becomes apparent, based on the plots of integrated excess currents below PDEV, such as those shown in Figure 7.1, that their decay may take minutes or even hours. This is a natural consequence of charge decay characteristics in solid-gas insulating media. The decay rate is however not only important below PDEV, above PDEV it is the balance between charge liberation by PDs and the recombination rate that determines the magnitude of the non-PD excess current. Studies of the decay rate are thus important for the understanding of the non-PD excess current.

The measurements performed showed however that the decay rate may vary even during the same experiment, not to mention between experiments and in this section two examples are elucidated for potentially inspiring future work. The two decay examples shown are extracted from previously presented tests: the twisted pair tests with occasionally reduced voltage level in section 7.1 and the PC-PA cavity specimen measured under constant voltage level in section 6.2.3. The decaying parts of the integrated excess current are extracted from these experiments and plotted in a logarithmic scale, which is appropriate for determining time constants of an exponential decay.

Figure 7.16 compares 6 decay curves extracted from the twisted pair measurement presented in Figure 7.1. These curves represent the first 6 occasions when the applied voltage level was temporally reduced below PDEV. The results indicate that more than one decay mechanism is active as the slope of the decays changes during the observed time. Further, it takes several decays for the curves to become repeatable.

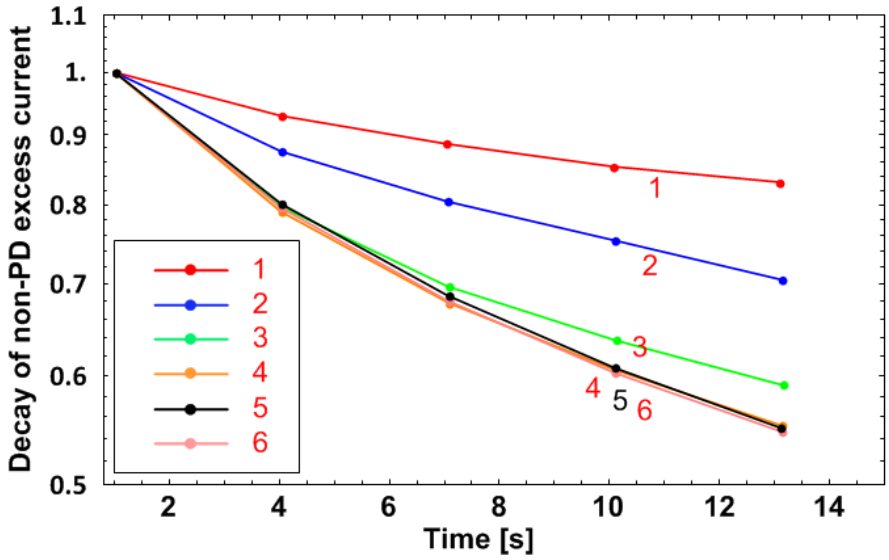

Figure 7.16. Logarithmic plot of 6 non-PD excess current decays measured on a twisted pair specimen as extracted from the first 6 occasions of voltage reduction in the measurement shown in Figure 7.1 and normalized in amplitude as well as in time.

Figure 7.17 compares the 6 decays of the integrated excess currents extracted from Figure 6.12. One should notice that these excess currents were measured with voltage level above PEIV. However, as no PD activity could be detected, which is confirmed by the current waveforms shown in Figure 6.14, the measured excess currents are presumably dominated by the non-PD excess current. The decay of the measured excess current should therefore mainly come from the decay of the non-PD excess current. The numbers marked in the curves indicate the measurement sequence over the time and are also found in Figure 6.12. The curves presented in this logarithmic plot indicate there are at least two different decay mechanisms control the process. In addition, the overall decay rate decreases over time and seem to stabilize towards the end of the experiment. However, compared to the results shown in Figure 7.16, the decay rate increases in the twisted pair object and it decreases in the cavity.

In general, based on numerous measurements not presented here, one may state that the decay of non-PD excess current seems to depend on many factors. However, one of the most important seems to be the environmental conditions during testing and further studies should be performed in a controllable and stable environment.

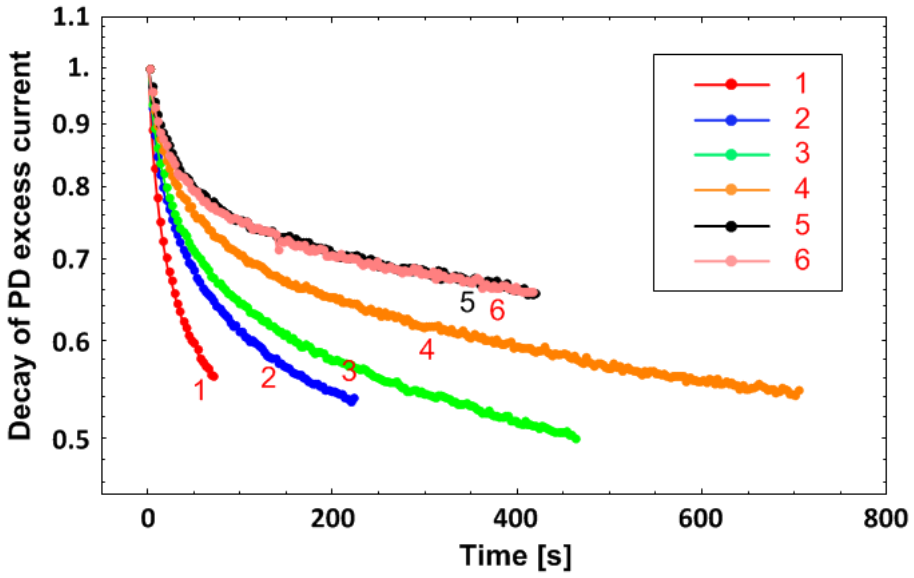

Figure 7.17. Log plot of 6 excess current decays of the PC-PA cavity specimen measured at voltage level above PDIV. The results are extracted from the measurement shown in Figure 6.12 and normalized in amplitude as well as in time.

7.6 Impedance spectrum of the non-PD excess current

It is worth to consider if non-PD excess current can be viewed in other ways, which eventually may yield additional information about its behavior. As the AWIS measurement technique is based on dielectric response measurements, where a frequency dependent impedance is deduced, it is natural and relatively easy to represent the non-PD excess currents in these terms. The semi-square test waveform is very useful here, as it provides a wide impedance spectrum of the object and an attractive feature is that it should be independent of the test waveform if the response is linear. The linear behavior of the non-PD excess currents has been demonstrated in the previous section and therefore the impedance representation is justified.

Calculation of the non-PD excess current impedance is based on an assumption that an in-parallel connected conduction path appears in the tested system. For an added parallel circuit, the impedance can be found by the difference in conductance, thus

$$Z_e = \frac{1}{\frac{1}{Z_T} - \frac{1}{Z_{to}}} = \frac{V_0}{I_{exc}} \tag{7.1}$$

where Z_{to} is the impedance obtained from the reference measurement. Z_T is the total impedance with non-PD excess current and Z_e is the impedance generating the non-PD excess current. V_0 and I_{exc} are the applied voltage and the excess current defined in equation (3.1). All harmonics with sufficient amplitude in the test voltage waveform can be utilized. In the below presented example this implies 500 Hz and its odd harmonics up to about 10 kHz.

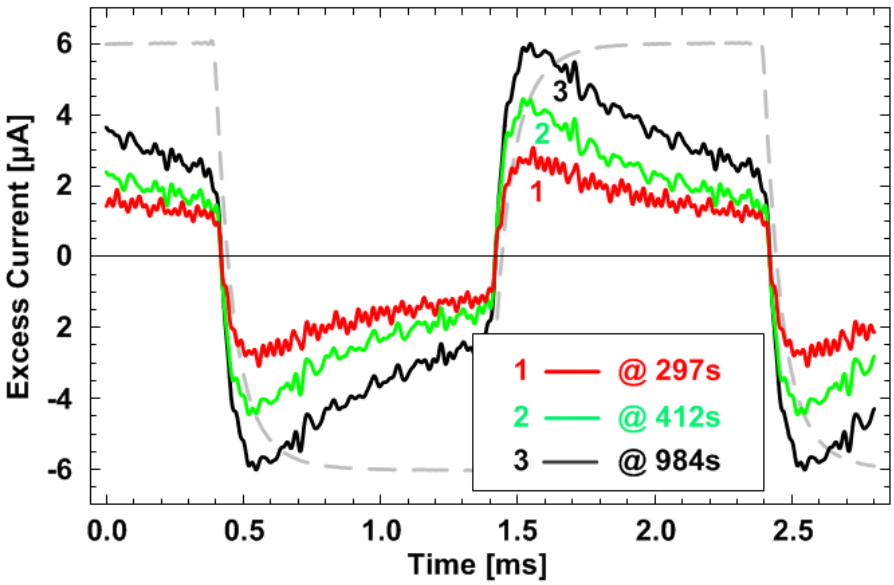

Figure 7.18. Non-PD excess currents from the measurement presented in section 7.1, for time points, marked as 1, 2, 3 in Figure 7.4.

As an example, the non-PD excess currents at reduced voltages in a twisted-pair specimen are studied. The measurement is described in section 7.1. The time instants chosen to clearly illustrate the impedance development are at 297 s, 412 s and 984 s, as respectively marked in Figure 7.4 as points 1, 2 and 3. Figure 7.18 shows the time domain currents at the chosen instants while the amplitude and phase of impedances obtained based on these currents are illustrated in Figures 7.19 and 7.20.

The amplitudes of the impedances obtained, as shown in Figure 7.19, decrease slightly with frequency up to about 10 kHz, while at higher frequencies a stronger decrease is observed. This might be the response from a parallel connection of a resistor with a small capacitor. Variable values of these parameters would however be required to represent different non-PD excess currents observed.

It is no surprise that the non-PD excess current impedance is predominantly resistive, as its wave shape has been found to follow the test voltage quite well at the rising front. The similarity to a resistance fails however when the impedance angle is considered as shown in Figure 7.20. Already at the lowest frequencies the angle is different from zero and thereafter stabilizes at about 20° for the all three currents. These results are consistent with the results using sinusoidal test voltages (seen Figure 7.6). Above 7 kHz, the accuracy of this estimation seems to degrade as large deviations appear in the results, presumably due to a reduced sensitivity.

One may speculate on the nature of the excess current based on the above presented results. The real part of the impedance should be viewed as a measure of the work performed by moving the charges constituting the current. If the work to move a single charge unit is constant during the experiment, then the real part of the impedance should reflect the energy lost by charge carriers and their number. If thus the active charge can be determined in another way, information on the charge transport properties could be obtained.

The angle frequency dependence could be interpreted as resulting from a capacitor with limited charge, which gives a voltage response equal to the charge divided by the capacitance. Then, if the active capacitance could be estimated, a measure on the active charge would be obtained. Further tests with more accurately calibrated sensors are required here to draw any firm conclusions.

The discussions above should however be viewed as an initial try to extract more information on the nature of the non-PD excess current. More work in the form of theoretical calculations and careful experiments is certainly needed.

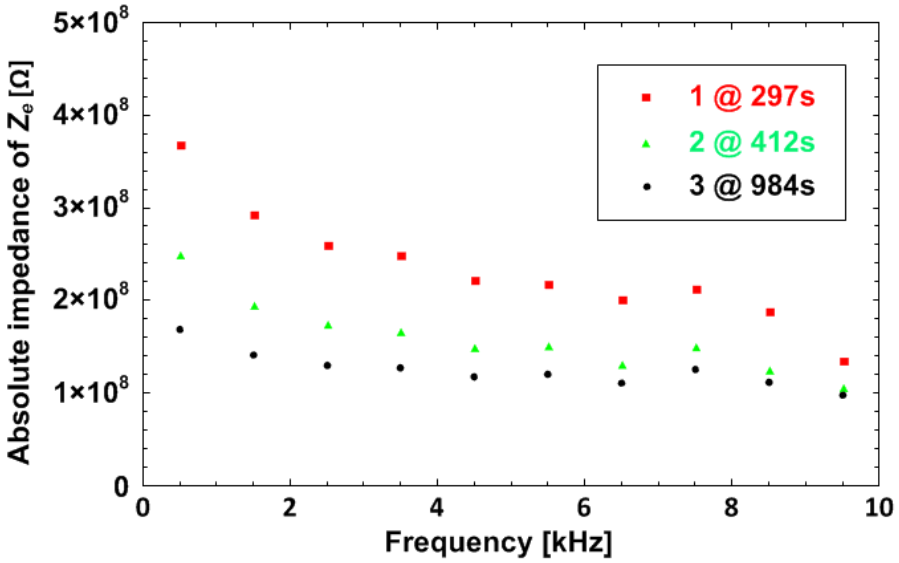

Figure 7.19. Frequency variation of the impedance amplitude obtained from the non-PD excess currents measured for a twisted pair test object.

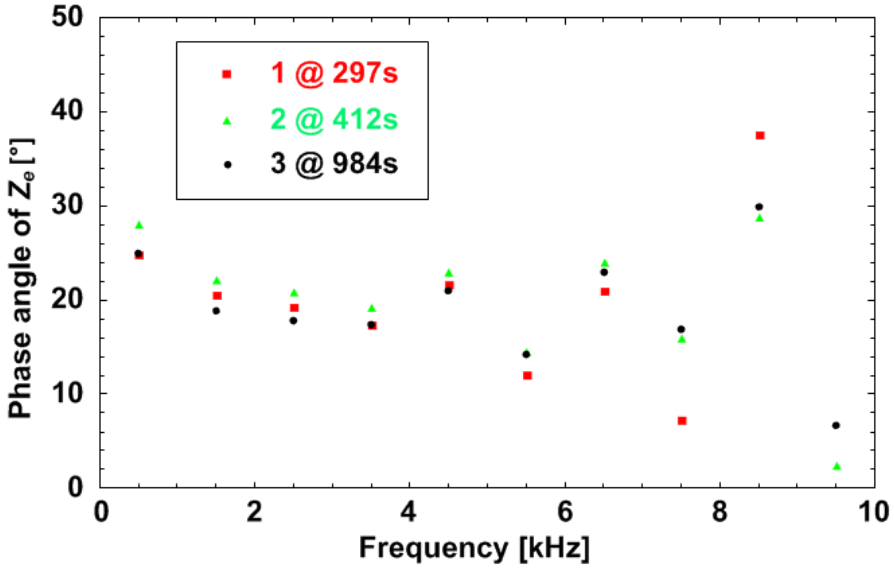

Figure 7.20. Frequency dependence of the impedance phase angle obtained from the non-PD excess currents measured for a twisted pair test object.

8 Conclusions

8.1 Partial discharge excess current

The aim of this work concentrated on complementing conventional pulse PD detection by measurements that could allow detecting both slow and fast charge movements of the PD activity. Further, as PD occurrence and its observed variation can be treated as an indicator of insulation system degradation, it becomes motivated to apply the developed technique for studying the long-term behaviour of PD activity in order to better understand how the variation influences insulation life time. This aim was achieved by using dielectric response measurements based on AWIS technique together with stochastic PD detection and is further summarized in the following three stages.

8.1.1 Partial discharge activity measured as excess current

The PD excess current measurement by means of AWIS technique secures sensitivity to all PD events by utilizing an integrating current shunt. To achieve a better resolution, a front resistor was implemented to slow down the fast discharge front, thus lowering the noise level. In addition, the choice between resolving the PD excess current in the time or in the frequency domain were discussed and exemplified with two test waveforms deficiencies that influence the choice.

Based on several verification examples, it has been illustrated that the excess current accounts for both number and amplitude of discharges and can thus be used for evaluating the impacts of many small against a few large discharges. Further, the measured excess current waveforms were compared with the currents that were estimated from simultaneously detected PD pulses by the stochastic PD detection. It was observed that, due to the pulse threshold required in the conventional PD detection methods, even the summed amplitude of all PD events could not properly account for the total discharge current if there appear many small PDs. The excess current is sensitive to all weak discharges as well as to other slower contributions that are below the conventional PD detection frequency range.

It is therefore claimed that measurements of the PD excess current can serve as an important complement providing useful and additional information about PD activity in various types of objects. However, it is conceivably not possible to apply this technique in all situations where pulse PD detection is presently used, as the PD excess current must constitute a significant fraction of the total measured current. Therefore, the application is limited to objects characterized by low capacitance, such as material samples or model insulation objects.

8.1.2 PD activity variations

For all the specimens studied, the detected PD activity quantitatively repeats a similar behaviour: it decays or even disappears after some initial significant discharges. In contrast, the measured excess currents show an increase and finally stabilization during the same period of time. From these experiments another significant current contribution, a non-PD excess current, was found.

More surprisingly, oscillations of PD activity were observed in dielectrically insulated cavity specimens and the effect seems to result from an interaction between PD activity and the non-PD excess current. Repetition times and amplitudes of the oscillations can apparently vary widely, which indicates that material properties, such as surface conductivity, play a role.

8.1.3 Non-PD excess current studies

The existence of the non-PD excess currents is demonstrated by performing experiments, in which the applied voltage is occasionally decreased below the PDEV, the PD and the non-PD excess currents can thus be separated. The non-PD excess current decays when the voltage is kept below PDEV. The non-PD excess current contribution to the total excess current under PD activity can be obtained by linear scaling with the voltage. The non-PD excess current follows the front of the voltage wave shape. There is however a phase shift observed, possibly indicating a certain influence of a capacitive component in the current.

It is shown, by circulating air around a twisted pair specimen during PD activity that the discharge amplitude can be influenced and the non-PD excess current forced to disappear. It is therefore assumed that the current results from ion movement in the gas and quickly move, reducing the local electric field and thus lowering the PD activity. In addition, tests under voltages of different rise times indicate that the part of the non-PD excess current at the polarity shift follows the voltage variation, despite the rise time has been varied by a factor of 20. Tests under even shorter rise times were not possible in this study due to equipment limitations, such as limited sampling rate of the DAQ card as well as switching jitter.

Changing of PD activity pattern into an oscillation mode is also possible in a cavity specimen by modifying its wall conductance. Together with the air flow experiment, showing that charges involved are present in the gas phase, we must conclude that other mechanisms may also operate for non-PD excess current to interact with PD activity. Further extensive studies on this topic are certainly required.

Impedance spectrum analysis was applied to the non-PD excess current to provide some alternative information on the nature of the current. Very weak frequency dependence, dominated by a predominantly resistive like component, is found. How the impedance function obtained from the non-PD excess current should be interpreted requires more consideration. The real part of the impedance could, for example, be viewed as the work done by the moving charges.

8.2 Philosophy of electrical measurement

From enhancements in over 100 years old dielectric response measurement to the latest discovery of non-PD excess current, this study uses the same technique and similar circuits but measured voltages range from a few microvolts up to tens of kilovolts and covering a frequency range from sub-mHz up to hundreds of kHz. Averaging and referencing push the accuracy level beyond the instrument specification, which, joined with powerful computational ability, facilitates these difficult investigations. Here, some reflections that have arisen during this project are presented with the hope to generate ideas for future explorations.

Improvement of measurement accuracy has always been one of the primarily goals in developing measurement techniques. In the electrical measurements, the noise level is a main burden. Proper shielding may reduce external noises a bit, some other noises, such as temperature and digitalization noises, are yet remaining. Here, averaging might be the most effective general way, as it can increase the signal-to-noise level with a factor of the square root of the number of measurements averaged. With increasing computational power of modern computers, extensive averaging becomes possible. In addition, averaging also facilitates statistic studies of stochastic phenomena, which serves as another advantage in high voltage applications. Though, limitations may eventually come from time resolution of the measurement. In all, averaging is central to all measurement techniques that were employed in this work.

Whether relative measurements of electrical parameters can be acceptable instead for absolute determinations can be debated. Considering the definition of many electrical quantities, an "absolute" measurement is often in practice a relative one. This provides an alternative to improve accuracy by referencing, as systematic errors are often dominating over relative ones. The systematic errors result from calibration of instruments and modelling of measurement setups. With referencing to a known measurement using identical setup and instrument, the systematic errors can largely be eliminated. Further, elaborate calibrations of all individual components may not be necessary. Referencing however require a carful design of the experimental procedure, linearity of instrumentation as well as some decent vertical accuracy and resolution. The word "decent" here depends on the specific experiment design. In this work, both the air referencing and the excess current are relative measurements of similar nature.

Sacrificing some accuracy may eventually be a gain. People are often reluctant to sacrifice a few percent of accuracy by introducing additional facilities even though these could simplify an elaborate testing procedure or eliminate some systematic errors. A balance between gain and drain may provide some alternative thinking on electrical measurements and may enable some more insights of entities that are presently not possible to measure. The contact-free electrode arrangement in dielectric response characterization is an example of sacrificing a little and gaining more.

Taking advantages of the excessive computational power offered by modern computers is another path to further explore in electrical measurement techniques. The algorithms employed to continuously pre-process measurement data and monitoring results in the excess current measurements would be impossible on a computer of the late 1990's. Rather complex algorithms may be used for on-line data pre-processing without hindering much of the time resolution. Meanwhile, measurement software

interface should preferably provide as detailed representation of the measured result as possible. With such a facility, many hours of failed experimental and further analysis time can be saved. In addition, horizontal expansion of measurement scale by many repeated measurements may turn quantitative data acquisitions into a qualitative understanding.

Future Work

This thesis introduced a current sensing method based on dielectric response technique to complement the conventional pulse PD detection method for partial discharge studies. Through studies of PD activity variations over time, a non-PD excess current that is closely related to PD activity variations has been observed. Some attempts were also carried out to study a few properties of the non-PD excess current. These studies are far from complete; therefore the future works in this field are to continue the studies of the non-PD excess current properties and to refine the measurement technique with the aim to obtain a better understanding of dielectric materials aging under PDs.

Further studies of the non-PD excess current could focus on to understanding its properties in the following three aspects: speed, existence and quantity. These aspects should be studied under the variation of pertinent parameters, such as voltage, temperature and pressure. The speed of the non-PD excess current is measured with respect to the applied voltage variation. Study of the non-PD excess current under faster voltage rise times may reveal a speed limitation and thus provide a measure of the charge-carrier mobility. "Existence" of the non-PD excess current should be interpreted as the mediums in which the dominating charges are moving to interplay with PDs. An understanding here may provide a possibility to control the non-PD excess current. Quantity of the non-PD excess current refers to the density of moving charges and their life-times. These may be understood thorough a study of non-PD excess current decay. A proper study of all the above mentioned properties of the non-PD excess current may eventually facilitate some control of PD activity.

Refinement of the PD excess current measurement technique would enable border applications. Increase of measurement resolution and sensitivity are of importance to evaluate weaker PD activities as well as for testing of insulation systems characterized with higher capacitances. Control of testing environments should also be refined for different test objects to ensure better repeatability of the PD excess current measurements. Comparison of material aging under PD activity of the same voltage but with and without presence of non-PD excess current would be valuable to illustrate the importance of this current for insulation lifetime.

Another much broader area for future studies is to apply PD excess current measurement technique to study various dielectric materials and insulation systems under PD activity for material characterization as well as insulation system design.

References

[1] J. E. H. Gordon, "Measurements of Electrical Constants. No. II On the Specific Inductive Capacities of Certain Dielectrics. Part I", Philosophical Transactions of the Royal Society of London, Vol. 170, pp. 417-446, 1879.

[2] D. Nattrass, "Partial discharge. XVII. The early history of partial discharge research", Electrical Insulation Magazine, IEEE, Vol. 9, Iss. 4, pp. 27-31, 1993.

[3] J. Hedberg and T. Bengtsson, "Straight Dielectric Response Measurements with High Precision", Nord-IS 05, Trondheim, Norway, pp. 174-177, 2005.

[4] B. Sonerud, T. Bengtsson, J. Blennow, and S. M. Gubanski, "Dielectric response measurements utilizing semi-square voltage waveforms", IEEE Trans. Dielectr. Electr. Insul., Vol. 15, Iss. 4, pp. 920-926, 2008.

[5] T. Bengtsson, E. Lindell, and T. Hammarström, "Stochastic Detection of Partial Discharges", IEEE Trans. Dielectr. Electr. Insul., Vol. 20, Iss. 6, pp. 2203-2211, 2013.

[6] T. Hammarström, "Partial Discharges at Fast Rising Voltages", Doctoral thesis, Chalmers University of Technology, 2014.

[7] F. H. Kreuger, *Partial Discharge Detection In High Voltage Equipment*, Oxford: Butterworth-Heinemann, 1989.

[8] G. C. Montanari, "Aging and life models for insulation systems based on PD detection", IEEE Trans. Dielectr. Electr. Insul., Vol. 2, Iss. 4, pp. 667-675, 1995.

[9] G. C. Stone and H. G. Sedding, "In-service evaluation of motor and generator stator windings using partial discharge tests", Industry Applications, IEEE Trans. on, Vol. 31, Iss. 2, pp. 299-303, 1995.

[10] P. H. F. Morshuis, "Degradation of solid dielectrics due to internal partial discharge: some thoughts on progress made and where to go now", IEEE Trans. Dielectr. Electr. Insul., Vol. 12, Iss. 5, pp. 905-913, 2005.

[11] L. Wang, A. Cavallini, G. C. Montanari, and L. Testa, "Patterns of partial discharge activity in XLPE: from inception to breakdown", Solid Dielectrics (ICSD), 2010 10th IEEE International Conference on, pp. 1-4, 2010.

[12] C. S. Kim, T. Kondo, and T. Mizutani, "Change in PD pattern with aging", IEEE Trans. Dielectr. Electr. Insul., Vol. 11, Iss. 1, pp. 13-18, 2004.

[13] P. H. F. Morshuis, "Partial discharge mechanisms", Doctoral thesis, Delft university of technology, 1993.

[14] L. Wang, "Physical model of PD behavior and relevant damage growth from micro-cavities in polyethylene-based material under AC voltage", Doctoral thesis, Università di Bologna, 2011.

[15] X. Xu, "Enhancements in Dielectric Response Characterization of Insulation Materials", Licentiate thesis, Materials and Manufacturing Technology, High voltage engineering, Chalmers University of Technology, Gothenburg, Sweden, 2013.

[16] L. Niemeyer, "A generalized approach to partial discharge modeling", Dielectrics and Electrical Insulation, IEEE Transactions on, Vol. 2, Iss. 4, pp. 510-528, 1995.

[17] D. König and Y. N. Rao, *Partial Discharges in Electrical Power Apparatus*, Vde Verlag GmbH, 1993.

[18] A. Reid and M. Judd, "Ultra-wide bandwidth measurement of partial discharge current pulses in SF6", Journal of Physics D: Applied Physics, Vol. 45, Iss. 16, p. 165203, 2012.

[19] IEC 60270, High Voltage Test Techniques – Partial Discharge Measurements 2000.

[20] E. Kuffel, W. S. Zaengl, and J. Kuffel, *High Voltage Engineering: Fundamentals*, Newnes, 2000.

[21] A. Kelen, "Critical Examination of the Dissipation Factor Tip-Up as a Measure of Partial Discharge Intensity", Electrical Insulation, IEEE Transactions on, Vol. EI-13, Iss. 1, pp. 14-24, 1978.

[22] T. W. Dakin, "The Relation of Capacitance Increase with High Voltages to Internal Electric Discharges and Discharging Void Volume", Power Apparatus and Systems, Part III. Transactions of the American Institute of Electrical Engineers, Vol. 78, Iss. 3, pp. 790-794, 1959.

[23] B. Sonerud, J. Blennow, S. M. Gubanski, S. Nilsson, and T. Bengtsson, "Continuous monitoring of dielectric properties of LDPE samples during electrical treeing", Solid Dielectrics (ICSD), 2010 10th IEEE International Conference on, pp. 1-4, 2010.

[24] J. T. Holbøll, H. Edin, and U. Gäfvert, "Time domain PD-detection vs. dielectric spectroscopy", IEEE 1997 Annual Report - Conference on Electrical Insulation and Dielectric Phenomena, Minneapolis, pp. 498-503, 1997.

[25] H. Edin and U. Gafvert, "Harmonic content in the partial discharge current measured with dielectric spectroscopy", Electrical Insulation and Dielectric Phenomena, 1998. Annual Report. Conference on, pp. 394-398 vol. 2, 1998.

[26] N. Taylor, "Dielectric response and partial discharge measurements on stator insulation at varied low frequency", Doctoral thesis, Electromagnetic Engineering, Royal Institute of Technology, Stockholm, 2010.

[27] N. Taylor; and H. Edin, "Differences between PD charges measured by Partial Discharge and Dielectric Spectroscopy systems", 21st Nordic Insulation Symposium (NordIS), Gothenburg, Sweden, pp. 69-73, 2009.

[28] B. Sonerud, T. Bengtsson, J. Blennow, and S. Gubanski, "Twisted pair sample subjected to square voltages: Measurements of dielectric properties during partial discharges", Proceedings of the 16th International Symposium on High Voltage Engineering, Cape Town, South Africa, pp. B-31, 2009.

[29] I. Shim, J. J. Soraghan, and W. H. Siew, "Digital signal processing applied to the detection of partial discharge: an overview", Electrical Insulation Magazine, IEEE, Vol. 16, Iss. 3, pp. 6-12, 2000.

[30] G. C. Stone, H. G. Sedding, N. Fujimoto, and J. M. Braun, "Practical implementation of ultrawideband partial discharge detectors", Electrical Insulation, IEEE Transactions on, Vol. 27, Iss. 1, pp. 70-81, 1992.

[31] X. Wang, B. Li, Z. Xiao, S. H. Lee, H. Roman, O. L. Russo, K. K. Chin, and K. R. Farmer, "An ultra-sensitive optical MEMS sensor for partial discharge detection", Journal of Micromechanics and Microengineering, Vol. 15, Iss. 3, p. 521, 2005.

[32] A. Zargari and T. R. Blackburn, "Application of optical fibre sensor for partial discharge detection in high-voltage power equipment", Electrical Insulation and Dielectric Phenomena, 1996., IEEE 1996 Annual Report of the Conference on, pp. 541-544 vol.2, 1996.

[33] R. Bartnikas, "Partial discharges. Their mechanism, detection and measurement", Dielectrics and Electrical Insulation, IEEE Transactions on, Vol. 9, Iss. 5, pp. 763-808, 2002.

[34] T. Bengtsson, H. Kols, and B. Jönsson, "Transformer PD Diagnosis using Acoustic Emission Technique", 10th Int. Symp. High Voltage Engineering (ISH), Montréal, Canada, pp. 73-79, 1997.

[35] H. Okubo and N. Hayakawa, "A novel technique for partial discharge and breakdown investigation based on current pulse waveform analysis", Dielectrics and Electrical Insulation, IEEE Transactions on, Vol. 12, Iss. 4, pp. 736-744, 2005.

[36] H. Okubo, A. Matsushita, S. Watanabe, N. Hayakawa, and T. Kumai, "Investigation of electrical insulation diagnosis of solid insulators in GIS by partial discharge current pulse waveform analysis (PD-CPWA)", Transmission and Distribution Conference and Exhibition 2002: Asia Pacific. IEEE/PES, pp. 925-930 vol.2, 2002.

[37] H. Okubo, N. Hayakawa, and A. Matsushita, "The relationship between partial discharge current pulse waveforms and physical mechanisms", Electrical Insulation Magazine, IEEE, Vol. 18, Iss. 3, pp. 38-45, 2002.

[38] G. P. Cleary and M. D. Judd, "UHF and current pulse measurements of partial discharge activity in mineral oil", Science, Measurement and Technology, IEE Proceedings -, Vol. 153, Iss. 2, pp. 47-54, 2006.

[39] R. Patsch and F. Berton, "Pulse Sequence Analysis-a diagnostic tool based on the physics behind partial discharges", Journal of Physics D: Applied Physics, Vol. 35, Iss. 1, p. 25, 2002.

[40] R. Patsch and F. Berton, "Pulse-sequence-analysis-chances to characterize defects", Electrical Insulation and Dielectric Phenomena, 1999 Annual Report Conference on, pp. 243-248 vol.1, 1999.

[41] J. Giddens, H. Edin, and U. Gafvert, "Measuring system for phase-resolved partial discharge detection at low frequencies", High Voltage Engineering, 1999. Eleventh International Symposium on (Conf. Publ. No. 467), pp. 228-231, 1999.

[42] C. Hudon and M. Belec, "Partial discharge signal interpretation for generator diagnostics", Dielectrics and Electrical Insulation, IEEE Transactions on, Vol. 12, Iss. 2, pp. 297-319, 2005.

[43] T. Tanaka, "Partial discharge pulse distribution pattern analysis", IEE Proceedings-Science, Measurement and Technology, Vol. 142, Iss. 1, pp. 46-50, 1995.

[44] N. C. Sahoo, M. M. A. Salama, and R. Bartnikas, "Trends in partial discharge pattern classification: a survey", Dielectrics and Electrical Insulation, IEEE Transactions on, Vol. 12, Iss. 2, pp. 248-264, 2005.

[45] A. Krivda, "Automated recognition of partial discharges", IEEE Transactions on Dielectrics and Electrical Insulation [see also Electrical Insulation, IEEE Transactions on], 2 (5), 1995.

[46] F. Kreuger, E. Gulski, and A. Krivda, "Classification of partial discharges", IEEE Transactions on Electrical Insulation, 28 (6)[see also IEEE Transactions on Dielectrics and Electrical Insulation], 1993.

[47] E. Gulski and A. Krivda, "Neural networks as a tool for recognition of partial discharges", Electrical Insulation, IEEE Transactions on, Vol. 28, Iss. 6, pp. 984-1001, 1993.

[48] B. A. Fruth and D. W. Gross, "Partial discharge signal generation transmission and acquisition", Science, Measurement and Technology, IEE Proceedings -, Vol. 142, Iss. 1, pp. 22-28, 1995.

[49] B. Sonerud, "Characterization of Electrical Insulation Exposed to Arbitrary Voltage Waveforms", Doctoral thesis, Department of materials and manufacturing technology, Chalmers University of Technology, Göteborg, 2010.

[50] E. Lindell, "Partial Discharges at Repetitive Rapidly Changing Voltages", Doctoral thesis, Chalmers University of Technology, Göteborg, 2009.

[51] B. Sonerud, T. Bengtsson, J. Blennow, and S. M. Gubanski, "Dielectric response measurements utilizing non-sinusoidal waveforms", Electrical Insulation and Dielectric Phenomena, 2006 IEEE Conference on, pp. 43-46, 2006.

[52] B. Sonerud, T. Bengtsson, J. Blennow, and S. M. Gubanski, "Dielectric response measurements utilizing semi-square voltage waveforms", Dielectrics and Electrical Insulation, IEEE Transactions on, Vol. 15, Iss. 4, pp. 920-926, 2008.

[53] B. Sonerud, T. Bengtsson, J. Blennow, and S. M. Gubanski, "Dielectric heating in insulating materials subjected to voltage waveforms with high harmonic content", Dielectrics and Electrical Insulation, IEEE Transactions on, Vol. 16, Iss. 4, pp. 926-933, 2009.

[54] B. Sonerud, T. Bengtsson, J. Blennow, S. M. Gubanski, and S. Nilsson, "Capacitance measurements and tree length estimation during electrical treeing in sub-picofarad samples", IEEE Trans. Dielectr. Electr. Insul., Vol. 16, Iss. 6, pp. 1707-1709, 2009.

[55] B. Sonerud, T. Bengtsson, J. Blennow, and S. Gubanski, "Measurement and analysis of partial discharge current during square voltage waveforms", Electrical Insulation and Dielectric Phenomena, 2009. CEIDP'09. IEEE Conference on, pp. 368-371, 2009.

[56] E. Lindell, T. Bengtsson, J. Blennow, and S. M. Gubanski, "Measurement of partial discharges at rapidly changing voltages", IEEE Trans. Dielectr. Electr. Insul., Vol. 15, Iss. 3, pp. 823-831, 2008.

[57] E. Lindell, T. Bengtsson, J. Blennow, and S. Gubanski, "Partial discharges measured at semi-square voltages", Electrical Insulation and Dielectric Phenomena, 2006 IEEE Conference on, pp. 631-634, 2006.

[58] E. Lindell, T. Bengtsson, J. Blennow, and S. M. Gubanski, "Influence of rise time on partial discharge extinction voltage at semi-square voltage waveforms", Dielectrics and Electrical Insulation, IEEE Transactions on, Vol. 17, Iss. 1, pp. 141-148, 2010.

[59] E. Lindell, T. Bengtsson, and F. Dijkhuizen, "Partial Discharge Frequency Dependence in Oil/Paper Test Object at Semi-Square Voltages", Proceedings of the 21st Nordic Insulation Symposium, pp., 2009.

[60] T. Hammarström, T. Bengtsson, J. Blennow, and S. M. Gubanski, "Resonant PD signal decoupling circuit for rapidly changing voltages", Nord-IS 11, Tampere, Finland, pp. 149-152, 2011.

[61] T. Hammarstrom, T. Bengtsson, J. Blennow, and S. M. Gubanski, "Evidence for changing PD properties at short voltage rise times", Dielectrics and Electrical Insulation, IEEE Transactions on, Vol. 18, Iss. 5, pp. 1686-1692, 2011.

[62] T. J. A. Hammarstrom, T. Bengtsson, J. Blennow, and S. M. Gubanski, "Partial discharges in motor wires at PWM voltages of different smoothness", Electrical Insulating Materials (ISEIM), Proceedings of 2014 International Symposium on, pp. 184-187, 2014.

[63] T. Hammarstrom, T. Bengtsson, J. Blennow, and S. Gubanski, "PD properties when varying the smoothness of synthesized waveforms", Dielectrics and Electrical Insulation, IEEE Transactions on, Vol. 20, Iss. 6, pp. 2035-2041, 2013.

[64] X. Xu, T. Bengtsson, J. Blennow, and S. M. Gubanski, "Harmonic Limited Test Waveforms for Fast AWIS Dielectric Studies", Nord-IS 11, Tampere, Finland, pp. 199-202, 2011.

[65] X. Xu, T. Bengtsson, J. Blennow, and S. M. Gubanski, "Arbitrary waveform impedance spectroscopy for accurate contact-free dielectric characterization", High Voltage Engineering and Application (ICHVE), pp. 170-173, 2012.

[66] X. Xu, T. Bengtsson, J. Blennow, and S. M. Gubanski, "Enhanced accuracy in dielectric response material characterization by air reference method", IEEE Trans. Dielectr. Electr. Insul., Vol. 20, Iss. 3, pp. 913-921, 2013.

[67] X. Xu, T. Bengtsson, J. Blennow, and S. M. Gubanski, "Correction of Geometric Influence in Permittivity Determination", NORD-IS 13, Trondheim, Norway, pp. 71-74, 2013.

[68] X. Xu, T. Bengtsson, J. Blennow, and S. M. Gubanski, "Enhanced accuracy in dielectric response material characterization by air reference method", Dielectrics and Electrical Insulation, IEEE Transactions on, Vol. 20, Iss. 3, pp. 913-921, 2013.

[69] H. Nyquist, "Certain topics in telegraph transmission theory", American Institute of Electrical Engineers, Transactions of the, Vol. 47, Iss. 2, pp. 617-644, 1928.

[70] E. Hewitt and R. Hewitt, "The Gibbs-Wilbraham phenomenon: An episode in fourier analysis", Archive for History of Exact Sciences, Vol. 21, Iss. 2, pp. 129-160, 1979.

[71] IEC 60851-5, Winding wires – Test methods, 1997.

[72] "OP-42GP datasheet", ed: Analog Devices.

[73] F. Massines, A. Rabehi, P. Decomps, R. B. Gadri, P. Ségur, and C. Mayoux, "Experimental and theoretical study of a glow discharge at atmospheric pressure controlled by dielectric barrier", Journal of Applied Physics, Vol. 83, Iss. 6, pp. 2950-2957, 1998.

[74] T. Ono, D. Y. Sim, and M. Esashi, "Micro-discharge and electric breakdown in a micro-gap", Journal of Micromechanics and Microengineering, Vol. 10, Iss. 3, p. 445, 2000.

[75] T. J. A. Hammarstrom, T. Bengtsson, J. Blennow, and S. M. Gubanski, "Partial discharges in motor wires at PWM voltages of different smoothness", Electrical Insulating Materials (ISEIM), Proceedings of 2014 International Conference on, pp. 184-187, 2014.